EMBRY-RIDDLE
Aeronautical University
SCHOLARLY COMMONS

Dissertations and Theses

5-1-2012

The Engineering Process for the Design of a Motorcycle Chassis and Suspension

Derek J. Noce
Embry-Riddle Aeronautical University - Daytona Beach

Follow this and additional works at: https://commons.erau.edu/edt

 Part of the Automotive Engineering Commons, and the Computer-Aided Engineering and Design Commons

Scholarly Commons Citation

Noce, Derek J., "The Engineering Process for the Design of a Motorcycle Chassis and Suspension" (2012). *Dissertations and Theses*. 112.
https://commons.erau.edu/edt/112

This Thesis - Open Access is brought to you for free and open access by Scholarly Commons. It has been accepted for inclusion in Dissertations and Theses by an authorized administrator of Scholarly Commons. For more information, please contact commons@erau.edu.

The Engineering Process for the Design of a Motorcycle Chassis and Suspension

Derek J. Noce

A Thesis Submitted to the Graduate Studies Office

in Partial Fulfillment of the Requirements for the Degree of

Master of Science in Mechanical Engineering

May 1, 2012

Embry-Riddle Aeronautical University

Daytona Beach, FL

The Engineering Process for the Design of a Motorcycle

Chassis and Suspension

By

Derek J Noce

This thesis was prepared under the direction of the candidate's Thesis Committee Chair, Dr. Jean-Michel M. Dhainaut, Professor, Daytona Beach Campus, and Thesis Committee Members Dr. Sathya N. Gangadharan, Professor, Daytona Beach Campus, and Dr. Dr. Ilteris Demirkiran, Professor, Daytona Beach Campus, and has been approved by the Thesis Committee. It was submitted to the Department of Mechanical Engineering in partialfulfillment of the requirements for the degree of

Master of Science in Mechanical Engineering
Thesis Review Committee:

Dhainaut

Dr. Jean-Michel M. Dhainaut date
Committee Chair

Sathya Narayan

Dr. Sathya N. Gangadharan date 05/14/2012
Committee Member

Ilteris May/14/2012

Dr. Ilteris Demirkiran date
Committee Member

5/14/12

Darris L. White, Ph.D. date
Graduate Program Chair,
Mechanical Engineering

CLR 5/14/12

Charles F. Reinholtz, Ph.D. date
Department Chair,
Mechanical Engineering

5/14/12

Maj Mirmirani, Ph.D. date
Dean, College of Engineering

8/7/12

Robert Oxley, Ph.D date
Associate Vice
President of Academics

ACKNOWLEDGEMENTS

First I want to offer gratitude to my advisor Dr. Jean-Michel M. Dhainaut. Thank you for your patience, knowledge and direction.

Second, I want to thank Dr. Ilteris Demirkiran for pushing me and playing negotiator.

Third, I want to thank Dr. Darris White for his help and giving me the possibility to study at this university.

Fourth, I want to thank Dr. Sathya N. Gangadharan. Your Structure Optimization Course helped shape my future with Pratt and Miller.

Finally, I want to thank my mother, Saundra F. Noce and father, James S. Noce . You both helped me make it this far. I love you very much. Thank you for your tolerance and sacrifice. You are great parents.

ABSTRACT

Author: Derek J Noce

Title: The Engineering Process for the Design of a Motorcycle Chassis and Suspension

Institution: Embry- Riddle Aeronautical University

Degree: Master of Science in Mechanical Engineering

Year: 2012

The thesis objective is to define and establish an engineering process for the design of a modern motorcycle chassis and suspension. The engineering process focuses on the interdisciplinary fields of engineering dealing with design and structural optimization. Specialized software, such as Motorcycle Kinematics, MATLAB, CATIA, HEEDS Professional, and NASTRAN are utilized. Motorcycle Kinematics is used to set up the preliminary motorcycle geometry, and MATLAB is a used to analyze the kinematics and stability of the motorcycle based on this geometry. CATIA (Computer Aided Three-Dimensional Interactive Application) is used to graphically illustrate the geometry of the motorcycle in three dimensional space. HEEDS Professional is optimization software that was used to minimize the weight of the motorcycle by searching the preliminary design space by automating the iterative design process, adjusting the criteria variables until it has reached an optimum value. NASTRAN (Finite Element structural program) is utilized for the calculations of stresses of the motorcycle frame components. HEEDS software interfaces with NEI Nastran until the optimal geometry ensuring structural reliability is obtained. The software was used to design, analyze and structurally optimize a race oriented motorcycle.

TABLE OF CONTENTS

ACKNOWLEDGEMENTS iii

ABSTRACT iv

LIST OF FIGURES vii

LIST OF TABLES viii

INTRODUCTION 1

LITERATURE SURVEY 2

Software: 2

MATLAB: 2

HEEDS: 2

CATIA: 4

NASTRAN & FEMAP: 4

NASTRAN, HEEDS Communication: 5

Frame: 5

Swingarm: 7

Front Suspension: 8

Rear Suspension: 9

THEORETICAL BACKGROUND 10

Kinematics of Motorcycle: 10

Acceleration: 12

Braking: 12

Motorcycle Vibrations Modes and Stability: 13

Suspension: 19

The damping rates are a function of the damping ratio(ζ), front or rear spring stiffness and the mass of the motorcycle. The damping ratio for non-areo race vehicle is between 0.5-0.7. [Milliken] 21

Steady Turning: 21

Motorcycle Trim: 22

RESULTS AND ANALYSIS 26

Structural Considerations: 26

Actual Design: 29

Parametric Study Results: 30

Design Results: ..... **Error! Bookmark not defined.**
Acceleration: 39
Braking: 40
Motorcycle Vibrations Modes and Stability: 42
Suspension: 45
Steady Turning: 48
Trim: 49
Curved Trim: 51
Discussion of Actual Results ..... **Error! Bookmark not defined.**
Structural Optimization Results 55
CONCLUSION 57
References ..... **Error! Bookmark not defined.**
APPENDIX A- MATLAB Programs 61
Acceleration Code: 61
Braking Code: 61
Weave, Wobble, and Capsize Modes Code: 62
Suspension Simulink Code: 66
Steady Turning Code: 69
Motorcycle Trim: 71
APPENDIX B – Structural Optimization Figures 76
Swingarm Structural Optimization Results: 76
Fork Structural Optimization Results: 78
Main Frame Structural Optimization Results: 80
APPENDICIES C- Front Suspension Data 82
Velocity Ratio for Four Link Front Suspension Program: 82
APPENDIX D – Rear Suspension Data 83

LIST OF FIGURES

FIGURE 1 DATA FLOW OF HEEDS 4
FIGURE 2 CATIA MOTORCYCLE MODEL 4
FIGURE 3 DIFFERENT CHASSIS CONFIGURATION 7
FIGURE 4 SWINGARM CONFIGURATION 8
FIGURE 5 FRONT SUSPENSION[FOALE,WIKI] 8
FIGURE 6 TYPES OF REAR SUSPENSION [COSSALTER] 10
FIGURE 7 GEOMETRY OF MOTORCYCLE [COSSALTER] 11
FIGURE 8 CAPSIZE MODEL WITH LATERAL ROLLING ON TIRE [COSSALTER] 16
FIGURE 9 WEAVE AND WOBBLE MODEL GEOMETRY [COSSALTER] 18
FIGURE 10 TWO DEGREE OF FREEDOM SUSPENSION MODEL 19
FIGURE 11 SQUAT AND LOAD TRANSFER LINES 24
FIGURE 12 REAR AND FRONT SUSPENSION DESIGNS 28
FIGURE 13 DRIVING FORCE AS A FUNCTION OF VELOCITY 30
FIGURE 14-ACCELERATION PARAMETRIC STUDY EQUATIONS 5 & 6 33
FIGURE 15-BRAKING PARAMETRIC STUDY, EQUATION 9, 10, 11 34
FIGURE 16-WEAVE AND WOBBLE PARAMETRIC STUDY, EQUATIONS 20-23 35
FIGURE 17- WEAVE AND WOBBLE DAMPING RATIO PARAMETRIC STUDY EQUATION 14, 20-24 36
FIGURE 18- CAPSIZE TIME CONSTANT PARAMETRIC STUDY 37
FIGURE 19-ROLL AND STEERING PARAMETRIC STUDY 38
FIGURE 20-ACCELERATION 39
FIGURE 21-CURVES OF DECELERATION AND DISTRIBUTION OF BRAKING 41
FIGURE 22-BRAKING DISTRIBUTION WITH OPTIMUM BRAKING LINE 42
FIGURE 23-TIME CONSTANT FOR CAPSIZE AS FUNCTION OF SPEED 43
FIGURE 24-NATRUAL FREQUENCIES OF WEAVE AND WOBBLE AS A FUNCTION OF SPEED 44
FIGURE 25-DAMPING RATIOS OF WEAVE AND WOBBLE AS A FUNCTION OF SPEED 45
FIGURE 26 NATURAL FREQUENCY VS SPRING STIFFNESS FOR FRONT AND REAR SPRINGS 46
FIGURE 27 WHEEL DISPLACEMENTS 48
FIGURE 28 ROLL AND STEERING ANGLES AS FUNCTION OF VELOCITY AND CURVATURE 49
FIGURE 29-SQUAT RATIO VS VERTICAL WHEEL MOVEMENT 49
FIGURE 30-FRAME PITCH ANGLE VS SQUAT RATIO 50
FIGURE 31-VERTICAL EXTENSION OF THE REAR SUSPENSION VS SQUAT RATIO 51
FIGURE 32- VERTICAL WHEEL MOVEMENT VS DEVIATION OF THE SQUAT RATIO 52
FIGURE 33-LOWERING OF THE CENTER GRAVITY VS CAMBER ANGLE 52
FIGURE 34- VARIATION PITCH ANGEL VS CAMBER ANGLE 53
FIGURE 35-SUSPENSION SIMULINK MODEL 69
FIGURE 36-MASS(LB) VS DESIGN ITERATION FOR SWINGARM 76
FIGURE 37-MAX ROTATION VS DESIGN ITERATION FOR SWINGARM 76
FIGURE 38- MAX VON MISES(PSI) VS DESIGN ITERATION FOR SWINGARM 77
FIGURE 39-MAX DISPLACEMENT(IN) VS DESIGN ITERATION FOR SWINGARM 77
FIGURE 40-MASS(KG) VS DESIGN ITERATION FOR FORK 78
FIGURE 41-MAX ROTATION(RAD) VS DESIGN ITERATION FOR FORKS 78
FIGURE 42-MAX VON MISES STRESS(PSI) VS DESIGN ITERATION FOR FORKS 79
FIGURE 43-MAX DISPLACEMENT(IN) VS DESIGN ITERATION FOR FORKS 79

FIGURE 44-MASS(LB) VS DESIGN ITERATION FOR MAIN FRAME 80
FIGURE 45-MAX ROTATION(DEG) VS DESIGN ITERATION FOR MAIN FRAME 80
FIGURE 46-MAX VON MISES STRESS(PSI) VS DESIGN ITERATION FOR MAIN FRAME 81
FIGURE 47-MAX DISPLACEMENT(IN) VS DESIGN ITERATION FOR MAIN FRAME 81

LIST OF TABLES

TABLE 1 STIFFNESS VALUES OF EACH COMPONENT 26
TABLE 2 MOTORCYCLE DESIGN PARAMETER 29
TABLE 3 ENGINE/TIRE PARAMETER 29
TABLE 4- MOTORCYCLE SPEC FOR PARAMETRIC STUDY 32
TABLE 5-FRONT AND REAR SPRING RATE AND DAMPING COEFFICIENT 46
TABLE 6- RESULTING NATURAL FREQUENCIES 47
TABLE 7- STRUCTURAL OPTIMIZATION CONSTRAINT PER COMPONENT 55
TABLE 8-STRUCTURAL OPTIMIZATION RESULTS 56

INTRODUCTION

The design and structural optimization of motorcycle frame was undertaken to document the thought process and to justify the selection of the motorcycle geometry. While designing the motorcycle, a literature review was completed to categorize the baseline characteristics of race type motorcycles. To add a more realistic parameter, this motorcycle frame is designed around a 2003 Yamaha R6 engine. Tony Foale's Motorcycle Kinematics software and MATLAB(Logic Package), were used to select the geometric characteristics. Theses softwares were used in evaluating effects of the chosen motorcycle geometry. The kinematics parameters, acceleration and braking were reviewed to verify how the motorcycle would perform. The stability of a motorcycle was also analyzed using eigenvalue analysis. The suspension was analyzed to determine the appropriate spring rates and damping rates. Finally the trim of motorcycle was reviewed to see how the motorcycle will behave in acceleration and cornering.

A portion of the project was to create a motorcycle frame with high structural efficiency, meaning high stiffness and low weight. Each component was evaluated for specific stiffness coefficients. The swingarm and fork were evaluated for lateral and torsional stiffness coefficients. The main frame was evaluated for lateral, torsional, and vertical stiffness coefficients. To evaluate the stiffness the component was put under load and the deflection was evaluated using finite element analysis software (Nei Nastran). Knowing the deflection and the reacting force the stiffness could be determined as the ratio of the force to the deflection.

The structural optimization aspect project involves the main frame, fork, and swingarm. The objective of this optimization was to minimize the weight of the

components without compromising the rigidity. The constraints on the system were maximum allowable Von Mises stress and the evaluated stiffness coefficient must fall within specified range per the torsional, lateral and vertical stiffnesses. The optimization occurs by running multiple iterations of predefined parameters, while searching for the best design. This optimization process took place by coupling optimization software (HEEDS) with FEA software (NEI Nastran).

The justification for this project was the multidisciplinary application of real world design. This project was not to reinvent the technology, but to make an attempt to utilize some of the best available software to design a high performance motorcycle. The software mentioned as well as the major structural components were discussed in detail below.

LITERATURE SURVEY

Software:

MATLAB:

MATLAB is a software environment used for numerical computation. Developed by Mathworks, MATLAB is used in both industry and academia. MATLAB has the ability to interface with a variety of languages [Mathworks]. The fundamental structure of MATLAB is arrays and matrices. MATLAB gives the user the ability to manipulate data in a variety of ways. MATLAB programming language is similar to other computer languages. Also, MATLAB contains a graphical interface. This GUI interface makes MATLAB powerful tool to utilize in many fields. [Palm]

HEEDS:

HEEDS is an optimization tool for any engineering discipline. It can be used in structures, fluids, thermodynamics, or acoustics. In the program the structural models

may be linear, nonlinear, static or dynamic. HEEDS interfaces with Computer Aided Engineering (CAE) applications to automate the design optimization process. The automated process takes a fraction of the time it would take to perform a handful of manual iterations. Within HEEDS, engineers can define design parameters and multidisciplinary design goals, and execute analysis models to judge a design's performance. During each design iteration, HEEDS manipulates values of design variables inside a file. Then the file is implemented, and HEEDS reads the resuling data from an output file. HEEDS performs multiple design iterations automatically while searching for design parameter values that simultaneously meet all targets and criteria. HEEDS effectively searches design spaces, so users can discover better designs faster.[HEEDS Professional | Red Cedar Technology., 3Pty - HEEDS Professional Design Optimization Software]

When utilized, HEEDS begins by choosing values for project variables within a set of pre-defined parameters of the previous step. During each evaluation, HEEDS dynamically alters its search based on the results. Next, HEEDS creates new model input files and evaluates each design with the same analysis software tools that produced the baseline input and output files. After each iteration, HEEDS extracts the corresponding response values from the output files. As the search progresses, HEEDS discovers relationships among variables and responses, and leverages this knowledge to identify higher-performing designs. The program creates a benchmark from the first design and then replaces it when it finds a better design. The last benchmark design obtained during a run is the best design.[HEEDS Professional | Red Cedar Technology]

Figure 1 Data Flow of Heeds

CATIA:

CATIA is a multi-platform **CAD/CAM/CAE** commercial software developed by the French company Dassault Systems and marketed worldwide by IBM. CATIA supports multiple stages of product development including Computer Aided Design(CAD), Manufacturing (CAM), and Engineering (CAE). The majority of the frame is modeled in CATIA can be view below. [CATIA]

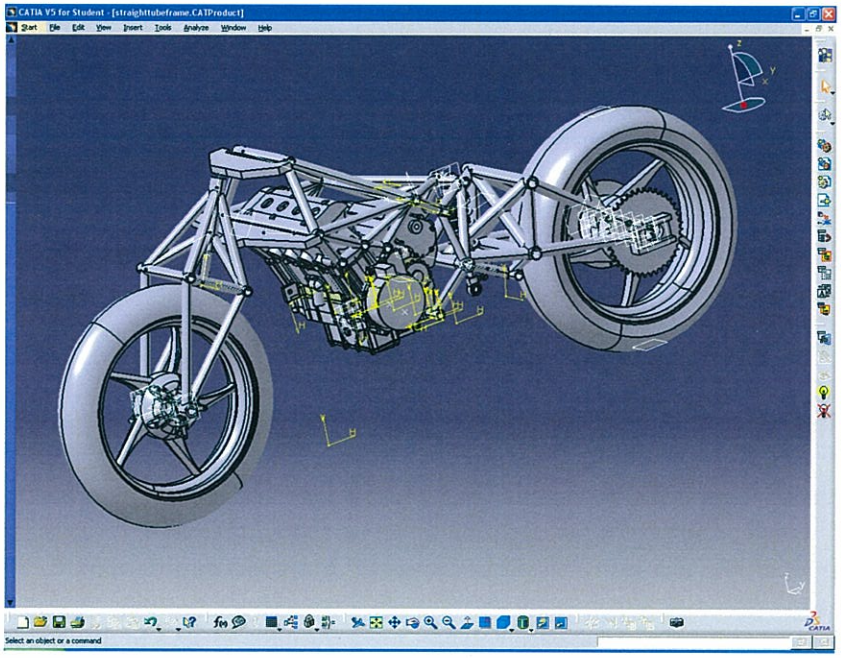

Figure 2 CATIA Motorcycle Model

NASTRAN & FEMAP:

NEi Nastran is an engineering analysis and simulation software product of NEi Software (formerly known as Noran Engineering, Inc.). Based on NASA's source analysis

program, the software is a finite element analysis (FEA) solver used to generate solutions for linear and nonlinear static and dynamic systems subjected to mechanical and thermal loading. In the present work NEi Nastran is used in conjunction with FEMAP.[NEI Nastran]

NASTRAN, HEEDS Communication:

As HEEDs runs, it begins by selecting the user specified project values. Using these values, new input and output files are created for baseline design. As the program runs, input and output files are created per iteration. The specified values are extracted to be used in creating the next set of files.

Geometry values are changed in the NASTRAN .nas file which is used to generate the model. The Nastran model is updated continuously per each iteration. Mathematical algorithms are used to find relationships among geometries and stiffness to weight characteristics. HEEDS continues to calculate until it converges to an optimal stiffness to weight value.

Frame:

The frame has a number of function requirements. There must be structurally sound attachments between the swingarm and main frame and the main frame and the forks. The engine can have rigid or flexible mounts. Also, the engine may be a stress member or not. There is no issue of strength when a motorcycle frame is designed for stiffness. A good evaluation of the structure performance is the stiffness to weight ratio, which can be referred to as structural efficiency. There are a number of frame types, such as tubular backbone, fabricated backbone, trellis, monococque and perimeter.[Cocco,Foale]

- Tubular backbone frames as shown in figure 3(a) have a single tube that passes over the engine and splits into two tubes, passing near the swingarm pivot. After the swingarm pivot, the down tube is still two tubes which converge into one before or at the steering head. .[Cocco, Foale]
- Fabricated backbone frame as shown in figure 3(b), has the profile that looks like a distorted capital letter "T". Fabricated backbone frames are typically heavier styled frames with high rigidity. This design has excess materials in low stress areas adding weight. Tubular and fabricated backbone frames typically have low structural efficiency values.[Cocco, Foale]
- Trellis frames, as shown in figure 3(c), are a truss structure. Fabrication of this structure involves welding and precise jigging. This style frame is light weight while having good rigidity, giving the overall structure high values of structural efficiency.[Cocco]
- Monococque frames, as shown in figure 3(d), are similar to aircraft style frames that have stress at the skin with underlying rib structure. These style frames have very high structural efficiencies when made out of composite material such as carbon fiber. Frames do not give good accessibility for maintenance. .[Cocco, Foale]
- Perimeter frames, as shown in figure 3(e), are most commonly used in the race industry and commercially. Most of these frames are made of cast aluminum or CNC milled aluminum. The large beam protrudes from the head stock leading to the subframe mounts and then onto the swingarm pivot. Perimeter frames have

high structural efficiency and are used in most of today's supersport motorcycles.[Foale]

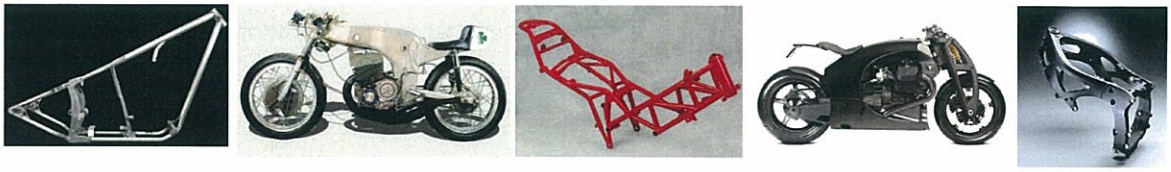

(a) (b) (c) (d) (e)

Figure 3 Different Chassis Configuration

Swingarm:

There are two types of swingarms; conventional(figure 4a) and single sided(figure 4b). Both types of swingarms can be manufactured out of casting or tubes. Conventional style swingarms can be triangulated or have the section between the two arms increased in size to increase stiffness or torsional rigidity.

The two advantages of single-sided swingarm are the ability to replace the wheel and a lower moment of inertia around the swingarm pivot. There are two disadvantages of a single side swing arm. First, the cooling of the rear brake is an issue because the rear brake is positioned inside of the rim obstructed by air flow. Second, the swingarm has different stiffness characteristics from left to right corning. Single sided swingarms have a tendency to flex towards the direction the motorcycle is being steered. This behavior has the tendency to make the bike take a wider turn than that of the radius of curvature which increases the stability of the motorcycle during a turn.[Cocco, Cossalter]

(a) (b)

Figure 4 Swingarm Configuration

Front Suspension:

Telescopic Forks consist of a stanchion and a tube. The stanchion runs along the inner tube creating a prismatic joint. This joint connects the sprung mass of the frame to the unsprung mass of the front wheel. With conventional telescopic forks the stanchion is on top. Alternatively, many modern sport bikes have inverted or upside down forks. With the stanchions on the bottom the bending and torsional stiffnesses of the forks are increased. Around the steering axis these forks have a low moment of inertia. When force is applied perpendicular to the axis of fork, a high friction force is created between the sliding joint of the stanchion and the tube. This suspension system has high unsprung mass. Also, to get a progressive spring rate from this system is by relying of the air captured in the fork tube.[Cossalter]

(a) (b) (c) (d) (e) (f)

Figure 5 Front Suspension [Foale,Wiki]

Other designs listed below are able to remedy the limitations of telescopic fork. With trailing arm(figure 5c) suspensions the pivot point is in front of the front axle. In push

arm (figure 5d) suspension the pivot point is behind the front axle. The four bar linkage can be connected to either directly to the frame or to the steering stem. If connected to the frame, the steering design is a Hossack/Fior (Duolever), as shown in figure 5(e). When connected to the steering head, the suspension is a Girder, as shown in figure 5(f). During braking this system can be designed to offer partial or total anti dive behavior. This suspension design does not contain any prismatic joints. These suspensions can be designed to provide greater torsional rigidity, lower unsprung mass and progressive spring rates. The disadvantages of these suspensions are when compressed, it causes the handle bars to turn. This behavior is also known as bump-steer. To solve this issue the steering revolute can fasten to the chassis.[Foale]

Rear Suspension:

Conventional or "*classic swingarm*" rear suspension shocks are mounted on both sides of the wheel near the axle connecting the swingarm to the subframe. The system has both advantages and disadvantages. Advantages of a conventional suspension are the simplistic design, heat dissipates from the shock easily, force input is directly to the shock causing little force to be transmitted to the chassis and gives a better response of following the profile of the road. Also, this system provides progressive force/displacement values if the shock is angled to the swingarm. The major disadvantages are different shock characteristics, low force /displacement coefficients, and limited travel of the shock. [Cossalter]

Another design is a "*cantilever*" mono shock. The advantages of this system over the dual shock design is greater wheel travel, lower unsprung mass, the system has higher values of torsional and bending stiffnesses, and it is easy to tune because there is one

shock. This system may have shock cooling issues. Also, this system provides progressive force/displacement values if the shock is angled to the swingarm. Another way, to achieve progressive force/displacement behavior is to add linkage to the suspension system. The linkage usually consists of a rocker and a push or pull rod.[Cocco, Foale]

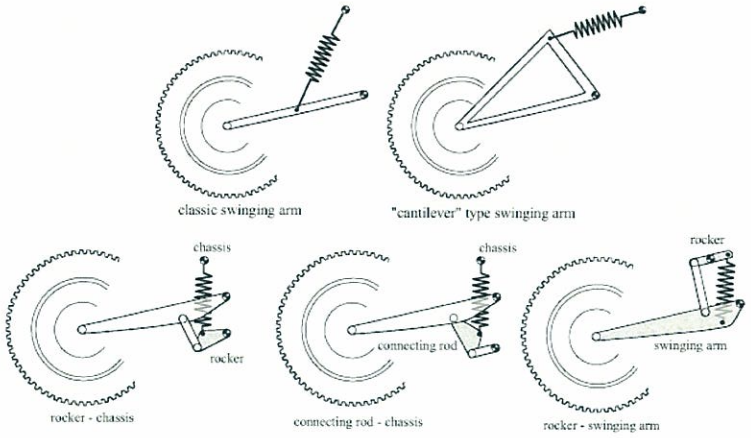

Figure 6 Types of Rear Suspension [Cossalter]

THEORETICAL BACKGROUND

Kinematics of Motorcycle:

There are number of geometric characteristics when describing a sport motorcycle. The wheelbase (p) is the distance from the contact patch of the front wheel to the contact patch of the rear wheel. Sport motorcycle typically has a shorter wheelbase which ranges 1350-1450 mm. The caster (ε) angle or rake of sport/competition bikes is 21-24°, which is the angle of the forks with respects to the vertical. The trail (a) is distance from where the steering axis intersects with the ground to the contact patch of the front tire. The trail ranges from 70 to 90 mm to for sportbikes. The front normal trail (a_n) is the perpendicular distance from the steering axis to the contact patch of the front tire. The rear normal trial (b_n) is the normal distance from the steering axis to the contact

patch of the rear wheel. The ratio of the front normal trail and rear normal trail for race/sports motorcycles is 6-6.5%.[Cossalter]

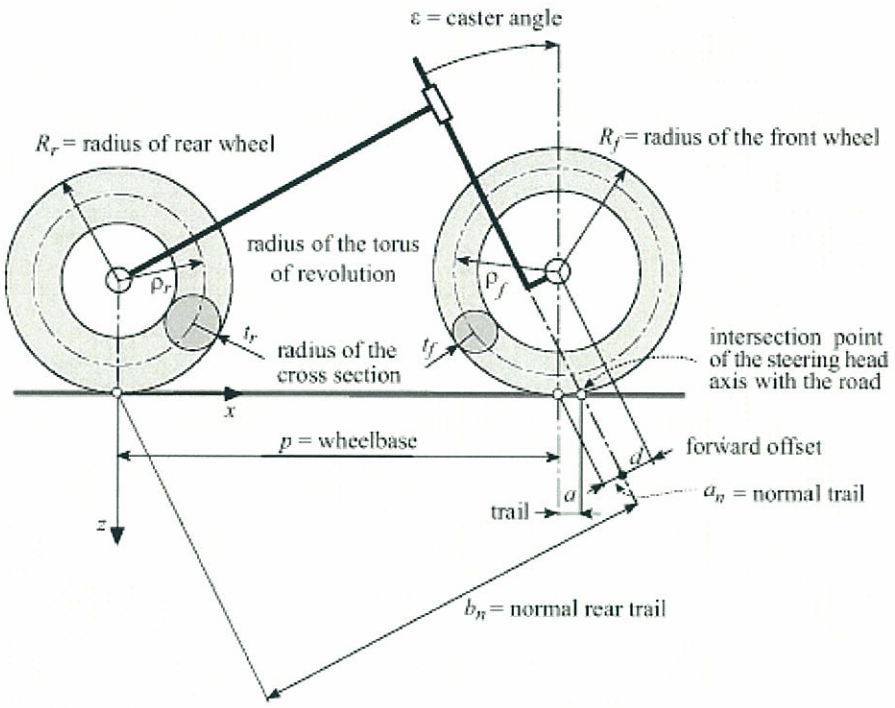

Figure 7 Geometry of Motorcycle [Cossalter]

$$a_n = a * \cos(\varepsilon) \quad (1)$$

$$b_n = (p + a)\cos(\varepsilon) \quad (2)$$

$$R_n = \frac{a_n}{b_n} = 6 - 6.5\% \quad (3)$$

The motorcycle center of gravity depends on the distances of the wheel base (p), the distance from the rear wheel contact patch to the CG (b), and height of the CG from ground (h).

$$\frac{\%front\ load}{\%rear\ \ load} = \frac{b/p}{(p-b)/p} \quad (4)$$

The weight distribution ranges from 50-57 % front to 43-50 % rear. Most modern sportbikes have a 50/50 weight distribution to perform equally as well in acceleration and braking.[Cossalter]

Acceleration:

During acceleration, load transfer causes a decrease in the normal force on the front tire and increases the normal force to the rear tire.

The dynamic load on the front tire (N_f) is given by

$$N_f = mg\frac{b}{p} - S\frac{h}{p} \tag{5}$$

The dynamic load on the rear tire (N_r) is given by

$$N_r = mg\frac{(p-b)}{p} + S\frac{h}{p} \tag{6}$$

The load transfer term in the above equations is the $S\frac{h}{p}$ term, where it is the driving force (S) multiplied by the ratio of the height to the center of gravity (h) to the wheelbase (p). The acceleration is limited by wheeling or loss of traction of the rear wheel which is a correlation ratio of the distance from the rear wheel contact patch to the CG to the height of the CG. If the traction coefficient (μ_p) is less the ratio the acceleration phase is traction limited. If the traction coefficient (μ_p) is greater than the ratio the acceleration is wheeling limited.[Cossalter]

$$if\ \frac{b}{h} > \mu_p\ , a_{traction\ limited} \quad if\ \frac{b}{h} < \mu_p\ , a_{wheeling\ limited}$$

Braking:

During braking, the signs of the load transfer term reversed because the thrus t(S) is negative. The dynamic equations become

$$N_f = mg\frac{b}{p} + S\frac{h}{p} \tag{7}$$

$$N_r = mg\frac{(p-b)}{p} - S\frac{h}{p} \quad (8)$$

Braking is limited by flipped over or when the rear wheel comes off the ground (N_r=0). The maximum deceleration ($\ddot{x}$) seen by the best race rider is 1.1 to 1.2 g's. The non-dimensionalized equations describe deceleration or force ($m\ddot{x}$) values for the overall motorcycle, the front tire force (F_f) and the rear tire force (F_r), respectively.[Cossalter]

$$\frac{\ddot{x}}{g} = \frac{p\mu_r + b(\mu_f - \mu_r)}{p + h(\mu_r - \mu_f)} \quad (9)$$

$$\frac{F_f}{F} = \frac{\mu_f(b + h\mu_r)}{p\mu_r + b(\mu_f - \mu_r)} \quad (10)$$

$$\frac{F_r}{F} = \frac{\mu_f((p-b) - h\mu_f)}{p\mu_r + b(\mu_f - \mu_r)} \quad (11)$$

Equations 9-11 are heavily influenced on the front braking coefficient (μ_f) and rear braking coefficient (μ_r).

The deceleration and force equations are dependent of the geometric values (CG height, wheelbase, distance of CG from the rear wheel) of the motorcycle and the friction coefficient of the tires (μ_r,μ_f).[Cossalter]

Motorcycle Vibrations Modes and Stability:

Multi-body models have two types of modes; in plane modes and out of plane modes. In-plane modes deal with the vertical planar motions of a motorcycle involving frame, suspension, and wheels. In-plane modes control road holding and rider comfort.

Out-of-Plane modes deal with motorcycle stability and handling. Out-of-Plane modes include roll, yaw, and lateral displacement of the steering head.

Eigenvalues (s) for both in-plane modes and out of plane modes are represented by the equations below

$$s = s_r + is_i \tag{12}$$

The complex number (s) equals the real part (s_r) plus imaginary part (is_i).

The natural frequency (ν) corresponds to the imaginary part of the eigenvalue.

$$\nu = \frac{s_i}{2\pi} \tag{13}$$

This imaginary part indicates oscillation. If the imaginary part is zero the mode does not oscillate.

The damping ratio depends on the real part of the eigenvalue and describes the damping. The damping ratio (ζ) is the calculated by the equation below.[Cossalter]

$$\zeta = \frac{s_r}{\sqrt{s_{r+}^2 s_i^2}} \tag{14}$$

The inverse of the real part equals τ, which describes stability of a system described by exponential law according to the equation below.

$$\alpha = \alpha_o e^{s_r t} = \alpha_o e^{\frac{t}{\tau}} \tag{15}$$

If τ is positive the system is unstable and if negative is stable. The complex modes can be clearly viewed on a locust chart. [Cossalter]

Motorcycle vibrations modes and stability are heavily dependent on velocity. Both the front and the rear of frames of a motorcycle can oscillate around the steering

axis. At low speeds motorcycle tends to fall over laterally. There are three major modes: wobble, weave, and capsize. Wobble is the oscillation of the front frame around steering axis. Weave is the oscillation of the rear frame around the steering axis. Capsize is the rotation of the entire bike around contact patches in the lateral direction. [Cossalter]

Capsize is the mode the riders used to roll the motorcycle. The motorcycle rolls when the rider moves the motorcycle from the equilibrium position. This mode appears always unstable, and is best represented as an inverted pendulum. The system can be quantified by eigenvalue analysis. Capsize mainly consists of rolling motion, but incorporates some lateral displacements along with steering and yaw movements. The capsize mode is affected by the factors listed below:

- the speed of the motorcycle
- wheel inertia
- center of gravity position
- motorcycle mass
- caster angle
- mechanical trial
- cross sectional radius of the tire
- slip and camber stiffness of tire

To see how geometric and inertial factors effect capsize mode, it is best to analyze the falling motion of motorcycle with the handlebars locked. With this assumption, capsize can be linearly approximated as an exponential equation. [Cossalter]

$$\varphi = \varphi_o e^{\frac{t}{\tau}} \tag{16}$$

Tau (τ) is positive time constant, which shows that the capsize mode is unstable. The following assumptions were made in the capsize are listed below:

- the motorcycle is moving in the horizontal direction at speed V
- the steering head is locked in place
- gyroscopic effects are negligible

The mathematical model used allows tires to slip laterally as the motorcycle leans over. The model has two degrees of freedom.

- Camber (φ) is the rotation around the x-axis
- lateral displacement (y) along the y axis

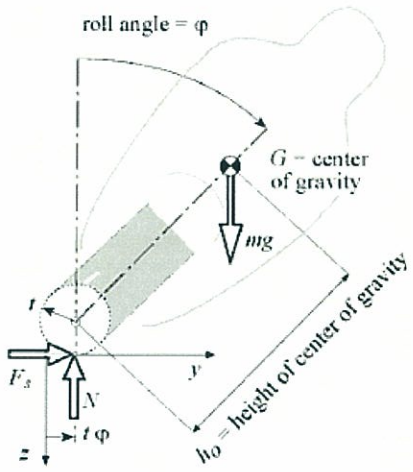

Figure 8 Capsize Model with Lateral Rolling on Tire [Cossalter]

The lateral force is a linear function of the slip angle (λ) and camber angle (φ). The k values are the lateral and camber stiffness of the tire. [Cossalter]

$$F_{LATERAL} = (k_\lambda \lambda + k_\varphi \varphi) mg \quad (17)$$

The slip angle is the ratio between the lateral velocity and linear velocity.

$$\lambda = \frac{\dot{y}}{V} \tag{18}$$

When using eigenvalue analysis for this two degree of freedom capsize model the equations take the form

$$\begin{bmatrix} mh_o & m \\ I_{xg} & mh \end{bmatrix} \begin{bmatrix} \ddot{\varphi} \\ \ddot{y} \end{bmatrix} + \begin{bmatrix} 0 & \frac{mgk_\lambda}{V} \\ 0 & \frac{-(h+t)k_\lambda mg}{V} \end{bmatrix} \begin{bmatrix} \dot{\varphi} \\ \dot{y} \end{bmatrix} + \begin{bmatrix} \frac{-k_\lambda}{mg} & 0 \\ mg((h+t)k_\varphi - h) & 0 \end{bmatrix} \begin{bmatrix} \varphi \\ y \end{bmatrix} = 0 \tag{19}$$

Many weave and wobble models assume that the steering head does not move laterally. The model used for eigenvalue analysis utilizes three degrees of freedom, which accounts for the lateral movement of the head. In Figure 9 Weave and Wobble Model Geometry, looking at the motorcycle along the steering axis, one can easily see the three degrees of freedom which are the rotation of the front assembly (θ_f), the rotation of the rear assembly (θ_r) and the lateral displacement of the head (y). All the modes of the in the model are independent of each other. [Cossalter]

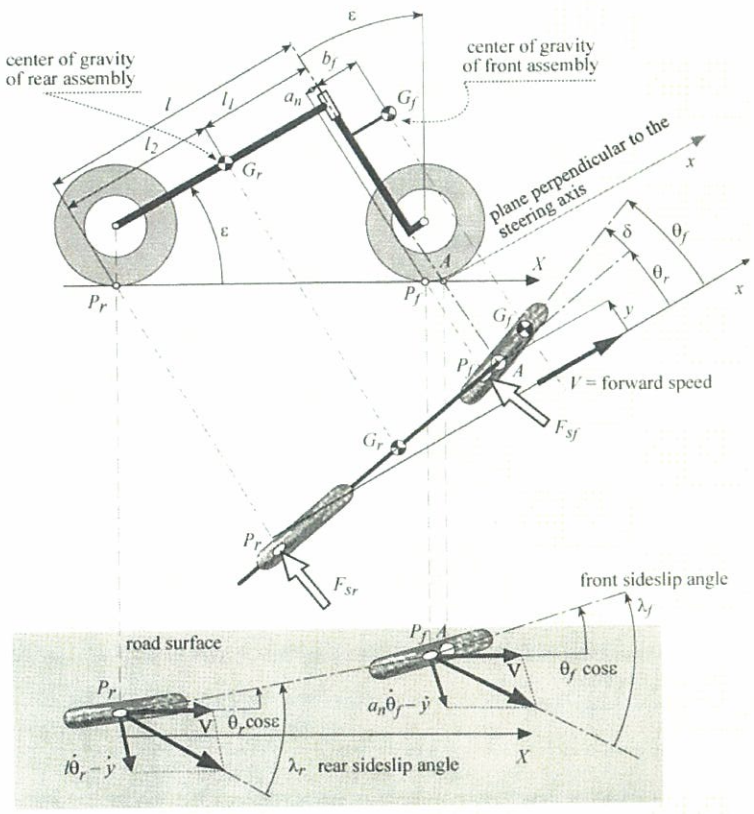

Fig. 7-18 Front-end and rear-end geometry.

Figure 9 Weave and Wobble Model Geometry [Cossalter]

Equation 21 is the homogenous equation describing the weave and wobble model is

$$[M]\begin{bmatrix}\ddot{y}\\ \ddot{\theta}_r\\ \ddot{\theta}_f\end{bmatrix}+[C]\begin{bmatrix}\dot{y}\\ \dot{\theta}_r\\ \dot{\theta}_f\end{bmatrix}+[K]\begin{bmatrix}y\\ \theta_r\\ \theta_f\end{bmatrix}=0 \tag{20}$$

Equation 22 is the mass matrix.

$$[M]=\begin{bmatrix}M_r+M_f & -M_r l_1 & M_f b_f\\ -M_r l_1 & M_r l_1^2+I_r & 0\\ M_f b_f & 0 & M_f b_f^2+l_f\end{bmatrix} \tag{21}$$

Equation 23 is the stiffness matrix

$$[K] = \begin{bmatrix} 0 & -K_{\lambda_r}\cos\varepsilon & -K_{\lambda_f}\cos\varepsilon \\ 0 & K_{\lambda_r} l\cos\varepsilon & 0 \\ 0 & 0 & K_{\lambda_f} a_n \cos\varepsilon \end{bmatrix} \quad (22)$$

Equation 24 is the damping matrix. The damping matrix is the only one which is influence by velocity of the motorcycle.

$$[C] = \frac{1}{V}\begin{bmatrix} K_{\lambda_r} + K_{\lambda_f} & -K_{\lambda_r} l & -K_{\lambda_f} a_n \\ -K_{\lambda_r} l & K_{\lambda_r} l^2 + cV & -cV \\ -K_{\lambda_f} a_n & -cV & K_{\lambda_f} a_n^2 + cV \end{bmatrix} \quad (23)$$

Suspension:

The model used to analyze the suspension two degrees of freedom. The two degrees freedoms are

- Vertical displacement of the sprung mass (z)
- Pitch of the sprung mass (μ)

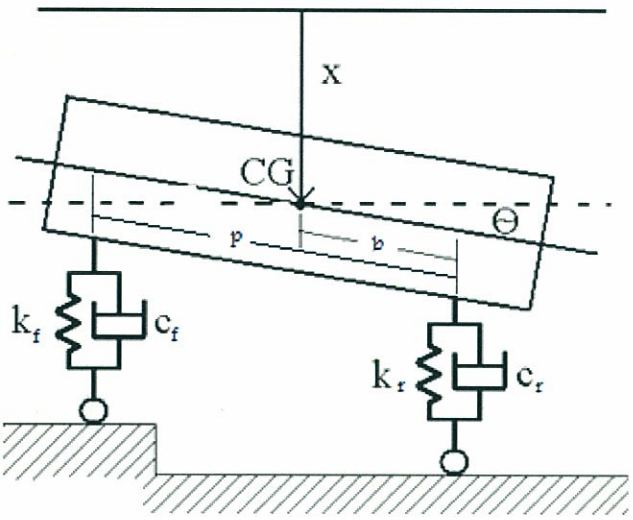

Figure 10 Two Degree of Freedom Suspension Model

The suspension system in Figure 10 is described by equations below

$$[M]\begin{bmatrix}\ddot{z}\\ \ddot{\mu}\end{bmatrix}+[C]\begin{bmatrix}\dot{z}\\ \dot{\mu}\end{bmatrix}+[K]\begin{bmatrix}z\\ \mu\end{bmatrix}=0 \tag{24}$$

$$[K]=\begin{bmatrix}k_r+k_f & (p-b)k_f-bk_r\\ (p-b)k_f-bk_r & (p-b)^2k_f-b^2k_r\end{bmatrix} \tag{25}$$

$$[C]=\begin{bmatrix}c_r+c_f & (p-b)c_f-bc_r\\ (p-b)c_f-bc_r & (p-b)^2c_f-b^2c_r\end{bmatrix} \tag{26}$$

$$[M]=\begin{bmatrix}m & 0\\ 0 & I_{yg}\end{bmatrix} \tag{27}$$

The natural frequency can be calculated by solving the eigenvalue problem. Racing motorcycles normally have natural frequencies of 2-2.6 Hz. Usually the front suspension is a lower stiffness then the rear suspension. The front natural frequency (υ_f) is 70 to 80 % of the rear natural frequency (υ_r). For quick calculation, the unsprung masses can be ignored. The equation for the natural frequency becomes the following equation:

$$\upsilon_r=\frac{1}{2\pi}\sqrt{\frac{K_r p}{m(p-b)}} \tag{28}$$

$$\upsilon_f=\frac{1}{2\pi}\sqrt{\frac{K_f p}{mb}} \tag{29}$$

The damping rates can also be calculated by

$$c_f=2\zeta\sqrt{\frac{K_f p}{mb}} \tag{30}$$

$$c_r = 2\zeta\sqrt{\frac{K_r p}{m(p-b)}} \tag{31}$$

The damping rates are a function of the damping ratio(ζ), front or rear spring stiffness and the mass of the motorcycle. The damping ratio for non-areo race vehicle is between 0.5-0.7. [Milliken]

Steady Turning:

A motorcycle in steady turning is subjected to two moments; a tilting moment due to the weight of the motorcycle and restoring moment generated by the centrifugal force. The following assumptions are made about a stead turning motorcycle:

- The motorcycle follows a constant a radius turn at constant velocity
- Gyroscopic effect are negligible

Equation 32 determines the effective roll angle necessary for equilibrium between moments of the weight of the motorcycle and the centrifugal force and given by

$$\varphi = \tan^{-1}\left(\frac{V^2}{gR_c}\right) + \frac{t\cdot\sin\left(\tan^{-1}\frac{V^2}{gR_c}\right)}{h-t} \tag{32}$$

The equation is a function of the velocity (V) and radius of curvature (R_c). The height of the motorcycle center of gravity (h) along with the thickness of the tire (t) affects the effective roll angle. The roll angle increases as the thickness of the tire increases and decreases as the height of the CG decreases.

The steering angle (δ) is influenced by the rake (ε) of the motorcycle, the radius curvature of the turn (R_{cr}), and the roll angle (φ). The steering angle (δ) is given by

$$\delta = \tan^{-1}\left(\frac{p \cdot R_{cr} \cdot \cos\varphi}{\cos\varepsilon}\right) \quad (33)$$

Looking at equations 32 and 33 together, one can see the velocity increases the steering angle decreases and the rolling angle increases. As the radius curvature increases the steering increases, but radius of curvature has no real effect on the roll angle

The motorcycle is heavily influenced by riding style. If the rider does not move and his center of gravity remains in plane and with the motorcycle's CG then the actual roll will be close to the theoretical roll angle. A racer will lean into a turn which reduces the actual roll angle of the motorcycle. If the rider leans to the exterior of the turn then the motorcycle has to be lean more than the theoretical roll angle. [Cossalter]

Motorcycle Trim:

Motorcycle trim exhibits various geometric configurations that a motorcycle takes as it is subjected to different forces during steady state and transient motion. Motorcycle trim is highly dependent on the suspension stiffness, forces operating on the motorcycle, and on the inclination angle of the swing arm and chain.

Squat and Dive refer to different pitching motions of the sprung mass. Dive is the forward pitching motion of the sprung mass, which occurs typically during braking. Squat is the backward pitching motion which typically occurs during acceleration. The load transfer causes squat and dive. Load transfer is influenced by inertia, aerodynamics, attitude and torque reaction between engine and sprocket during acceleration. Motorcycle geometry, along with braking and driving forces may cause the suspension to extend or compress [Cossalter].

With chain driven motorcycles, the chain pulls backs and down on the sprung mass and the swingarm pushes up and forward. Depending on the angle of the swingarm and the geometry of the motorcycle, the chain force and swingarm forces can be additive or subtractive in turn causing the motorcycle to exhibit pro-squat or anti-squat effects. The anti-squat effect can change over the full range of the suspension. For example, as the suspension is compressed, anti-squat effect can decrease and may even become a pro-squat effect. There are four moments acting on the swingarm, that influence of anti-squat or pro-squat effect on a motorcycle, are listed below:

- Load transfer moment, compresses the suspension
- Driving force moment, which extends the suspension
- Chain force moment, compresses the suspension
- Moment generated to suspension movement

The squat ratio will describe partial trim of the motorcycle and is dependent on the four moments listed above.

Referring to Figure 11, point A is the force center, which is determined by drawing line through the chain and swingarm. The squat line is drawn for the contact patch of the rear wheel through point A. The squat angle (σ) is the angle of the squat line with the horizontal. The load transfer line is drawn through the contact patch of the rear wheel to the intersecting point of a horizontal line drawn through the CG and vertical line drawn through the contact patch of the front wheel. The load transfer angle (τ) is the angle between the load transfer line and the horizontal [Cossalter, Foale].

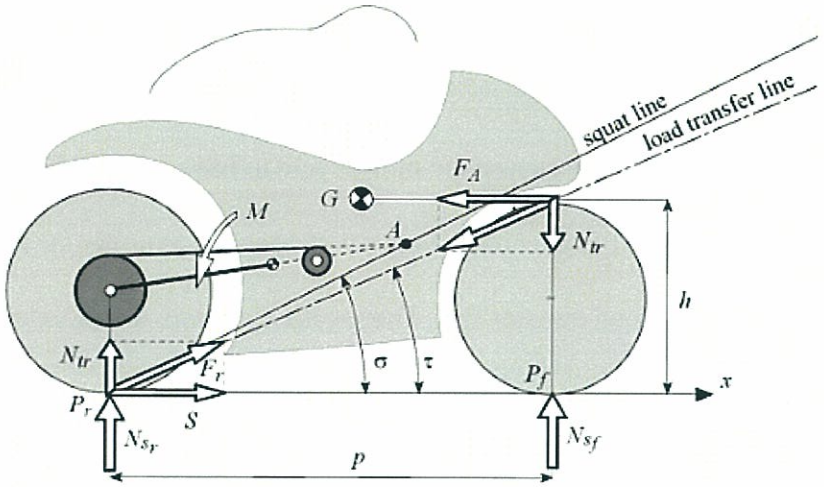

Figure 11 Squat and Load Transfer lines

The Squat Ratio ($\Re$) is the ratio between the moment generated by the load transfer and the moment generated by the addition of the chain force and the driving force.

$$\Re = \frac{h\cos\phi}{p(\sin\phi + \frac{R_r}{r_c}\sin(\phi - \eta)} = \frac{\tan\tau}{\tan\sigma} \quad (34)$$

The variables of the equation are the CG height (h), angle of the swingarm with the horizontal (ϕ), the angle of the chain relative the horizontal (η), radius of the rear wheel (R_r), and radius of the drive sprocket (r_c).

There are three cases of how the load transfer angle (σ) affects the squat angle (τ):

- Load transfer angle equals squat angle (σ = τ), Squat Ratio=1 ($\Re$=1). The virtual pivot A lies directly on the load transfer line. When the motorcycle is accelerating the thrust does not compress or extend the suspension

- Load transfer angle is greater than squat angle ($\sigma < \tau$), ($\Re > 1$). The virtual pivot A lies below the load transfer line. During acceleration, thrust compresses the suspension. This causes the motorcycle to have pro squat behavior.
- Load transfer angle is less than squat angle ($\sigma > \tau$), ($\Re < 1$). The virtual pivot A lies above the load transfer line. During acceleration, thrust extends the suspension give the motorcycle anti squat behavior [Cossalter]

As the squat ratio of the motorcycle varies the front suspension extends and the rear may extend or compresses depending on the value of squat ratio. The vertical extension of the front suspension is expressed as

$$\Delta L_f = \frac{N_{tr}}{k_f} \tag{35}$$

The compression or extension of the rear suspension is equated by

$$\Delta L_r = \frac{N_{tr}}{k_r} \left(\frac{1 - \Re}{\Re}\right) \tag{36}$$

Both above expressions are dependent on the load transfer (N_{tr}). The vertical extension of the front is also dependent on the front spring stiffness. Rear deformation is dependent the squat ratio and the rear spring stiffness.

As a motorcycle moves at a constant velocity from a straight line to a curve the motorcycle will pitch forward and the center gravity lowers. The pitching motion and lowering of the center of gravity are inversely proportional the roll angle. The pitch is motion ($\Delta\mu$) is

$$\Delta\mu = \frac{mg\left(\frac{1}{\cos\varphi} - 1\right)}{\frac{p^2 k_f k_r}{bk_f - (p-b)k_r}} \tag{37}$$

The lowering of the center gravity (Δh) is

$$\Delta h = \frac{mg\left(\frac{1}{\cos\varphi} - 1\right)}{\frac{p^2 k_f k_r}{(p-b)^2 k_f + b^2 k_r}} \tag{38}$$

RESULTS AND ANALYSIS

Structural Considerations:

The frame can be separated into three components; main frame, fork and swingarm. The frame is evaluated for the torsional, lateral and vertical stiffness. Both the lateral and torsional stiffness is evaluated for the fork and swingarm. The designed swingarm must be able to withstand longitudinal force such as braking and thrust. The designed fork must withstand the longitudinal braking. Both the swingarm and fork need to be able to withstand lateral forces. The stiffness of each component is in a range specified by Vittore Cossalter in "Motorcycle Dynamics". The values in the following table were taken from that text:

Table 1 Stiffness Values of Each Component

Component	Torsional(kNm/°)	Lateral (kN/mm)	Vertical(kN/mm)
Main Frame	3-7	1-3	5-10
Swingarm	1-2	0.8-0.16	n/a
Fork	0.1-0.3	0.07-0.018	n/a

The above values were used to construct some constraints used in the optimization software, HEEDS . The components were treated as linear and torsional springs. Since the applied forces and torques along with the stiffness coefficients in the

literature were known, the maximum angular and linear displacements could be calculated. The desired design is to have a frame of high stiffness and low weight. Too much of one kind of stiffness versus another is undesirable. To make sure we have the right ratios of the stiffness, the values from the literature review were used as guidelines. A range of values was given in Table 1, from the range the upper limit was chosen for the calculation of the maximum torsional and the lateral displacement.

To find the minimum wall thickness for the tubes used to construct the components, each component is subjected to maximum forces. The maximum lateral load is 1.6 times the normal load. The maximum acceleration is 1.2g and the maximum deceleration is 1.2g. All forces are translated at the contact patch between the tire and the road. Since the frame is broken into components, the reactions forces were calculated for each component as the force translates from the road to the frame. When reaction forces were calculated each component is considered a rigid body.

The structural stiffness of a motorcycle is an important classification for defining the performance. Motorcycles with high values structural stiffness give quick response to rider input. This sensitivity gives precision in trajectory and, in turn, causes the motorcycle to feel jumpy or unstable. The lateral flexibility of the front fork or flexibility near the steering head stabilizes the wobble mode at high speed but creates instability of the wobble mode at low speeds. Torsional flexibility of the frame has no real influence on the stability of the vehicle. Lateral flexibility of rear swingarm gives stability to the motorcycle at very high speeds. The torsional flexibility of the swingarm gives stability to the motorcycle at high rate of speeds. Lateral forces create lateral displacements of the wheels. As the wheel displaces laterally, the plane of the wheel rotates. The lateral

displacement with rotation wheel causes an increase in the angle of slip which increases the damping of structural vibration. Torsional deformation of the wheel plane does not increase damping effect of structural vibration

Overall, a motorcycle performs best with moderate lateral stiffness and high torsional stiffness.

One must also consider the force transferred through the motorcycle as the suspension is compressed. As the shock is compressed the force from the compressed spring translates both to the swingarm shock mount and the shock suspension frame mount. The compression happens both in the front and rear. The rear suspension design chosen is a floating rocker and link suspension. The front suspension design chosen is a Hossack suspension. Profile images of the front and rear suspension designs can be viewed below.

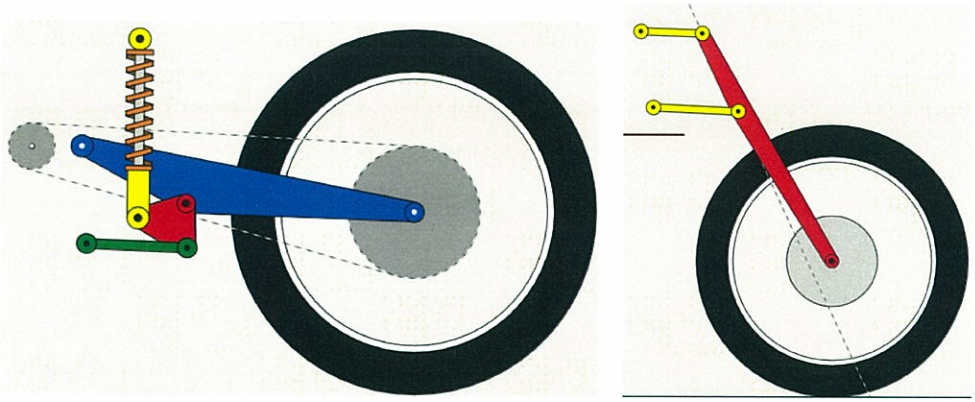

Figure 12 Rear and Front Suspension Designs

The suspensions are not unique. The rear suspension comes from 2003 Yamaha R6 which has been one the of most popular sport bikes to convert to a track motorcycle. The 2003 Yamaha R6 design is still being manufactured today and is known as R6s. The front suspension is also known as the Duolever which is produced on the BMW K1200.

The frame design chosen to be used was a trellis frame. As stated in the previous pages, trellis frames are a truss structure. This style frame is light weight while having good rigidity, giving the overall structure high values of structural efficiency. Again, the structure efficiency is the stiffness to weight ratio. [Tony Foale]

Actual Design:

The geometry of the motorcycle was chosen based on competitive motorcycles from industry and information from the literature review. Table 2 outlines the parameters of the actual motorcycle design.

Table 2 Motorcycle Design Parameters

Parameter:	
Wheelbase(p):	1380mm
Distance from the rear contact patch to the GG(b):	690mm
Height to the CG(h):	580mm
Weight Distribution:	50/50
Rake:	24°
Trial:	86mm
Target Mass:	189kg

The motorcycle was designed around 2003 Yamaha R6 engine.

Table 3 Engine/Tire Parameters

Engine:	600cc-2003 Yamaha R6
Redline:	16000 rpm
Max Torque:	44.1 @ 12000 rpm
Max Power:	104 HP @ 13500 rpm
Gear Ratio:	1^{st} - 2.846 2^{nd} - 1.947 3^{rd} - 1.556 4^{th} - 1.33 5^{th} - 1.19 6^{th} - 1.083
Primary Reduction:	1.955
Secondary Reduction:	3
Tire Radius:	303mm (0.994in)

Based on the available motorcycle engine data Figure 13 Driving Force as a Function of Velocity was constructed to determine available driving force and the approximate maximum velocity. Figure 13 describes the force available in each gear for 1st to 6th as function as a function of the velocity. The purple line in Figure 13 indicates the available driving force in 6th gear. Where the purple line crosses the velocity axis indicates the top speed of the motorcycle. The maximum available driving force is 2588.4 N at 12000 rpm in 1st gear. The maximum velocity is 260 k/hr.

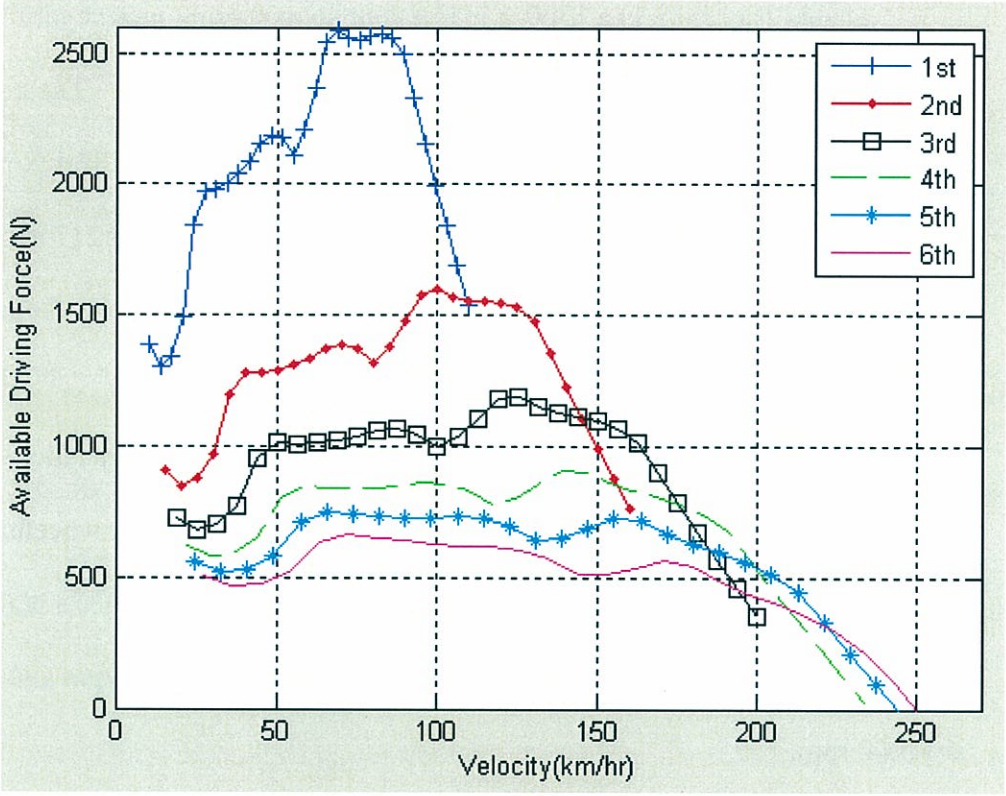

Figure 13 Driving Force as a Function of Velocity

Parametric Study Results:

The parametric study was constructed to better understand on how the geometry affects the performance of the motorcycle. The situations analyzed were acceleration, braking,

stability, and steady turning. The study was conducted using four different cases; Suzuki SV650, Suzuki Hayabusa, Yamaha R6, and Triumph Daytona 955i.

Suzuki SV650 is 650cc V twin naked bike. Essentially, the motorcycle is considered to be a medium performance motorcycle on a budget. The motorcycle has a max power and torque of 73.4 hp (54.7 kW) at 8800 rpm and 47.2 lbf·ft (64.0 N·m) @ 7000 rpm. Out of the study group, this motorcycle has the lowest CG height and weighs the least at 165kg.

Suzuki Hayabusa is a 1300cc in line four sport touring motorcycle. This motorcycle has top speed of the 303 to 312 km/h(188 to 194 mph). The motorcycle has a max power and torque of 121.3 kW(162.6 hp) @ 9750 rpm and 132.1 N·m (97.4 lb·ft) @ 7000 rpm. The Hayabusa weighs the most of the study group at 217 to 250 kg. This motorcycle has a longer wheelbase and lower CG height, which gives the motorcycle greater straight line stability.

The Yamaha R6 is a 600cc inline four sport motorcycle. This motorcycle is based race technology. The motorcycle has a high CG height and shorter wheelbase which makes the motorcycle more unstable but more nimble. The motor has a high power to weight ratio. The max horse power and torque are 104hp @ 13500rpm and 44.7Nm @12000 rpm.

The Triumph Daytona 955i is 950cc 3 cylinder engine sport bike. The max power and torque are 108.8 kW(149.00 hp) @ 10700 rpm and 100.00 N·m (73.8 ft·lbf) @ 8200 rpm. When comparing the Daytona to the other motorcycles in the study, it is mainly middle of the pack.

For comparison, Table 4 displays all geometric characteristics per each motorcycle

Table 4- Motorcycle Spec for Parametric study

Motorcycle	Weight Distribution	Wheelbase (mm)	Rear Contact Patch to CG(mm)	Height to CG (mm)	Mass (kg)	rake(°)	Trail(mm)
Suzuki SV650	0.55/0.45	1455	800.25	475	165	25	101
Suzuki Hayabusa	0.49/0.51	1485	727.65	519	217	24	97
Yamaha R6	0.5/0.5	1380.5	690.25	580	166	24	97
Triumph Daytona 955i	0.51/0.49	1431	729.81	517	188	24	86

Figure 14 displays the maximum acceleration of the motorcycles at the friction limit of the rear wheel. The acceleration is limited by wheeling or loss of traction of the rear tire. The maximum acceleration is a correlation ratio of the distance from the rear wheel to the contact patch to the CG to the height of the CG. The blue star lines represent the maximum acceleration which motorcycle can reach without wheeling. The red dotted lines represent the maximum acceleration as a function the rear driving coefficient.

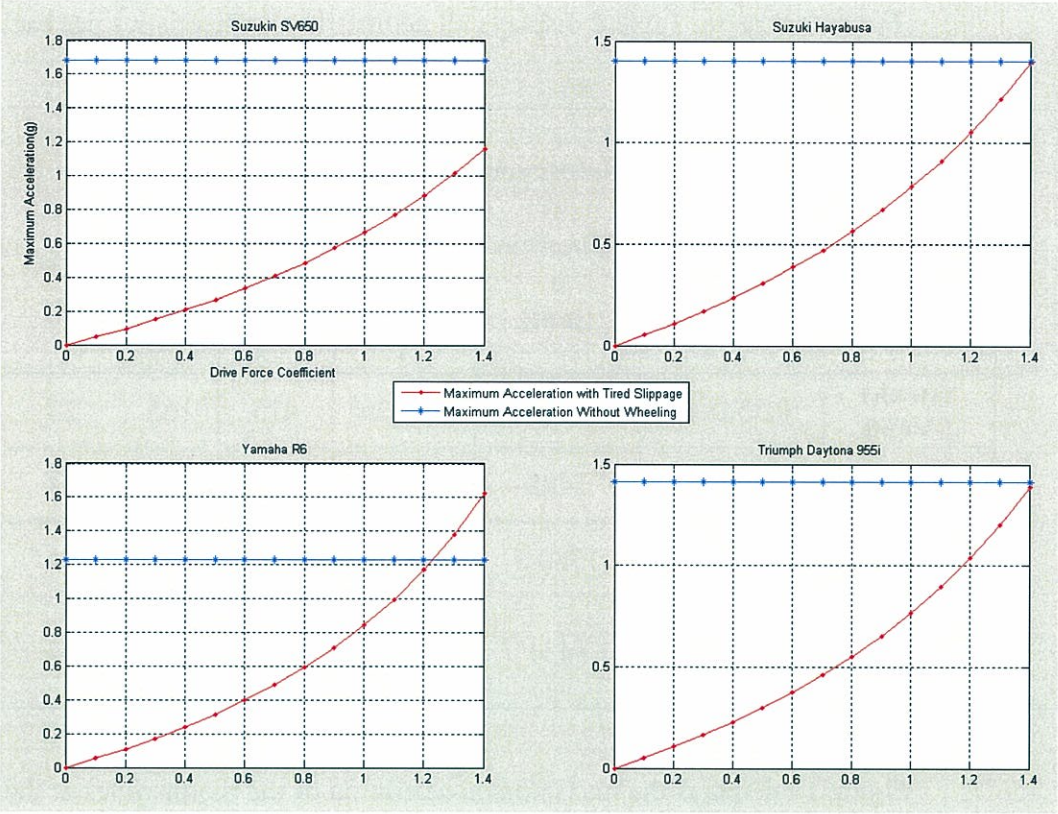

Figure 14-Acceleration Parametric Study Equations 5 & 6

Viewing Figure 14, all the motorcycles in the case study are traction limited except for the Yamaha R6. Even still, the Yamaha R6 is traction limiting up to a driving coefficient of 1.2, then the motorcycle is wheeling limited. Both the Triumph Daytona 955i and Suzuki Hayabusa can be wheeling limited at a driving force coefficient of 1.5, but this effectively means the motorcycle needs to accelerate greater 1.45g's for the motorcycle to wheelie.

Figure 15 displays braking and deceleration forces in terms of the braking coefficients of the front and rear wheels. The figure describes the overall braking behavior of the motorcycle from which the optimum braking can be determined. The blue lines describe the maximum deceleration forces in g's. The red lines describe the

braking distribution between the front and rear wheel. The red line number values in Figure 21 are the braking distribution on the front wheel which varies 0.1-1. For example, at the value of 0.4, the braking distribution is 40% front and 60% rear. The horizontal axis represents braking of the rear wheel only (100% rear). The vertical axis represents the braking of the front wheel only (100% front).

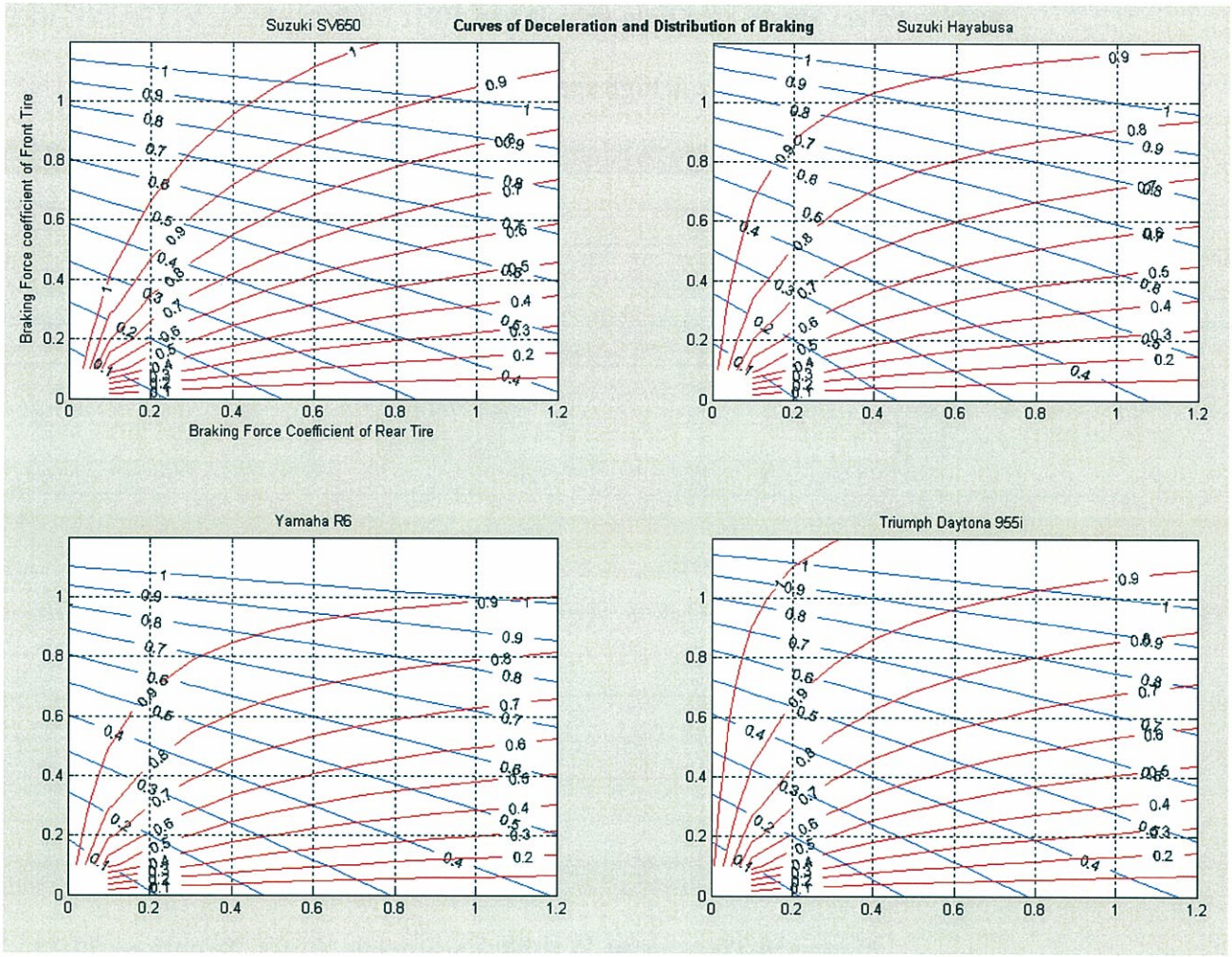

Figure 15-Braking Parametric Study, Equation 9, 10, 11

The maximum deceleration of each motorcycle appears to be very similar. The R6 appear to be the most responsive during braking. The R6 is the most responsive because it is able to reach higher decelerations at lower braking force coefficients. The SV650 and the

Daytona 955i are the middle of the pack. The Hayabusa appears to be the least responsive meaning it requires high braking coefficient to reach high deceleration levels of braking.

Figure 16 displays frequency verses speed for the wobble and weave modes for each motorcycle. The two modes are significantly independent of each other. Typical wobble values are 4Hz for light vehicle and 10Hz for heavy vehicle. Usually, weave values varies from 0-4Hz at high speeds.

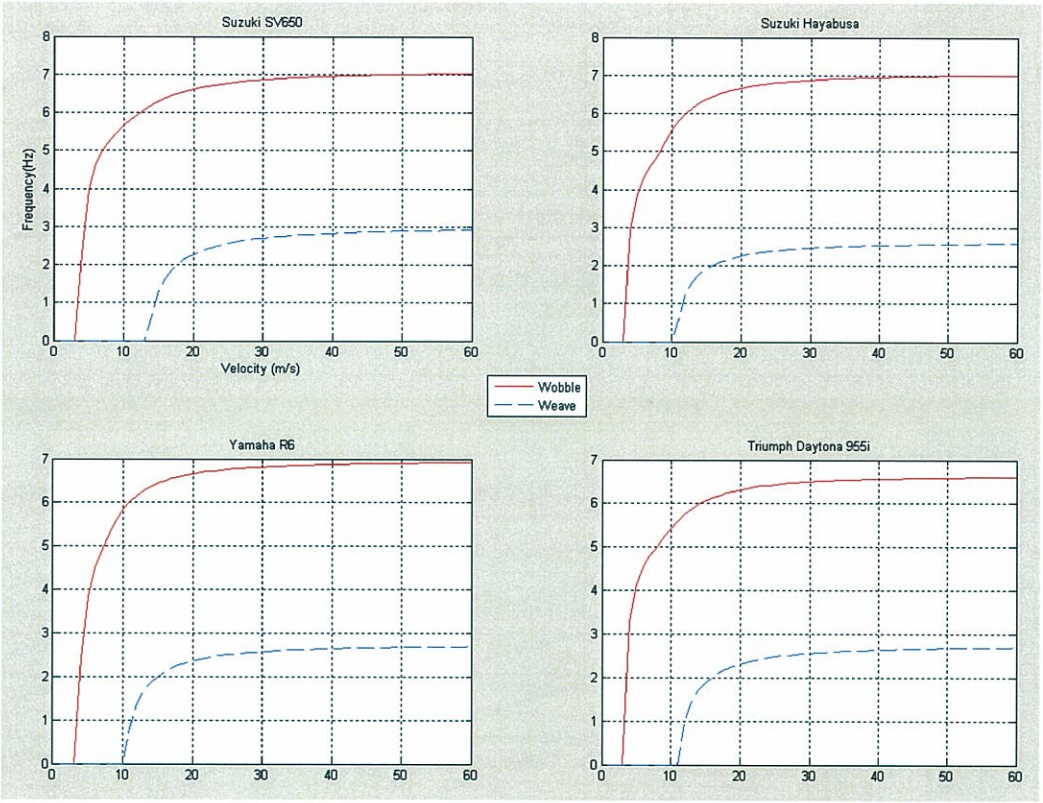

Figure 16-Weave and Wobble Parametric Study, Equations 20-23

All of the motorcycles in the study have a wobble frequency of approximately 7 Hz and a weave frequency of approximately 3 Hz. All the motorcycles in the study are mid weight sport motorcycles. The frequency values are actually negative which means that each motorcycle is stable in the weave and wobble modes. Also, the motorcycles become

more stable as the velocity increases, but both modes become asymptotic. From inspection of Figure 16, the R6, Hayabusa , and SV650 have all about the same wobble stability. The wobble mode of the 955i is the less stable for motorcycles. The SV650 has the most stable weave mode. All the other motorcycles have are less stable weave mode values, but all are approximately the same value. This figure is obtained by solving the eigenvalue problem in equations 20-23

The damping of the weave and wobble modes is to reduce the excitability of the motorcycle and make the motorcycle more stable in unstable zones of speed. The damping ratio decreases as the velocity increases. Figure 17 shows the damping ratio for weave and wobble modes.

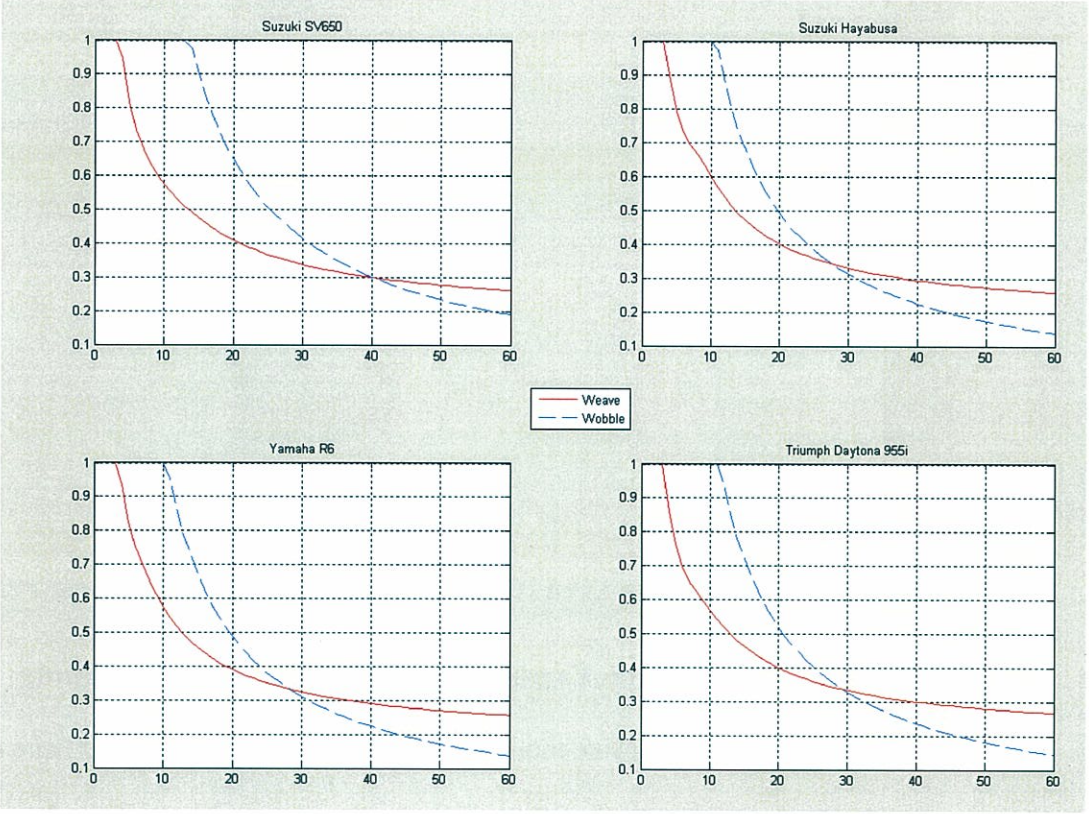

Figure 17- Weave and Wobble Damping Ratio Parametric Study Equation 14, 20-24

The damping ratio for weave mode for each motorcycle declines at similar rate with the increase in velocity. For the wobble mode, the SV650 has more damping at higher velocity which helps the motorcycle to be more stable. The three remaining motorcycle all have similar values for the wobble mode. Wobble mode, which is the oscillation of the front frame around the steering axis, can easily be stabilized by the induction of a steering damper.

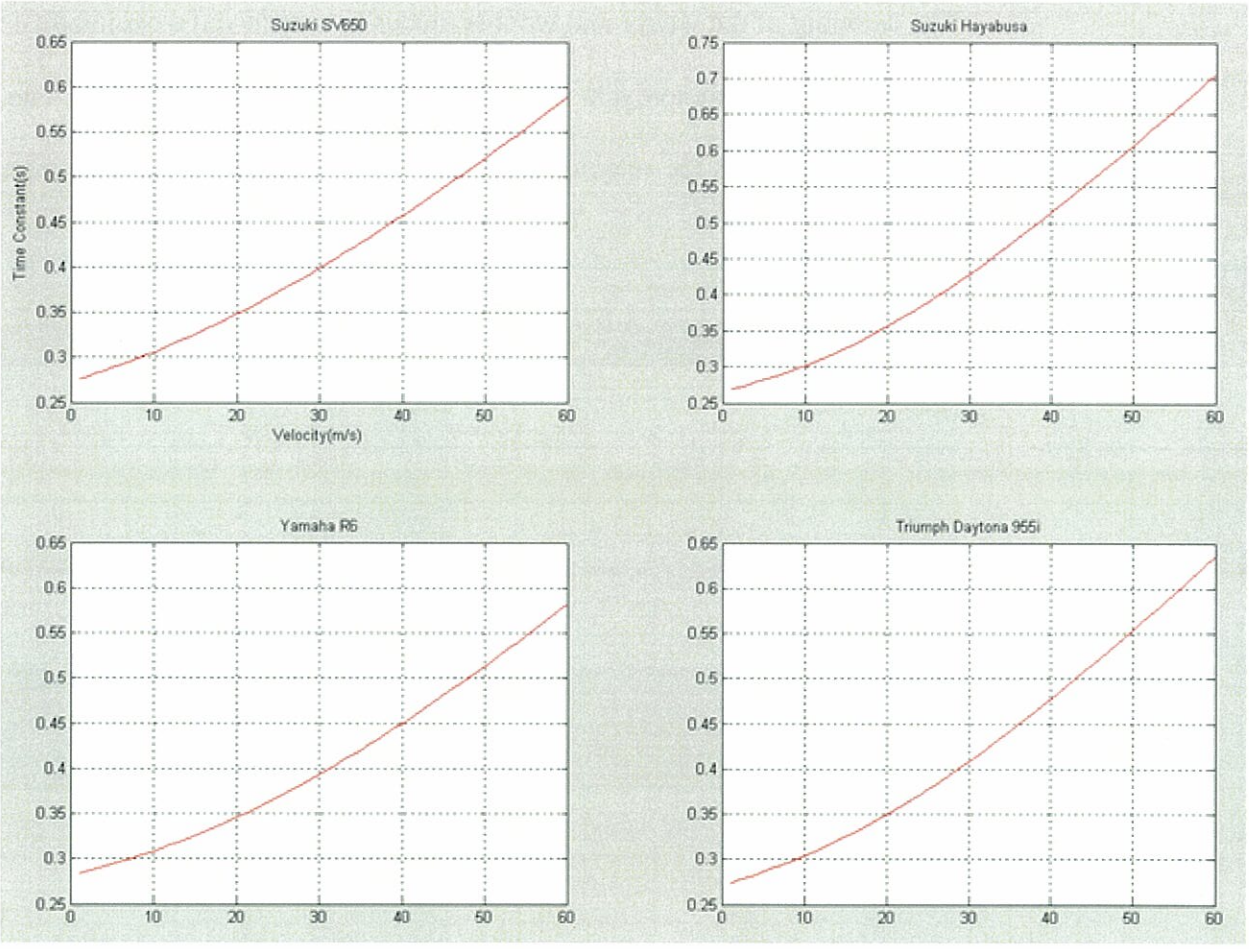

Figure 18- Capsize Time Constant Parametric Study

Figure 18 exhibits the capsize mode time constant which is obtained from eigenvalue analysis of equation 19 for the camber angle(φ). The figure shows as the time constant increases with the increase in velocity. The time constant (τ) is inversely proportional to

the eigenvalue. In these instances, the time constant increases the capsize mode becomes less unstable. The R6 is the most unstable, but this instability makes the motorcycle more nimble and easier for the ride to roll the motorcycle into the corner at speed. The Hayabusa is the most stable of the group at speed because of the long wheelbase and low center of gravity. The Daytona 955i is more stable than the SV650.

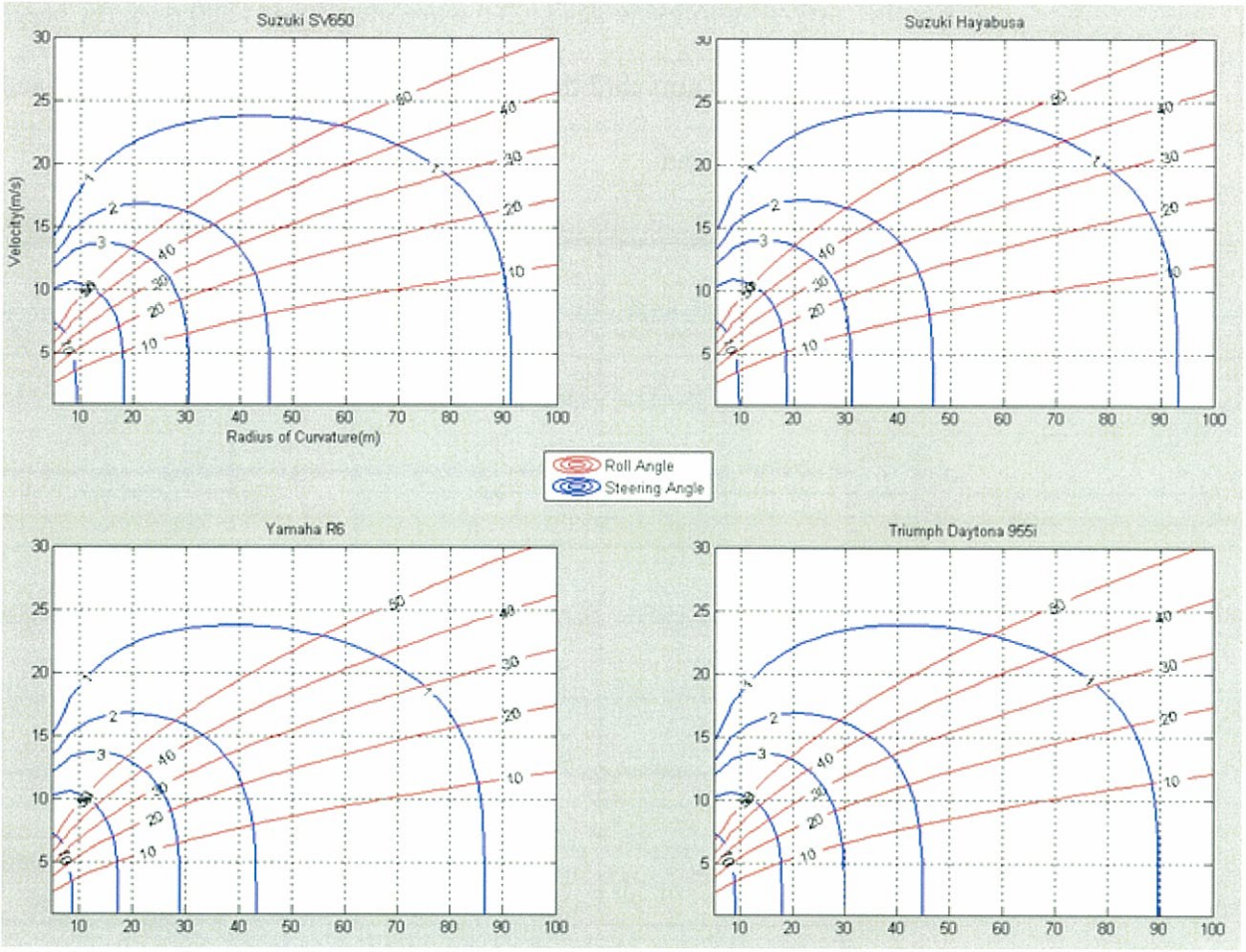

Figure 19-Roll and Steering Parametric Study

Figure 19 describes the roll and steering angles as a function of velocity and radius of curvature and was constructed from equation 32-33.Reviewing the above figure, some of the motorcycles require more steer while the other motorcycles require more roll to make certain turns at velocity. All the roll angle contour lines of each plot are similar but the

steering angle contour lines are different. The R6 has the tighter turning radius when compared to the rest of the case study. The SV650 and Daytona 955i having similar turning radius while the Hayabusa has the largest turning radius.

DESIGN RESULTS

Acceleration:

For the current motorcycle design the wheelbase (p) is 1380 mm, the height to the center of gravity (h) is 580 mm anfd the distance from the rear wheel contact patch to the center of gravity (b) is 690 mm.

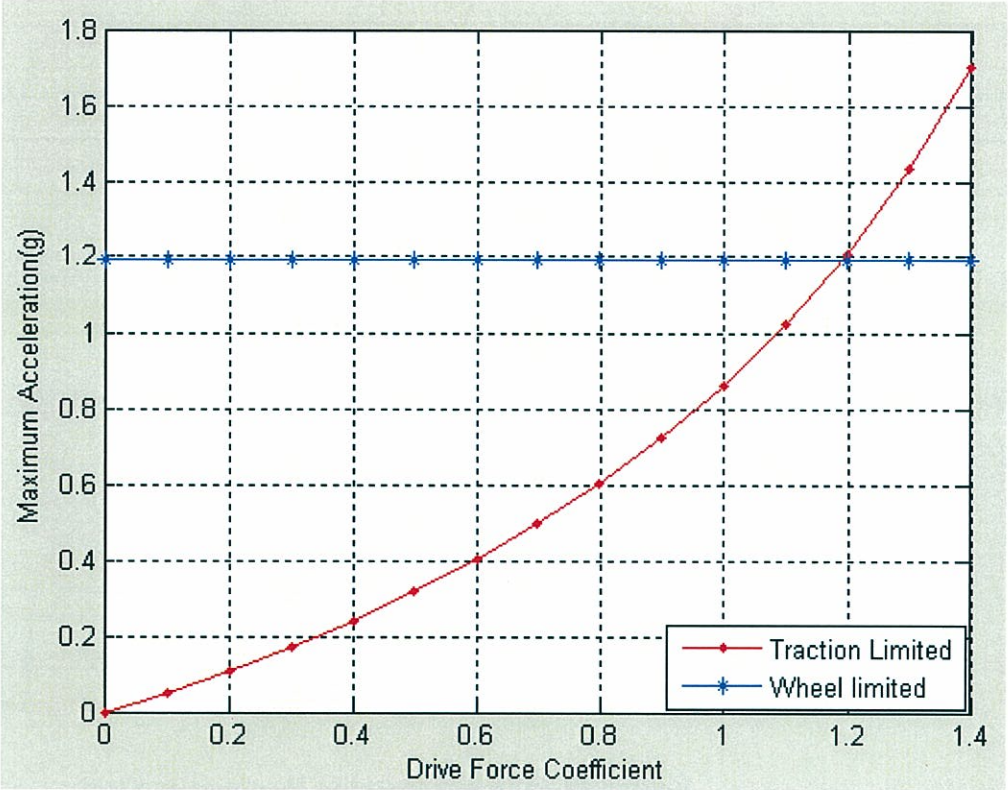

Figure 20-Acceleration

Figure 20 shows the maximum acceleration of the motorcycle as the friction limit of the rear wheel. The acceleration is limited by wheeling or loss of traction of the rear wheel,

which is the correlation ratio of the distance from the rear wheel to the contact patch to the CG to the height of the CG.

$$if\ \frac{b}{h} = \frac{690}{580} = 1.189 > \mu_p\ , a_{traction\ limited}$$

$$if\ \frac{b}{h} = \frac{690}{580} = 1.189 < \mu_p\ , a_{wheeling\ limited}$$

The red dotted line in the above figure represents the traction limited acceleration as a function of the driving force coefficient. This is the maximum acceleration the motorcycle achieves without the slipping of the rear tire. The blue star line is a constant which describes the wheeling limited acceleration or maximum acceleration the motorcycle achieves without wheeling. If the driving force coefficient is below 1.189 the motorcycle is traction limited. Comparably, for driving force coefficients greater than 1.189 the motorcycle is wheeling limited. In turn, this gives the motorcycle a maximum acceleration of 1.189g's without wheeling.

Braking:

Figure 21 displays braking and deceleration forces in terms of the braking coefficients of the front and rear wheels. The figure describes the overall braking behavior of the motorcycle from which the optimum braking can be determined. The blue lines describe the maximum deceleration forces in g's. The red lines describe the braking distribution between the front and rear wheel. The red line number values in Figure 21 are the braking distribution on the front wheel which varies 0.1-1. For example, at the value of 0.1, the braking distribution is 10% front and 90% rear. The horizontal axis represents braking of the rear wheel only (100% rear). The vertical axis represents the braking of the front wheel only (100% front). Maximum braking force achievable is 1.21g's, but this braking distribution is 100% on the front wheel. To obtain

deceleration of 1.2g's the front tire must have a braking force coefficient of approximately 1.2. At a deceleration of 1.2g's, the rear wheel will come off the ground.

When braking force coefficients are the same, the rider can achieve the maximum possible braking coefficient. Cossalter says, "The optimal line of braking is always tangent at the origin to the braking distribution line having the same distribution between the static loads on the two wheels."

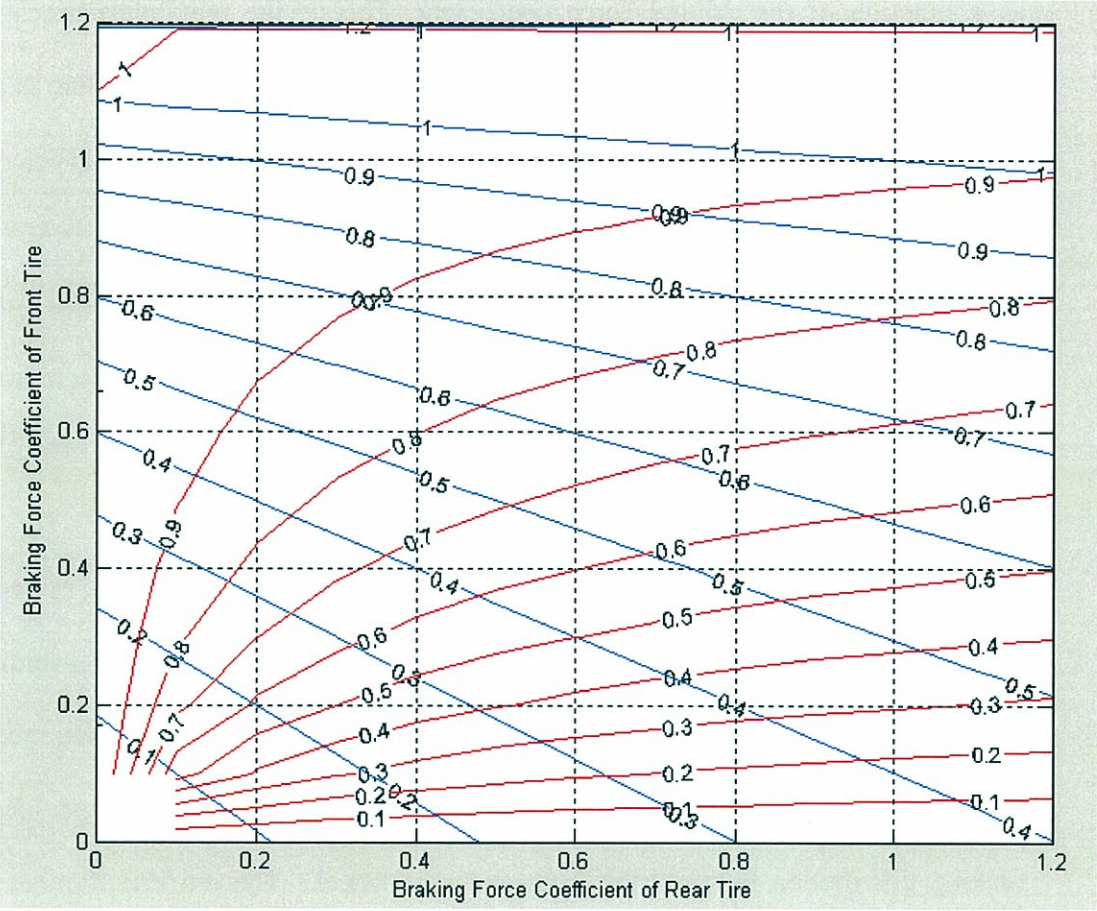

Figure 21-Curves of Deceleration and Distribution of Braking

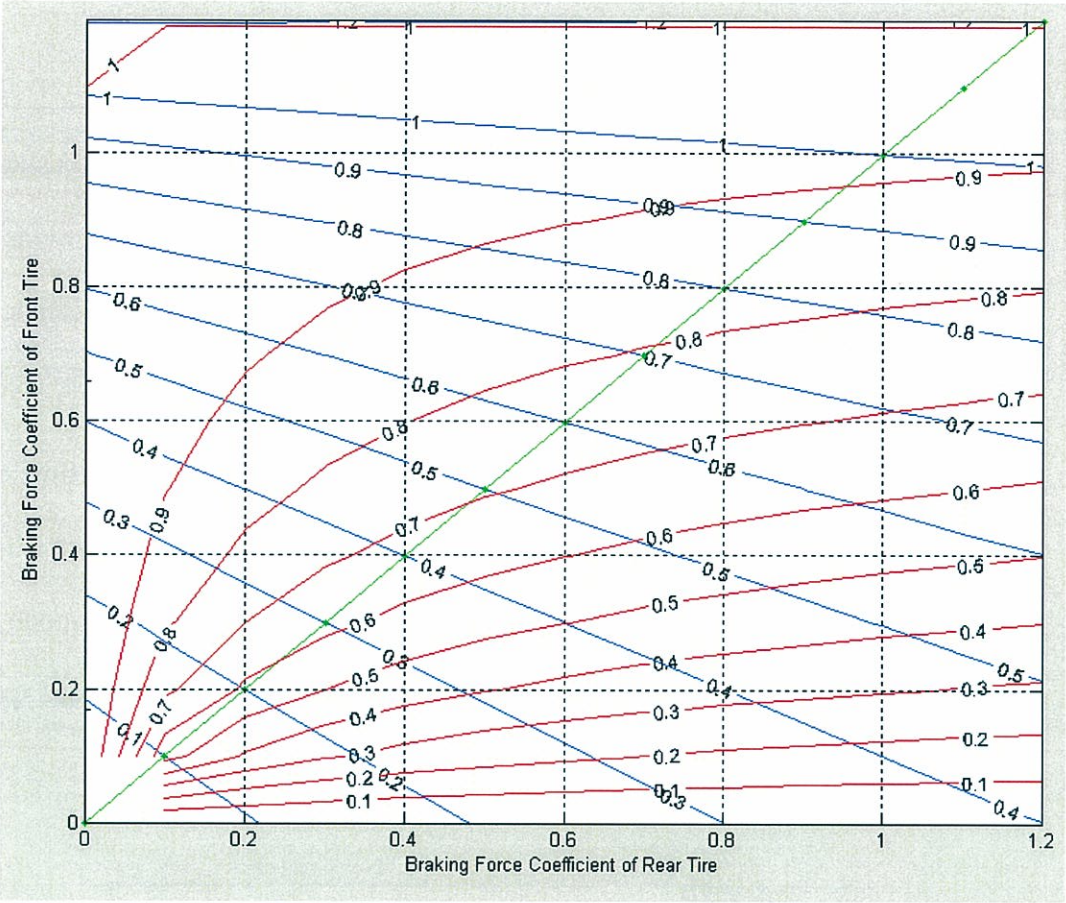

Figure 22-Braking Distribution with Optimum Braking Line

Figure 22 shows the optimum braking line, according to a 50/50 static weight distribution which is represented by the green line. Optimum braking line indicates that it is not good idea for the rider to use the rear brake greater than the front braking. To achieve high decelerations, the rider needs to operate in the red contour lines which range from 0.7 to 1.0. This means that front braking force is 70 to 100 percent of the total braking force which produces maximum decelerations of 0.7g to 1.2g.

Motorcycle Vibrations Modes and Stability:

There are three major modes wobble, weave, and capsize. Wobble is the oscillation of the front frame around steering axis. Weave is the oscillation of the rear

frame around the steering axis. Capsize is the rotation of the entire bike around contact patches in the lateral direction. [Cossalter]

Capsize is best described as an inverted pendulum and is always unstable. Figure 23 describes the time constant of the designed motorcycle. The capsize model is heavily dependent tire camber stiffness which varies 0.7 to a1.5 rad^{-1}. Value of camber stiffness used was from an example in the book "Motorcycle Dynamics" by Vittore Cossalter.

Capsize mode can be describes as an exponential law, □ = □□ □□. The time constant (τ) is positive because the capsize mode is always unstable. The time constant is inversely proportional to the eigenvalue, so as time constant increases the capsize mode is becoming less unstable. Figure 23 shows the time constant as a function of speed for the current cycle design.

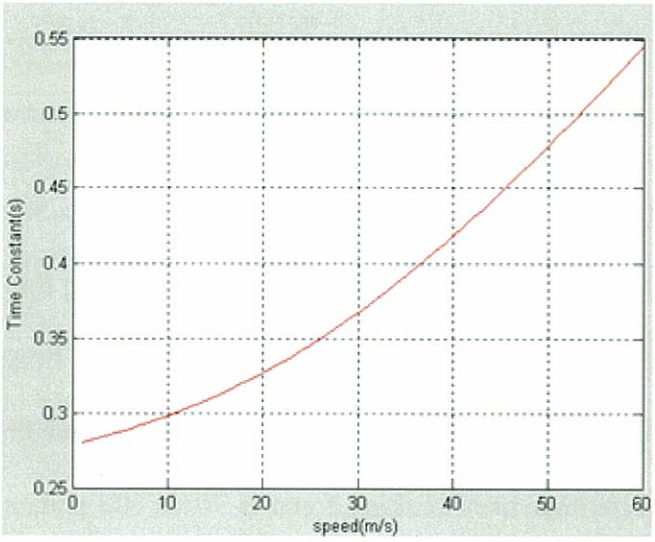

Figure 23-Time Constant for Capsize as Function of Speed

Based on a camber stiffness of 0.93 rad^{-1}, τ varies from 0.2804 to 0.5449 s. The time constant increases as the speed increases. This increase τ causes the system to less unstable at higher speeds. The camber tire stiffness causes a dragging effect on the

capsize mode. The resisting torque created the camber tire stiffens is a product of the camber stiffness coefficient, camber angle, normal force and tire radius. [Cossalter]

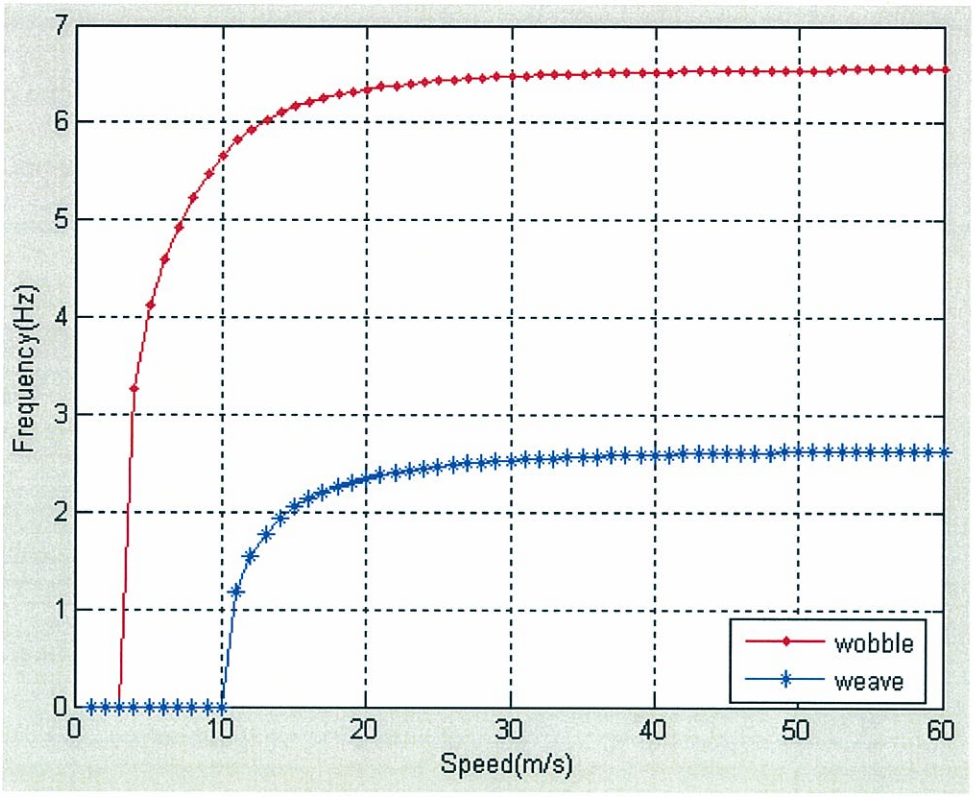

Figure 24-Natrual Frequencies of Weave and Wobble as a Function of Speed

Figure 24 displays frequency verses speed for the wobble and weave modes. The two modes are significantly independent of each other. Typical wobble values are 4Hz for light vehicle and 10Hz for heavy vehicle. At 10-20 m/s the wobble mode is slightly unstable and the addition of a steering damper aids stability. The wobble frequency in this model varies from 0 to 6.5596Hz. Usually, weaves values varies from 0-4Hz at high speeds. From 7-8 m/s weave mode is unstable, but as the motorcycle reaches the midrange speeds it stabilizes. [Cossslter]. In this mode weave frequency varies from 0 to 2.6399Hz.

The damping of the weave and wobble modes is to reduce the excitability of the motorcycle and make the motorcycle more stable in unstable zones of speed. The reduction of the damping coefficient in the system does not greatly affect the natural frequencies. As the velocity increases the damping ratio decreases, so the damped natural frequency (ω_d) approaches the natural frequency (ω_n). Figure 25 presents damping ratio as a function of velocity.

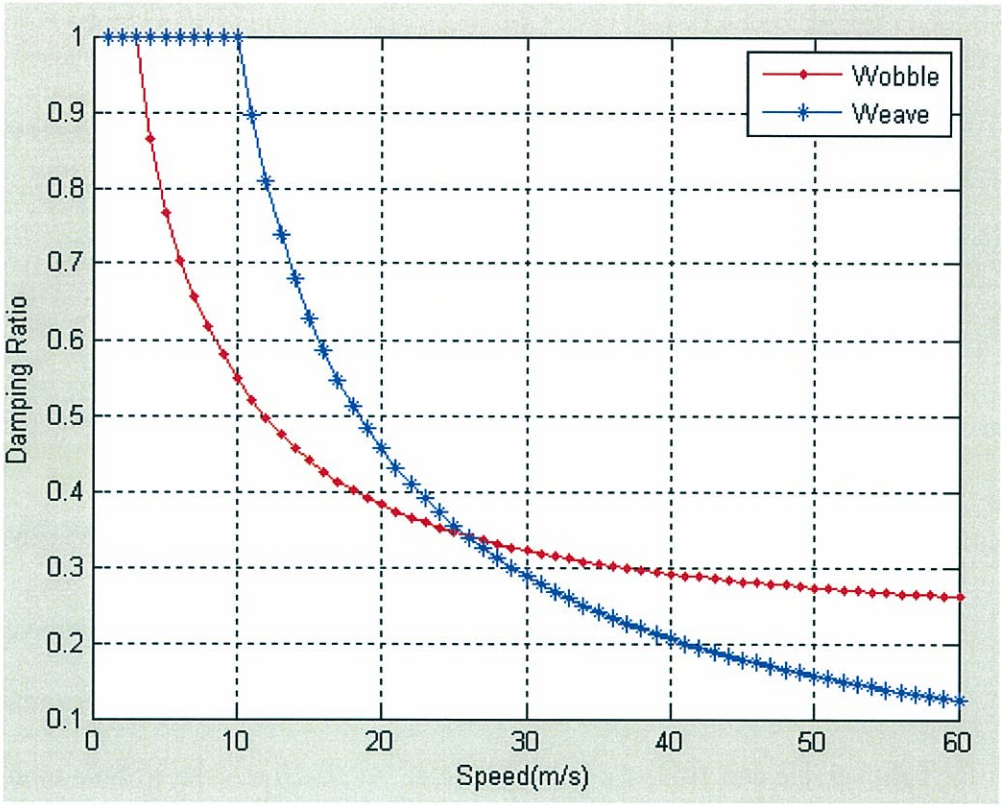

Figure 25-Damping Ratios of Weave and Wobble as a Function of Speed

Suspension:

The two degree freedom model was used to determine the natural frequencies and spring stiffness coefficients. For racing motorcycles the natural frequency of the spring mass system is 2-2.6Hz. Race vehicle damping ratios are from 0.5 to 0.7, so the damping ratio of 0.6 was chosen. [Milliken] Also, the front natural frequency is the 70 to 80% of

the rear natural frequency. The spring rates and damping coefficients for the front and rear suspension can be viewed in the Table 5 below.

Table 5-Front and Rear Spring Rate and Damping Coefficient

Rear		Front	
Spring Rate	**Damping Coefficient**	**Spring Rate**	**Damping Coefficient**
34.039 k N/m	2.6004 Ns/m	21.785 kN/m	2080.3 Ns/m

The spring rates were chosen from Figure 26 below based on the statements above. The figure displays available spring per the range of natural frequencies of 2-2.6Hz. The natural frequency of 2 Hz was chosen for the front shock and 2.5 Hz was calculated for the rear shock. The front natural frequency is 80 percent of the rear (2/2.5=0.8).

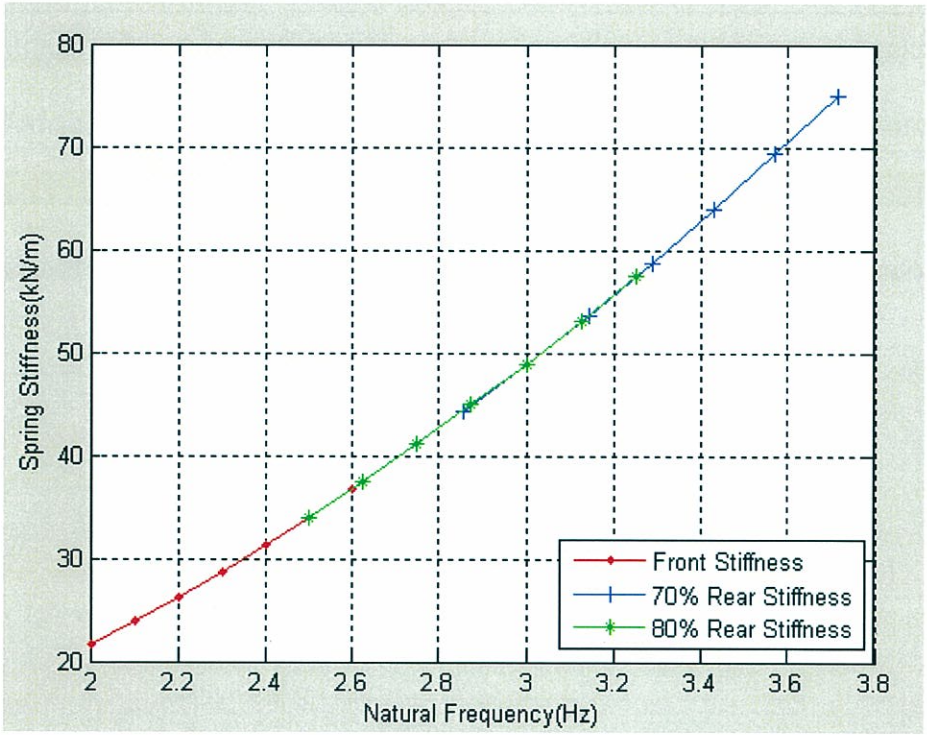

Figure 26 Natural frequency vs Spring Stiffness for Front and Rear Springs

Natural Frequencies(Hz)

Pitch	Bounce	Front	Rear
3.6148	2.2638	2.0	2.5

displays the results of front and rear spring rates and damping ratio gives the following natural frequencies:

Table 6- Resulting Natural Frequencies

Natural Frequencies(Hz)			
Pitch	**Bounce**	**Front**	**Rear**
3.6148	2.2638	2.0	2.5

The motorcycle passes over a step 0.1 m high at velocity of 13 m/s (46 km/hr). To mimic this in the Simulink model step functions were used. The first step function impulse occurs at 1 s and the second function occurs at a time of 1+p/V or 1.1062 seconds. p/V is the vehicle wheel base length divided by the velocity of the vehicle. This value creates a delay between the front and rear impulses of 0.1062 seconds. The oscillations of the front and rear suspension should return to zero at the same time. This behavior can be observed below in Figure 27. This is to reduce the pitching feeling of the vehicle. The bounce sensation is said to be more pleasant to people than the pitching sensation.

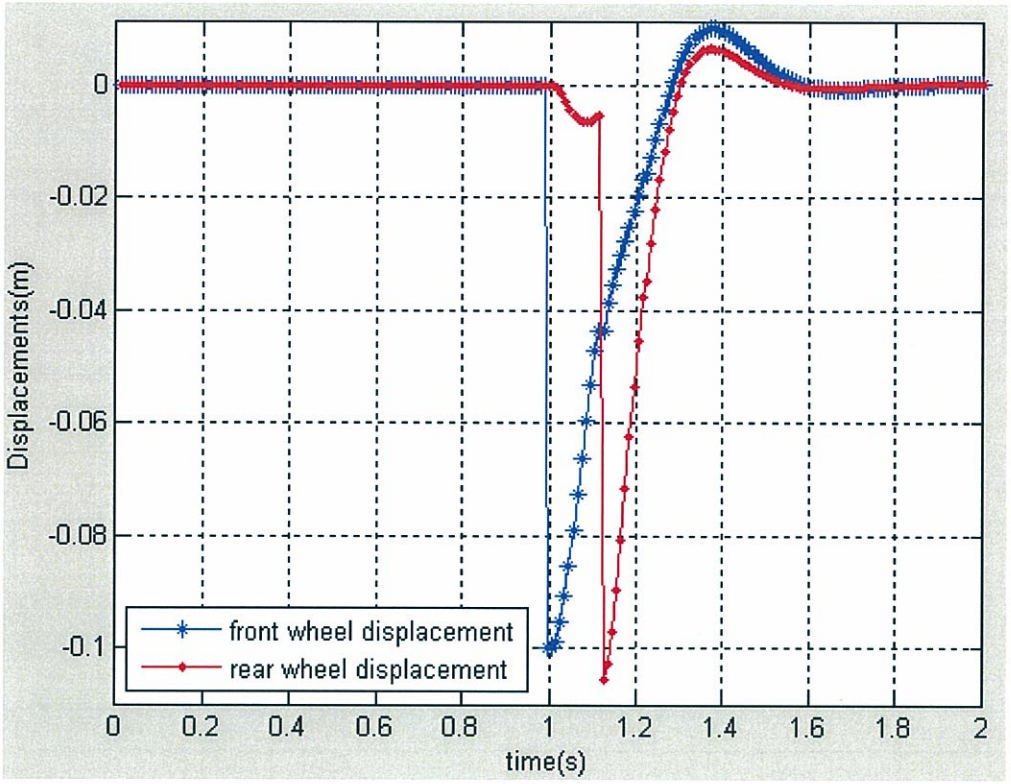

Figure 27 Wheel Displacements

Steady Turning:

Figure 28 shows affects rolling and steering angle as a function of velocity. The blue contour lines are the steering angle. The red contour lines are the roll angle. The contour lines shows how roll steering angle need to change to hold constant velocities and radii of curvature. From reviewing figure one can see that as the velocity increases the steering angle decreases and the rolling angle increases. As the radius curvature and velocity increases the steering angle decreases and the contour lines for roll angle become further apart. So this means the rider needs to roll the motorcycle more and steer the motorcycle less. In this model, the slip angles are the zero, so the motorcycle follows a kinematic trajectory. [Cossalter]

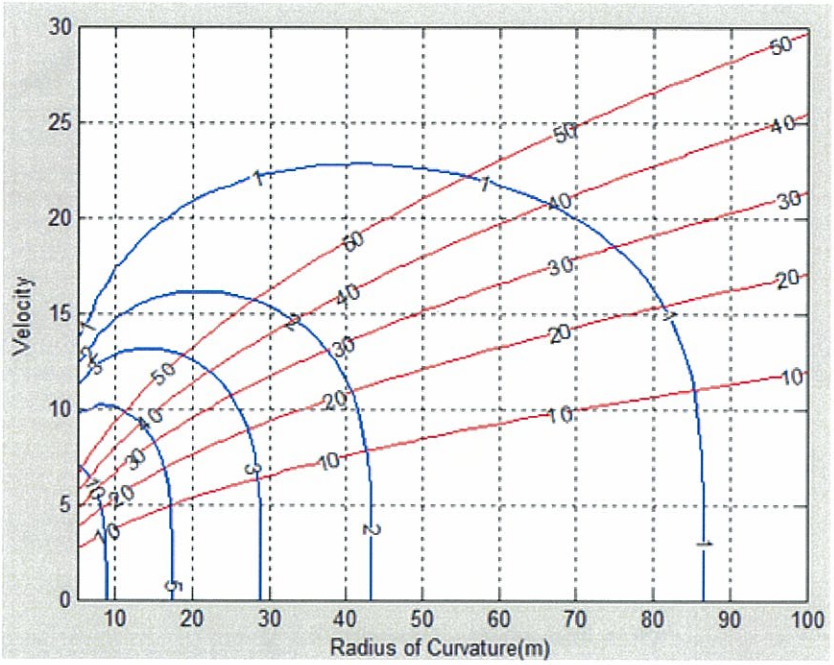

Figure 28 Roll and Steering Angles as function of Velocity and Curvature

Trim:

The squat ratio is the function of the rear wheel travel which is a 120 mm at full compression. Over the range of the shock travel, the squat ratio varies from 0.8 to 1.9.

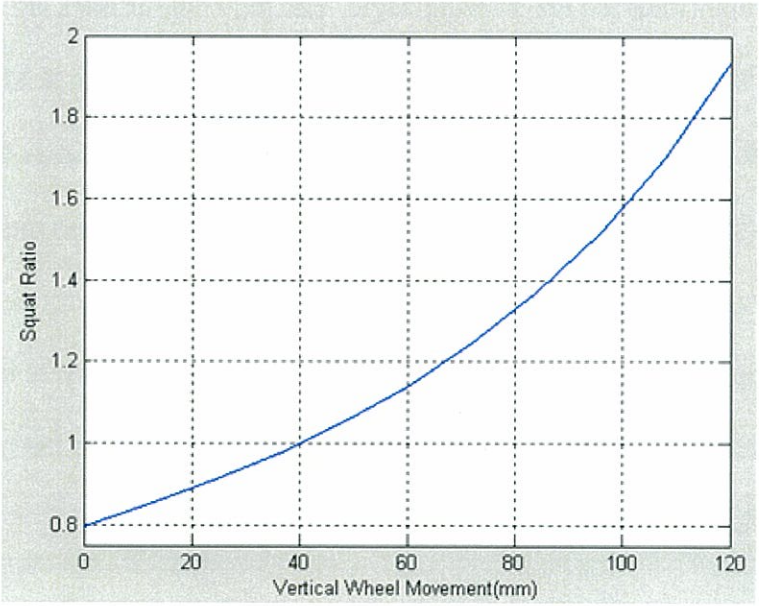

Figure 29-Squat Ratio vs Vertical Wheel Movement

As the squat ratio increases the motorcycle pitches forward and the center of gravity lowers. These two motions are not only influenced by the squat ratio but are also influenced by load transfer. The load transfer is a proportional to the driving force as the driving force increases the pitching increases and the center gravity lowers more. Figure 30 shows how the frame pitch angle varies with increase of squat ratio. The three different lines on the plot represent three different driving force values. The lowest line is the maximum driving force of 2588 N provide by the engine. The lines above the maximum drive force line are fractional values of the maximum drive force. As the driving force and squat ratio increases, so does the frame pitch angle. The pitch angle varies from -0.005 to -0.035 deg. The pitching angle is very small as it is only a fraction of a degree.

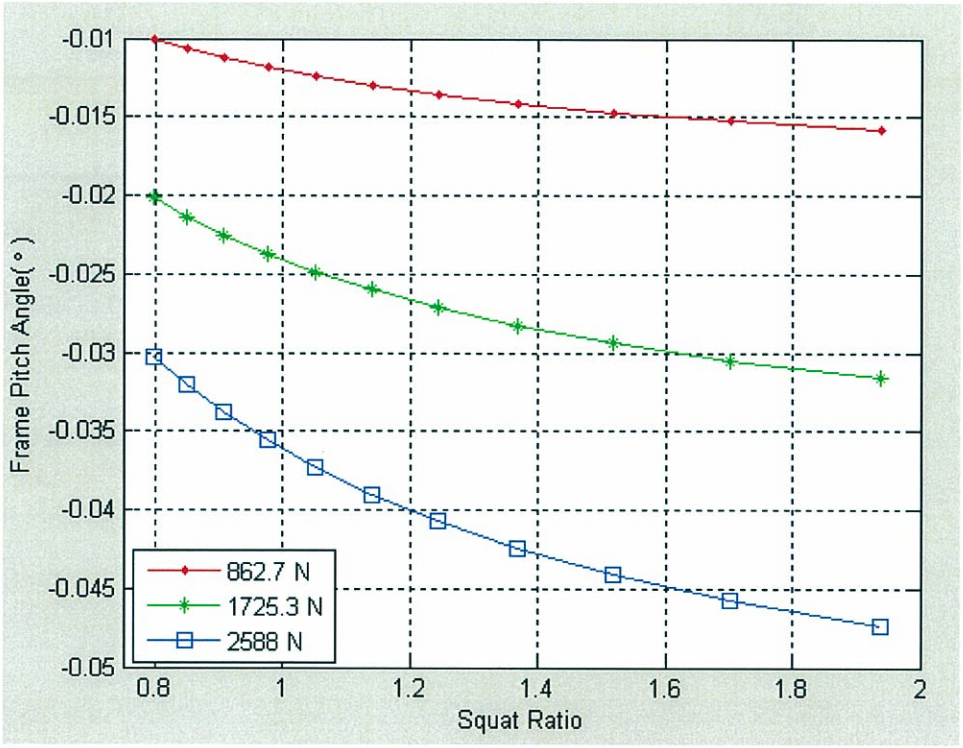

Figure 30-Frame Pitch Angle vs Squat Ratio

Figure 31 describes the extension or compression of the rear suspension as a function of the squat ratio. Reviewing the figure, if the squat ratio is less than one, the suspension extends and if it greater than one the suspension compresses. Like Figure 30, Figure 31 has multiple contour lines which are varying values of the maximum driving force of 2588 N. The rear suspension extends by 15 mm and compresses increases to 25 mm.

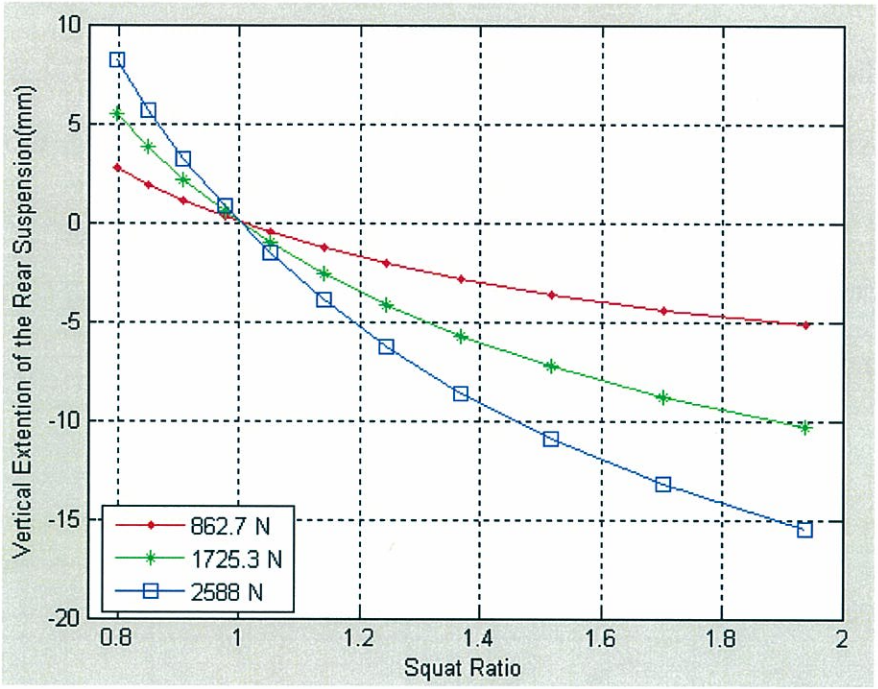

Figure 31-Vertical Extension of the Rear Suspension vs Squat Ratio

Curved Trim:

The squat ratio is a function of the vertical movement as shown in Figure 32. The squat ratio is also a function of the camber angle. The camber angle does not greatly affect the squat ratio, but as camber angle increases the squat ratio reduces.

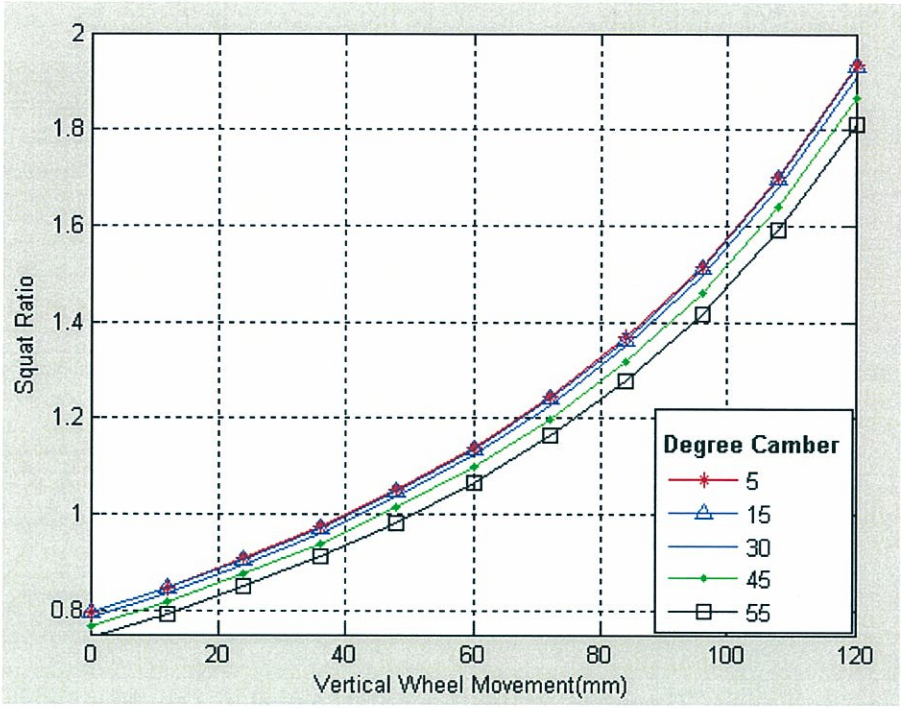

Figure 32- Vertical Wheel Movement vs Deviation of the Squat Ratio

A motorcycle pitches and the center of gravity lowers as motorcycle goes through the turn. Figure 33 and Figure 34 describes the lowering of the CG and pitching of the frame respectively.

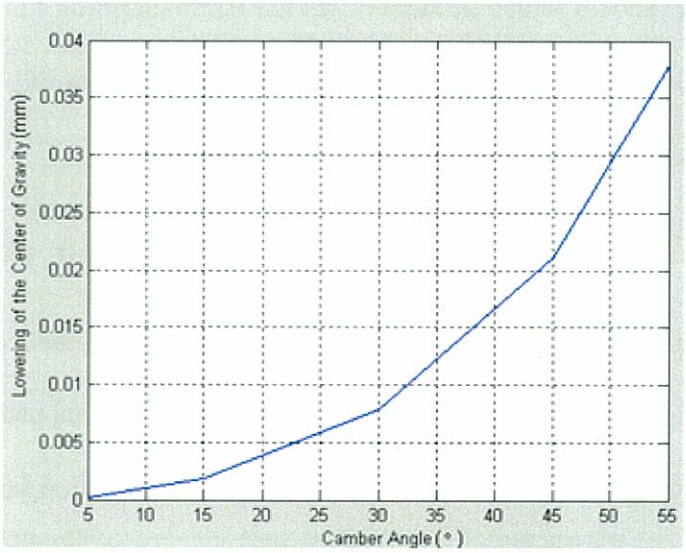

Figure 33-Lowering of the Center Gravity vs Camber Angle

As the camber angle increases the CG of the motorcycle lowers by a small amount.

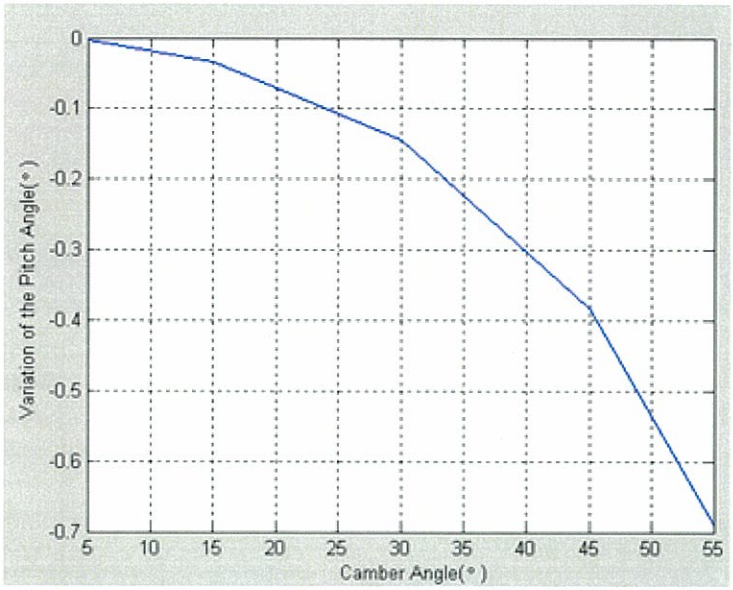

Figure 34- Variation Pitch Angel vs Camber Angle

As the camber increases the motorcycle pitches forward by fraction of degree. The pitching motion due to rear suspension is greater than the front suspension stiffness. As a motorcycle enters a turn, the rider brakes causing the motorcycle to pitch even more than the values indicate in the above figures. As a motorcycle pitches the trail of the motorcycle reduces which in turn causes the lateral aligning force to reduce. This reduction of the aligning enables the rider to camber the motorcycle more easily.[Cossalter]

DISCUSSION AND RESULTS

The geometry of the actual design most resembles the R6 from the parametric study. The goal was to design a light weight modern race motorcycle. The maximum acceleration and deceleration is 1.189g. This gives the motorcycle symmetric performance in acceleration and braking. The wheelbase and the location of the center of gravity are the same as the Yamaha R6. The target weight for this motorcycle was

189kg or less, which is the wet weight of a Yamaha R6. The resulting geometry of the motorcycle is viewable in Table 2 Motorcycle Design Parameter. From the review of capsize model of the actual design, the time constant is equal to that of the R6. The problem with the capsize model is that it was difficult to calculate a realistic value for the moment inertia of the motorcycle. In the case study, an experimental value was calculated from examples in the literature. The weave and wobble stability for this motorcycle is easily influenced by addition of a steering damper so results of the model were not as valuable as previously thought.

The suspension was designed to perform as a race bike. This was accomplished using a two degree of freedom model and information from the literature review. The issue with the model is the spring stiffness coefficient calculated off the reduced spring stiffness. This model assumes that the front and rear wheel are directly in line with shocks. In reality, this is not true. The velocity ratio is the ratio of the shock travel to the wheel travel. For the rear suspension the velocity ratio is roughly 2.0, which was extrapolated from the suspension data created by Tony Foale's Kinematic Software which can be view in appendix D. Multiplying the velocity ratio by the reduced spring stiffness will give approximate tuned spring stiffness. The front suspension is a four link suspensions. A program was created to calculate the velocity of the front suspension. The desired velocity ratio for the front suspension is 2. The best calculated value was about 2.8. This program can be found in Appendix D. Overall, the suspension provided gave good simulation data to accurately fit spring to a motorcycle and to supply the appropriate damping rates.

Structural Optimization Results

The frame, swingarm, and fork were only optimized because lateral loading appeared to cause the highest stress values in each component. Some analysis was completed for the effects of driving force on the swingarm and frame. The driving force as it translates through the swingarm and frame does not appear to have great affect when compared to that of the lateral force. The braking force on the front fork is significant due to the long moment arm from the contact patch of the front tire to the steering head. The analysis of the vertical stiffness of the main frame was not completed. The braking force most directly tests the vertical stiffness of the main frame. The braking force pulls the fork legs to the rear causing the steering head to deflect in towards the engine. This in turn causes the main frame to bend around itself on the lateral axis. The results the structure optimization are outlined in the following paragraphs.

Table 7- Structural Optimization Constraint per Component

	Constraints				
Component	**Lateral Load(N)**	**Torsion Load(Nm)**	**Max Rotation(°)**	**Max Displacement(mm)**	**Max Yield Stress(MPa)**
Main Frame	4330	1314.1	0.18	1.44	173.74
Swingarm	4330	1305.996	0.65	2.69	173.74
Fork	4330	1297.95	4.32	24.053	173.74

The maximum displacement and rotation constraints on the system were constructed from the upper limit of the linear and torsional spring coefficients of Table 1 and the lateral and torsional loads in Table 7. Based on Table 1, the components go from greatest to least lateral and torsional stiffness in the following order; main frame, swingarm, and fork. The torsional and lateral loads were calculated from the translation of a 1.6g force at the contact patch between the tire and the road. Some of the loading is not clearly defined so a safety factor of 2.5 was used to calculate a maximum allowable

yield stress. 4130 steel tubing was used in the design of the frame, swingarm, and forks. 4130 has a Maximum Yield Stress of 434.6MPa and with the safety factor of 2.5 this made the maximum allowable yield stress 173.7MPa.

Table 8-Structural Optimization Results

Results with Both Lateral and Torsion Load Applied				
Component	**Max Rotation(°)**	**Max Displacement(mm)**	**Max Von Mises Stress(MPa)**	**Mass(kg)**
Main Frame	0.18	0.66	173.74	12.96
Swingarm	0.31	1.65	102.65	3.41
Fork	0.00	0.006	14.507	6.82

Table 8 shows the structural optimization results. Again, these results are only of the torsion and lateral loads created by lateral force between the road and the tire. The fork appears deflected least and does not twist at all. The main frame displaces 0.66 mm and rotates 0.18°. The swingarm deflects 1.65mm and rotates 0.31°. The mass is 12.96kg, 3.41kg, and 6.82kg for the main frame, swingarm, and forks, respectively. The von Mises stress of each component is less than or equal to the maximum allowable yield stress. The lateral force generates the least amount of force in the forks and the greatest amount of stress in the main frame as it translates through the motorcycle.

To help achieve the desired mass of 189kg, structural optimization was completed to minimize the mass of the main frame, swingarm, although some analysis was completed to see what affect the driving force has on the components. The driving force does not affect the components as much the lateral force between the tire and the road. Also the braking force on the front fork is significant due to the long moment arm from the steering to the steering head, but it was not as necessary the lateral force. An analysis of the vertical stiffness of the main frame was not completed. The braking force most

directly tests the vertical stiffness of the main frame. The vertical stiffness of the main frame needs to be evaluated to make this thesis more relevant.

Also, the models used were of simple 3-dimensional truss structures. To get more realistic results, one must use volume mesh models. The truss models are good estimation of stresses throughout the structure and are an easy way to construct a simple model for structural optimization. The components in the current design have members that are over built and too stiff. The parts are also too stiff because they were designed using the upper limits of the spring stiffness coefficients listed in the Table 1 Stiffness Values of Each Component. Also, the diameter of the tubing was limited to sizes available in the market place.

CONCLUSION

The parametric study helped because it reinforces what the designer can learn from the literature. Basically the parametric study shows that a short wheelbase with high center gravity makes a motorcycle more unstable. Also, short wheel bases with high centers of gravity causes limitation of high acceleration and deceleration. With high center of gravity the motorcycle will be more unstable but this will enable the rider to lean the motorcycle more easily in order to corner. Mass of a motorcycle has no effect on the acceleration and deceleration calculation as it is purely based on the geometry of the motorcycle. The mass comes into effect when calculating the vibration modes of a motorcycle. From the parametric modes, the weave and wobble of all the motorcycles are about the same and the mass show no great influence. Capsize mode is affected by the mass. The heavier the motorcycle, the greater the time constant, which causes the motorcycle to be less unstable.

HEEDS gives the ability to cut significant amount weight from the components in a short amount of time. The model used by HEEDS was simple, but effective enough to ballpark the internal stresses in each component. For further development of the optimization model, HEEDS coupled with CAD software and FEA software gives a more detailed analysis. Instead having a simple three dimensional truss model, a three dimensional solid model of a weldment with all the necessary details should be constructed. Having a more detail analysis will help give more accurate internal stresses. More accurate inaccurate internal stresses will allow for the elimination of the redundant members and excess material.

Overall, this thesis gives good insight to what needs to be considered in the design of a sport motorcycle. Where this thesis comes short is it does completely explore each field to the necessary depth for a capable design. Each section should be further explored for more detailed mathematical models and greater understanding needs to be applied to current mathematical models.

REFERENCES

1. "HEEDS Professional | Red Cedar Technology." *Accelerating Innovation in Design Optimization | Red Cedar Technology*. Web. 11 Feb. 2011.
    a. <http://www.redcedartech.com/products/heeds_professional>.
2. "3Pty - HEEDS Professional Design Optimization Software" - Workflow Automation, Multidisciplinary Design
3. " *MathWorks - MATLAB and Simulink for Technical Computing*. Web. 20 Feb. 2011. <http://www.mathworks.com/products/connections/product_detail/product_39246.html>.
4. "CATIA." *Wikipedia, the Free Encyclopedia*. Web. 20 Feb. 2011. <http://en.wikipedia.org/wiki/CATIA>.
5. "NEi Nastran." *Wikipedia, the Free Encyclopedia*. Web. 20 Feb. 2011. <http://en.wikipedia.org/wiki/NEi_Nastran>.
6. "Femap and NEi Nastran FEM Analysis Engineering Software." *NEi Software Nastran Finite Element Analysis FEA Femap Engineering Virtual Stress Test Simulation*. Web. 20 Feb. 2011. <http://www.nenastran.com/engineeringsoftware/femap>.
7. Cocco, Gaetano. *Motorcycle Design and Technology*. Vimodrone [Milano: Giorgio Nada Editore, 1999. Print.
8. Cossalter, Vittore. *Motorcycle Dynamics*. 2nd ed. Padova: Vittore Cossalter, 2006. Print.

9. Foale, Tony. *Motorcycle Handling and Chassis Design: the Art and Science.* 2n ed. Spain: Tony Foale, 2006. Print.

10. "Motorcycle Frame Technology." *Diseno-art.com | From Concept Cars to Power Boats*. Web. 15 Jan. 2011. <http://www.disenoart.com/encyclopedia/archive/motorcycle_frames.html>.

11. Palm, William J. "Chapter 1/An Overview of MATLAB." *Introduction to MATLAB 7 for Engineers*. Boston, Mass. [u.a.: McGraw-Hill, 2005. 3-5. Print.]

12. (Milliken, William F., and Douglas L. Milliken. *Race Car Vehicle Dynamics.* Warrendale, PA, U.S.A.: SAE International, 1995. Print.

13. "Suspension (motorcycle)." *Wikipedia*. Wikimedia Foundation, 05 June 2012. Web. 09 May 2012. <http://en.wikipedia.org/wiki/Suspension_(motorcycle)>.

APPENDIX A- MATLAB Programs

Acceleration Code:

```
clc,clear all,close all;

p=1380/1000;     %Wheelbase
perb=0.50;       %Weight Distribution
h=580/1000;      %Height to CG
b=perb*p;        % distance to CG from the rear contact patch

Mp=0:0.1:1.4; %drive force coefficient

        for o=1:length(Mp)
        TL(o)= (Mp(o)*(p-b)/p)/(1-(Mp(o)*h/p)); %traction limited
        WL(o)= b/h; % wheel limited
        end


figure
plot(Mp,TL,'r',Mp,WL)
legend('Traction Limited','Wheel limited')
xlabel('braking force coeficcient of rear tire')
ylabel('braking force coeficcient of front tire')
title({'Curves of deceleration and distribution of braking';'[p=1.38m;
h=0.580m; b= 0.69m]'})
grid on
```

Braking Code:

```
clc,close all, clear all;
p=54.331*25.4/1000; %wheelbase
b=0.5*p;  % distance from rear contact patch to CG

h=580/1000; % height from ground to the CG

Mf=0:0.1:1.2;
Mr=0:0.1:1.2;


for n=1:length(Mf)
    for m=1:length(Mr)
    xdd(n,m)=(p*Mr(m)+b*(Mf(n)-Mr(m)))/(p+h*(Mr(m)-Mf(n)));

    Ff(n,m)=Mf(n)*(b+h*Mr(m))/(p*Mr(n)+b*(Mf(m)-Mr(n)));

    Fr(n,m)=Mr(m)*((p-b)-h*Mr(n))/(p*Mr(n)+b*(Mf(m)-Mr(n)));

    end
end
```

```
% figure
% plot3(Mf,Mr,xdd)

figure(1)
[C,h]=CONTOUR(Mr,Mf,xdd,[0.1 0.2 0.3 0.4 0.5 0.6 0.7 0.8 0.9 1
1.2],'b') ;
clabel(C,h);
hold on
grid on
%figure
[C,h]=contour(Mr,Mf,Ff,[0.1 0.2 0.3 0.4 0.5 0.6 0.7 0.8 0.9 1],'r');
clabel(C,h);
xlabel('Braking Force Coefficient of Rear Tire')
ylabel('Braking Force coefficient of Front Tire')
title({'Curves of Deceleration and Distribution of Braking';'[p=1.38m;
h=0.580m; b= 0.69m]'},'FontWeight','bold')
% figure(2)
% [C,h]=contour(Mr,Mf,Fr,[0.1 0.2 0.3 0.4 0.5 0.6 0.7 0.8 0.9 1]);
% clabel(C,h);



figure(2)
% [C,h]=CONTOUR(Mr,Mf,xdd,[0.1 0.2 0.3 0.4 0.5 0.6 0.7 0.8 0.9 1
1.2],'b') ;
% clabel(C,h);
plot(Mr,Mf,'g')
hold on
grid on
%figure
[C,h]=contour(Mr,Mf,Ff,[0.1 0.2 0.3 0.4 0.5 0.6 0.7 0.8 0.9 1],'r');
clabel(C,h);
xlabel('Braking Force Coefficient of Rear Tire')
ylabel('Braking Force coefficient of Front Tire')
title({'Braking Distribution with Optimum Braking Line';'[p=1.38m;
h=0.580m; b= 0.69m]'},'FontWeight','bold')
axis([0 1.2 0 1.2])
% figure(2)
% [C,h]=contour(Mr,Mf,Fr,[0.1 0.2 0.3 0.4 0.5 0.6 0.7 0.8 0.9 1]);
% clabel(C,h);
```

Weave, Wobble, and Capsize Modes Code:

```
clc,close all, clear all;


%BOTH
p=54.331*25.4/1000; %wheelbase
b=0.5*p;  % distance from rear contact patch to CG
h= 580/1000;   %height to the CG from ground
m=189.148018;  %mass
```

```
V=1:1:60;    % velocity

%WEAVE AND WOBBLE

Mr=m*(217.5/(217.5+30.7)); % rear mass
Mf=m*(30.7/(217.5+30.7)); % mass front

bf=0.024;

R=300/1000;  %wheel radius
l=1.3578;%52.99*25.4/1000;  %
l2= 0.823;%sqrt(b^2-(h-R)^2); %
l1=l-l2; %

Ir=21.08;
If=0.44;


E=24*pi/180; %caster

a=86/1000;    % trial
an=a*cos(E); %normal trial

c=2.3;%6.8;        % steering damping coefficient


Klr=10000;    %10-25 rad-1
Klf=10000;

M=[Mr+Mf, -Mr*l1,Mf*bf;-Mr*l1,Mr*l1^2+Ir,0;Mf*bf,0,Mf*bf^2+If];

K=[0,-Klr*cos(E),-Klf*cos(E);0,Klr*l*cos(E),0;0,0,Klf*an*cos(E)];


%CAPSIZE
t= 75/1000; %tire radius

Igx=20; % moment of inertia
g= 9.81; %gravity

klr=11; %Klr/(m*g*0.5); %rear corner stiffness
klf=11; %Klf/(m*g*0.5); %front corner stiffness

kp=0.93; %1;    %camber stiffness

M1=[m,m*h;m*h,Igx];

K1=[0,-kp*m*g;0,m*g*h*(kp-1)];


syms w s s1
```

```
for n=1:length(V)

C=(1/V(n))*[Klf+Klr,-Klr*l,-Klf*an;-Klf*l,Klr*l^2+c*V(n),-c*V(n);-
Klf*an,-c*V(n),Klf*an^2+c*V(n)];

BB= det(M*s^2+C*s+K);

CC= solve(BB,s);

DD(1:6,n)= CC;

DD1(1,n)= CC(1,1);
DD1real(1,n)=real(CC(1,1));
DD1imag(1,n)=imag(CC(1,1));

DD2(1,n)= CC(2,1);
DD2real(1,n)=real(CC(2,1));
DD2imag(1,n)=imag(CC(2,1));

DD3(1,n)= CC(3,1);
DD3real(1,n)=real(CC(3,1));
DD3imag(1,n)=imag(CC(3,1));

DD4(1,n)= CC(4,1);
DD4real(1,n)=real(CC(4,1));
DD4imag(1,n)=imag(CC(4,1));

DD5(1,n)= CC(5,1);
DD5real(1,n)=real(CC(5,1));
DD5imag(1,n)=imag(CC(5,1));

DD6(1,n)= CC(6,1);
DD6real(1,n)=real(CC(6,1));
DD6imag(1,n)=imag(CC(6,1));

L3(1,n)=DD3real(1,n)/sqrt(DD3real(1,n)^2+DD3imag(1,n)^2);

L6(1,n)=DD6real(1,n)/sqrt(DD6real(1,n)^2+DD6imag(1,n)^2);


%CAPSIZE CALCULATION
C1=[(m*g*klr)/V(n),0;-(m*g*klr*h)/V(n),0];

BB1= det(M1*s1^2+C1*s1+K1);

CC1= solve(BB1,s1);


EEE(1:4,n)=double(CC1);

EE1(1,n)= CC1(1,1);
EE1real(1,n)=real(CC1(1,1));
EE1imag(1,n)=imag(CC1(1,1));
```

```
EE2(1,n)= CC1(2,1);
EE2real(1,n)=real(CC1(2,1));
EE2imag(1,n)=imag(CC1(2,1));

EE3(1,n)= CC1(3,1);
EE3real(1,n)=real(CC1(3,1));
EE3imag(1,n)=imag(CC1(3,1));

EE4(1,n)= CC1(4,1);
EE4real(1,n)=real(CC1(4,1));
EE4imag(1,n)=imag(CC1(4,1));

L7(1,n)=EE2real(1,n)/sqrt(EE2real(1,n)^2+EE2imag(1,n)^2);

Tua1(n)=1/EE1real(n);
Tua2(n)=1/EE2real(n);
Tua3(n)=1/EE3real(n);
Tua4(n)=1/EE4real(n);

% %%%%%CAPSIZE CALCULATION FROM BOOK%%%%%
%
Z=solve(V(n)*Igx*s^3/(m*g)+klr*(Igx/m+(h+t)*h)*klr*s^2+V(n)*kp*(h+t)*s-
kp*g*h,s);
%  ZZ(1:3,n)=Z;
%
%  Tuaz1(n)=1/real(ZZ(1,n));
%  Tuaz2(n)=1/real(ZZ(2,n));
%  Tuaz3(n)=1/real(ZZ(3,n));

end
%WEAVE AND WOBBLE
ImagDD1=DD1imag/(2*pi);
ImagDD2=DD2imag/(2*pi);
ImagDD3=DD3imag/(2*pi);
ImagDD4=DD4imag/(2*pi); %Weave
ImagDD5=DD5imag/(2*pi);
ImagDD6=DD6imag/(2*pi); %Wobble

%CAPSIZE
ImagEE1=EE1imag/(2*pi);
ImagEE2=EE2imag/(2*pi);
ImagEE3=EE3imag/(2*pi);
ImagEE4=EE4imag/(2*pi);

% %WEAVE AND WOBBLE
figure(1)
plot(V,abs(ImagDD6),'r',V,abs(ImagDD4),'b')%,V,abs(ImagEE2)ui,'g')
legend('wobble','weave')
grid on
xlabel('speed(m/s)')
ylabel('frequency(Hz)')
title('Natural Frequencies for Weave, Wobble and Capsize as a function
of Speed','FontWeight','bold')
```

```
figure(2)
plot(V,abs(L6),'r',V,abs(L3),'b')%,V,abs(L7),'g')
legend('Wobble','Weave')
grid on
xlabel('speed(m/s)')
ylabel('Damping Ratio')
title('Damping Ratio for Weave and Wobble as a function of
Speed','FontWeight','bold')

%CAPSIZE
figure(3)
 plot(V,Tua4,'r')%,V,Tua2)
  grid on
  xlabel('speed(m/s)')
  ylabel('Time Constant(s)')
  axis([0 60 0.25 0.55])
  title('Time Constant for Capsize as function of
Speed','FontWeight','bold')

figure(4)
 plot(V,EE4,'k')
% hold on
% plot(V,EE4,'m')
% plot(V,EE1,'r+') %0
% plot(V,EE2,'g.')
  grid on
  xlabel('speed(m/s)')
  ylabel('Real Part of the Eigenvalue(1/s)')
  title('TIme Constant for Capsize as function of
Speed','FontWeight','bold')
```

Suspension Simulink Code:

Set up M-Code:

```
clc,clear all, close all;

% % FRONT FORK SPRINGS
% % Recommended Fork Spring Rate: 0.838 kg/mm (use closest
available)
% % Stock Fork Spring Rate: .900 kg/mm(stock)
% KFFS=0.838*9.81*2
% % RESULT FORK SHOCK
% % NATURAL FREQUENCY 2.0Hz @ SPRING CONSTANT 23kN/m
%
% % REAR SHOCK SPRINGS
% % Recommended Shock Spring Rate: 9.564 kg/mm (use closest
available)
% % Stock Shock Spring Rate: 10.8 kg/mm (stock)
% KRSS=9.564*9.81
% %RESULT REAR SHOCK
% % NATURAL FREQUENCY 3.0639Hz @ SPRING CONSTANT 92kN/m
%
% m=(357+190)*2.2; %mass
```

```
%
% p=54.331*25.4/1000; %wheelbase_m
% b=0.5*p;  % distance from rear contact patch to CG
% h=580/1000; % height to the center of gravity
%
% I=(h^2+(p/3)^2)*m/12; %inertia
%
% kf=23*1000;%kN/m
% kr=92*1000;
%
% cf=3.56028*10^3;
% cr=4.7470*10^3;

%%%%%STOCKSETUP%%%%%
WD      = [.50 .50];    %Weight distribution
m=(417+190)/2.2;        % (kg) Vehicle Mass is 1655.9

h       = 580/1000; % (m) Vehicle Height
l       = 54.331*25.4/1000; % (m) Vehicle Wheelbase
% CG_h    = 580/1000; % (m) Height to the CG

%k1 = 23967.5%23000;  % front suspension stiffness in (N/m)
%k2 = 38648 %92000;  % rear suspension stiffness in (N/m)

DR=0.6;

l1 = WD(1)*l    %m
l2 = WD(2)*l    %m

Mf=m*l1/l
Mr=m*l2/l

vf=2

k1=Mf*(vf*2*pi)^2

c1 = DR*2*sqrt(k1*Mf)%3560;    % front suspension damping in (N
sec/m)

j    =(h^2+l^2)*m/12;    %2856.6;  %Iyy;    %kg*m^2 %from carsim
2856.6 kg m s^2

v    = 13;  %velocity of motorcycle

%Velocity Delay
delay =l/v+1  %delay = 1.2085


%vr=(1/(2*pi))*sqrt(k2/Mr)
%vf=(1/(2*pi))*sqrt(k1/Mf) % Front natural frequecy
```

```
vr=vf/0.80              %rear natural frequecy

k2=Mr*(vr*2*pi)^2     % rear suspension stiffness in (N/m)

c2 = DR*2*sqrt(k2*Mr) % 4747;    % rear suspension damping in (N
sec/m)

%bounce natural frequencies
Vb=(1/(2*pi))*sqrt((k1+k2)/m)   %Vb = 1.1657
%pitch natural frequencies
Vp=(1/(2*pi))*sqrt((k1*l1^2+k2*l2^2)/j)   %Vp = 1.3257


%Eigenvalues(Coupled Equation)
A=[(k1+k2)/m,(l2*k2-l1*k1)/m;(l2*k2-l1*k1)/j,(l2^2*k2+l1^2*k1)/j]

z=sqrt(eig(A))/(2*pi)

Vbc=z(1)   %Vbc =

Vpc= z(2) %Vpc =
```

Simulink Model:

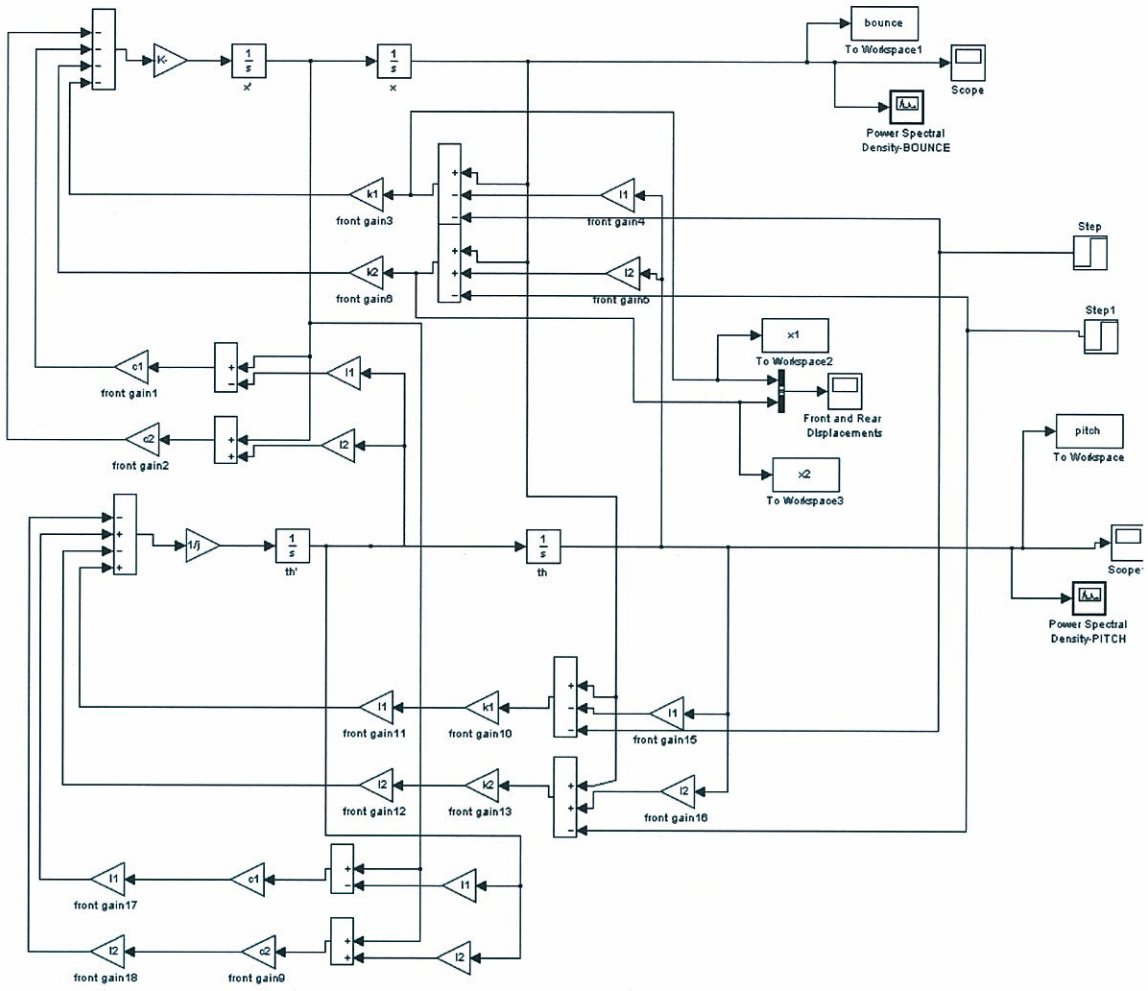

Figure 35-Suspension Simulink Model

Plot M-Code:

```
t=0:(3-0)/304:3;

figure
plot(t,x1,t,x2,'r')
xlabel('time(s)')
ylabel('Displacements(m)')
title('Wheel Displacements','FontWeight','bold')
legend('front wheel displacement','rear wheel displacement')
grid on
 axis([0 2 -0.11 0.011])
```

Steady Turning Code:

```
clc,close all,clear all;
```

```
d=(1:0.25:10)*pi/180;%1:(10-1)/29:10;%
Rcr=5:(100-5)/(length(d)-1):100;
V=0:(30-0)/(length(d)-1):30;
lr=1*pi/180;%0:1:4;
lf=1*pi/180;%0:1:4;
%constants
%geometry
p=1380/1000;
b=0.5*p;
h=580/1000;
t=100/1000;

rake=24*pi/180;

%Tire Stiffnesses
klf= 25;    %10-25
krf= 25;   %10-25
klr= 1.5;   %0.7-1.5
krr= 1.5;   %0.7-1.5

m=189+87;
g=9.81;
rr=0.3;
rf=0.3;

%Force Drag
CdA=0.3;      %Drag Coefficient*Area
rho=1.167;    %Air Density

%interia
Izg=1;
Iyg=1;
Ixzg=1;

Iwf=0.33;
Iwr=0.66;


for m=1:length(V)

    for n=1:length(Rcr)
        iRcr(n)=1/Rcr(n);
             for  o=1:length(d)


   yaw(n,m)=V(m)/Rcr(n); %pg109

   roll(n,m)=atan(V(m)^2/(Rcr(n)*g))+t*sin(atan(V(m)^2/(Rcr(n)*g)))/(h-
t); % pg 107

   Fa(o,n,m)=0.5*rho*CdA*(V(m))^2; %Drag Force

   beta(o,n,m)=roll(n,m)+d(o)*sin(rake); %pg25
```

```
   Or(o,n,m)=V(m)/(rr);    %pg109---torus of the tire is zero


   dd(n,m)=atan(p*cos(roll(n,m))/(cos(rake)*Rcr(n)));

   D(o,n,m)=cos(rake)*dd(n,m)/cos(roll(n,m))+lr-lf;%current is from pg
28,,,,,+lr-lf; %pg110


        end
    end
end

aaa=length(d);



figure
[C,hh]=contour(Rcr,V,roll'*180/pi,[10,20,30,40,50],'r');
clabel(C,hh);
hold on
[CC,hhh]=contour(Rcr,V,dd(:,:)'*180/pi,[10,5,3,2,1],'b');
grid on
clabel(CC,hhh);
ylabel('Velocity')
xlabel('Radius of Curvature(m)')
title('Roll & Steering Angle as Function of Velocity and Curvature')
```

Motorcycle Trim:

Straight Trim:

```
clc,close all, clear all;

p=1380;      %motorcycle wheelbase
rc = 111.3; %rear sprocket radius
rp = 43.2;  %drive sprocket radius
L = 580;    %length of swingarm
h = 580;    %height of the center gravity
Rr = 303;   %rear wheel radius

aa=-2;           %upper angle
zz=10;           %lower angle

phi   =  aa:abs((aa-zz))/10:zz;   %angle range
phia = (pi/180)*phi;             %radian range
xp    = 4.516*25.4;   %sprocket horizontal position compared with
swinging arm pivot
yp    = 0.018*25.4;   %sprocket vertical postion compared with
swinging arm pivot

T=-100:(20-(-100))/(length(phi)-1):20;
```

```
for n=1:length(phi);
        a(n)= L*cos(phia(12-n))+xp;
        b(n)= L*sin(phia(12-n))+yp;
        Lc(n) =sqrt(a(n)^2+b(n)^2);

        nue(n)=asin((L*sin(phia(12-n))-(rc-rp))/Lc(n));

        SqR(n) = h*cos(phia(12-n))/(p*(sin(phia(12-
n))+(Rr/rc)*sin(phia(12-n)-nue(n))));
end
figure(1)
plot(T,SqR)
axis([-100 20 0.75 2])
grid on
xlabel('Vertical Wheel Movement(mm)')
ylabel('Squat Ratio')
title('Deviation of the Squat Ratio vs Vertical Wheel
Movement','FontWeight','bold')

%%Trim as the squat ratio varies

kf=21.785; %N/mm-front spring stiffness
kr=34.039 ; %N/mm-rear spring stiffness
%m=(417+190)/2.2;%189.148018; %mass


%1 mph = 1.609344 kph
%1 pound force = 4.44822162 newtons


S=[2588*1/3,2588*2/3,2588]; %driving force ____ 2003 Yamaha R6
Engine Torque 68.50 Nm @ 12000 RPM

for m=1:length(S)
    for o=1:length(SqR)

        Ntr(m)=S(m)*h/p;     %Load Transfer

        Lf(m)=Ntr(m)/kf; % vertical extention of front suspension

        Lr(m,o)=(Ntr(m)/kr)*((1-SqR(o))/SqR(o)); %vertical
extention of the rear suspension

        Mue(m,o)=(pi/180)*(Lr(m,o)-Lf(m))/p;
    end
end


figure(2)
plot(SqR,Mue(1,:)*180/pi,'r',SqR,Mue(2,:)*180/pi,'g',SqR,Mue(3,:)
*180/pi)
```

```
grid on
legend('1303.3N','2606.7N','2588.0N')
xlabel('Squat Ratio')
ylabel('Frame Pitch Angle( \circ )')
title('Deviation of the Frame Pitch Angle vs Squat
Ratio','FontWeight','bold')
%axis([0.8 2.0 -0.01 -0.08])

figure(3)
plot(SqR,Lr(1,:),'r',SqR,Lr(2,:),'g',SqR,Lr(3,:))
grid on
legend('1303.3N','2606.7N','2588.0N')
xlabel('Squat Ratio')
ylabel('Vertical Extention of the Rear Suspension(mm)')
title('Deviation of the Vertical Extention of the Rear Suspension
vs Squat Ratio','FontWeight','bold')
axis([0.8 2.0 15 -25])
% figure(4)
% plot(S,Lf,'r')%,S,Lf)
% grid on
```

Curved Trim:

```
clc,close all, clear all;

p=1.380;     %motorcycle wheelbase
h = 0.580;    %height of the center gravity
b=0.5*p;  % distance from rear contact patch to CG
kf=21785; %N/m-front spring stiffness
kr=34039 ; %N/m-rear spring stiffness
m=(417+190)/2.2;%189.148018; %mass

g=9.81;       %gravity

rc = 0.1113; %rear sprocket radius
rp = 0.0432;  %drive sprocket radius
L =  0.580;    %length of swingarm

Rr = 0.303;   %rear wheel radius

aa=-2;           %upper angle
zz=10;           %lower angle

phi   =  aa:abs((aa-zz))/10:zz;   %angle range
phia = (pi/180)*phi;            %radian range
xp    = 4.516*25.4/1000;   %sprocket horizontal position compared
with swinging arm pivot
yp    = 0.018*25.4/1000;   %sprocket vertical postion compared
with swinging arm pivot

T=-100:(20-(-100))/(length(phi)-1):20;
```

```
Cd=[5,15,30,45,55];
C = (pi/180)*Cd;%camber angle

 for o=1:length(C)

 Dh(o)=m*g*((1/cos(C(o)))-1)/((kf*kr)*p^2/(kf*(p-b)^2+kr*b^2));
%lowering of the center of gravity

 Dmue(o)= -m*g*((1/cos(C(o)))-1)/((kf*kr)*p^2/(kr*b-kf*(p-b)));
%Variation of the Pitch Angle

    for n=1:length(phi);
            a(n)= L*cos(phia(12-n))+xp;
            bb(n)= L*sin(phia(12-n))+yp;
            Lc(n) =sqrt(a(n)^2+bb(n)^2);

            nue(n)=asin((L*sin(phia(12-n))-(rc-rp))/Lc(n));

            SqRC(n,o)=(h-Dh(o))*cos(phia(12-n))/(p*(sin(phia(12-
n))+(Rr/rc)*sin(phia(12-n)-nue(n))));
    end
 end


figure(1)
plot(T,SqRC)
axis([-100 20 0.75 2])
grid on
k=legend('5','15','30','45','55');
LEGENDTITLE(k,'Degree Camber')
xlabel('Vertical Wheel Movement(mm)')
ylabel('Squat Ratio')
title('Deviation of the Squat Ratio vs Vertical Wheel
Movement','FontWeight','bold')

figure(2)
plot(Cd,Dh)
grid on
%axis([0 55 0 0.02])
xlabel('Camber Angle')
ylabel('Lowering of the Center of Gravity')
title('Lowering of the Center of Gravity vs Camber
Angle','FontWeight','bold')

figure(3)
plot(Cd,Dmue*180/pi)
grid on
%axis([0 55 0 0.018])
xlabel('Camber Angle')
ylabel('Variation of the Pitch Angle( \circ ) ')
title('Variation of the Pitch Angle vs Camber
Angle','FontWeight','bold')
```

APPENDIX B – Structural Optimization Figures

Swingarm Structural Optimization Results:

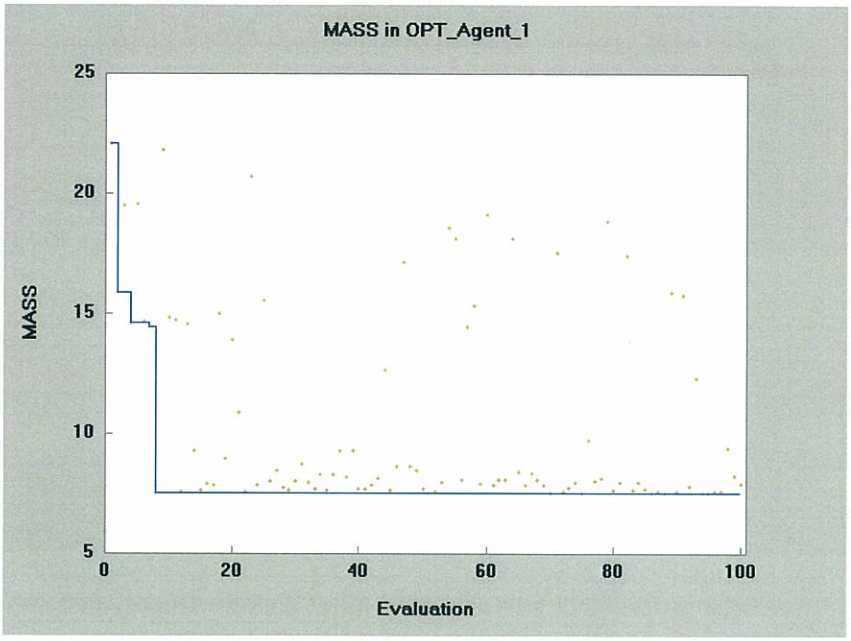

Figure 36-Mass(lb) vs Design Iteration for Swingarm

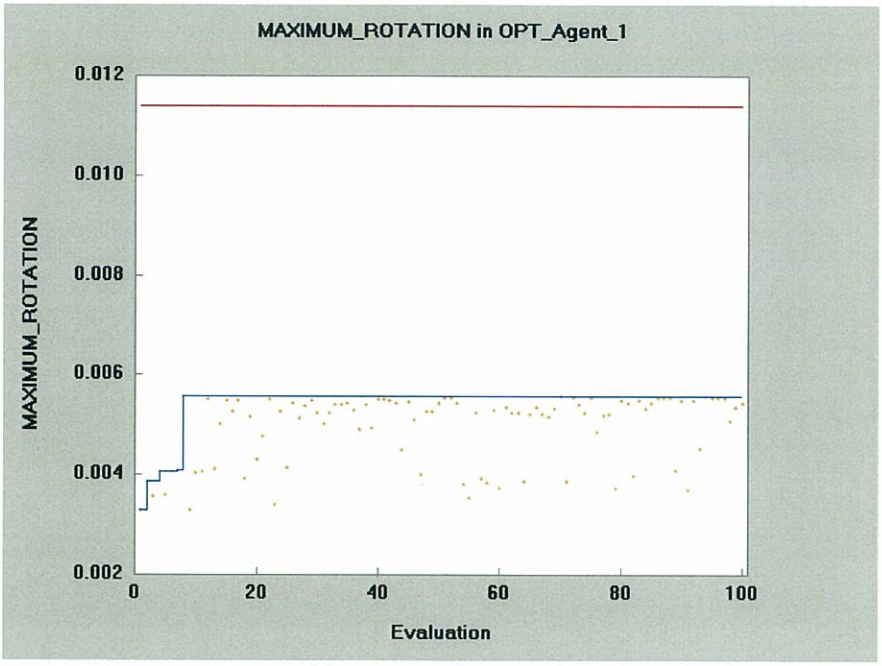

Figure 37-Max Rotation vs Design Iteration for Swingarm

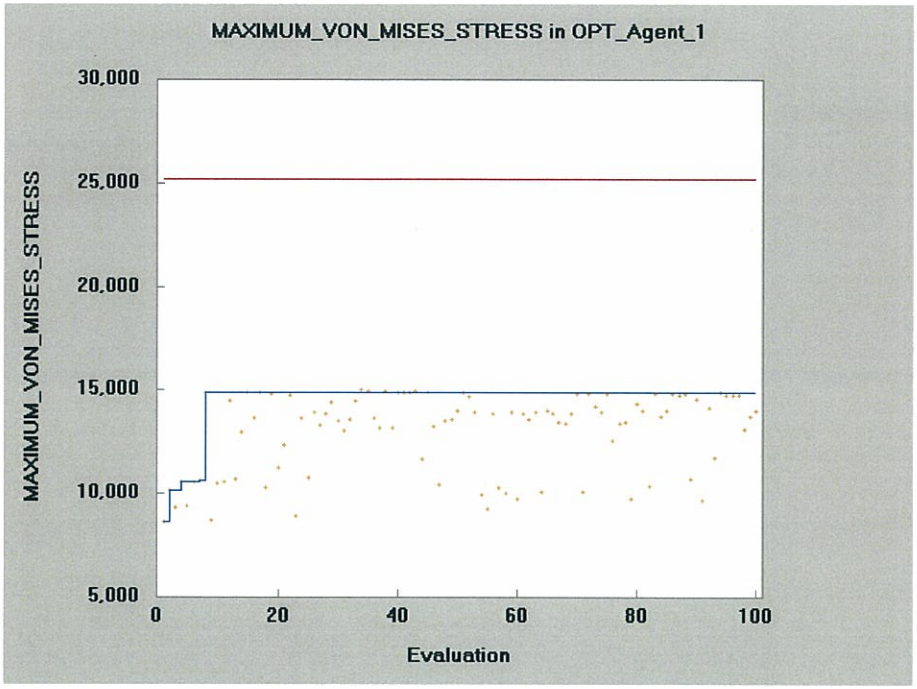

Figure 38- Max Von Mises(psi) vs Design Iteration for Swingarm

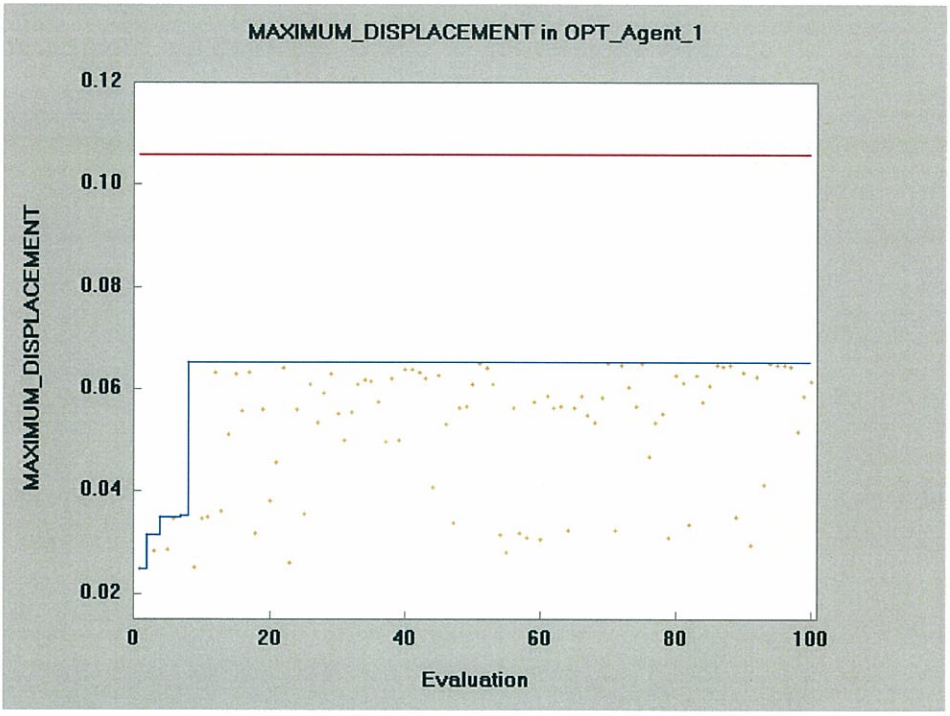

Figure 39-Max Displacement(in) vs Design Iteration for Swingarm

Fork Structural Optimization Results:

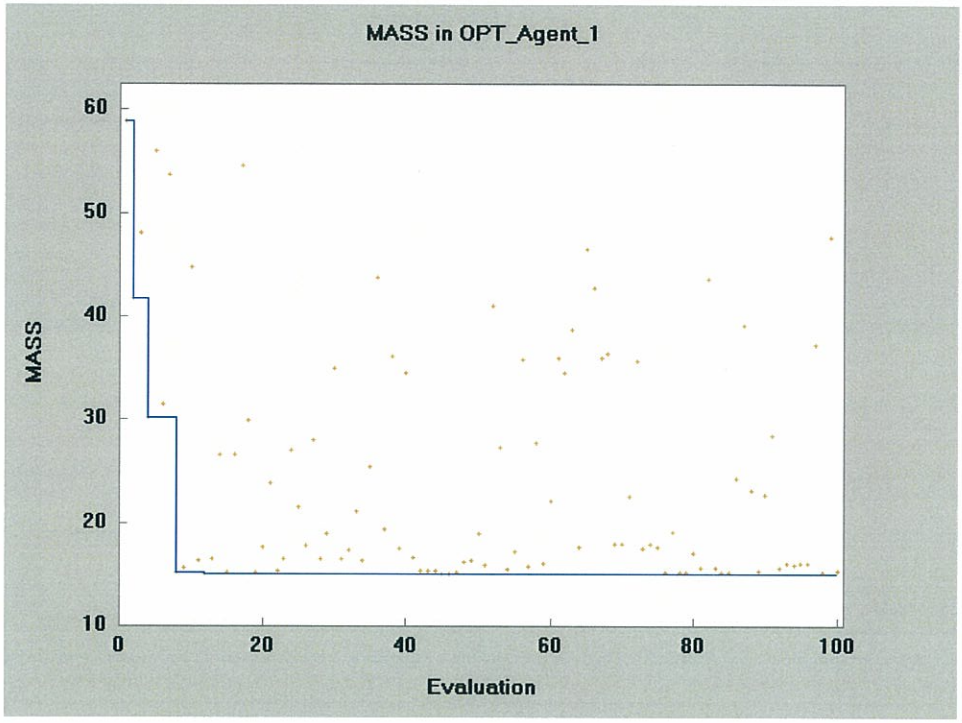

Figure 40-Mass(kg) vs Design Iteration for Fork

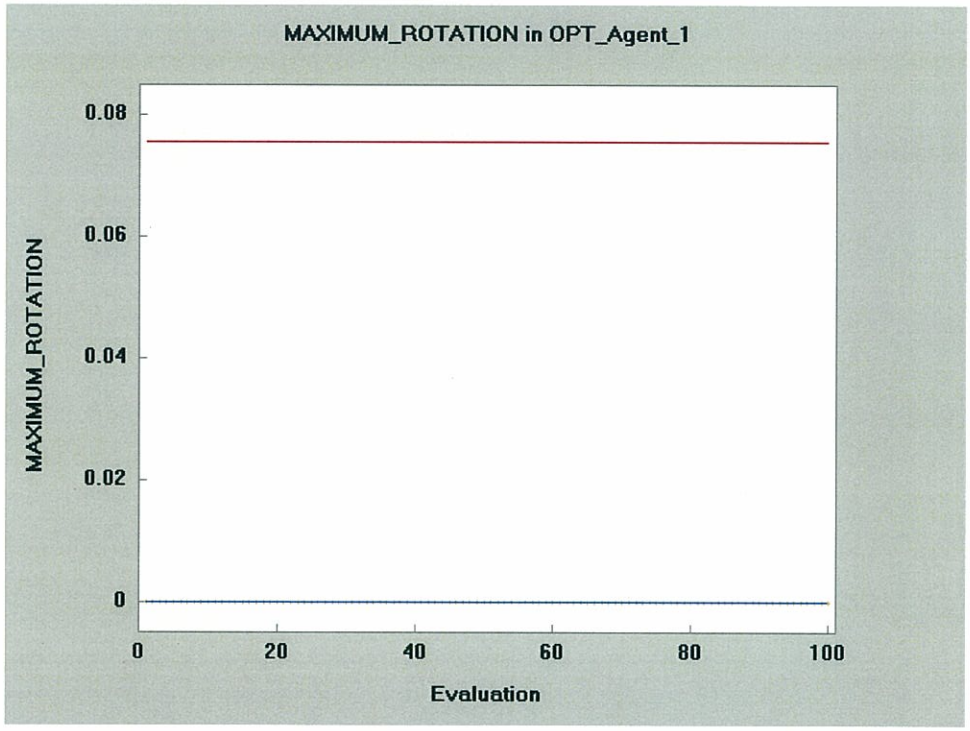

Figure 41-Max Rotation(Rad) vs Design Iteration for Forks

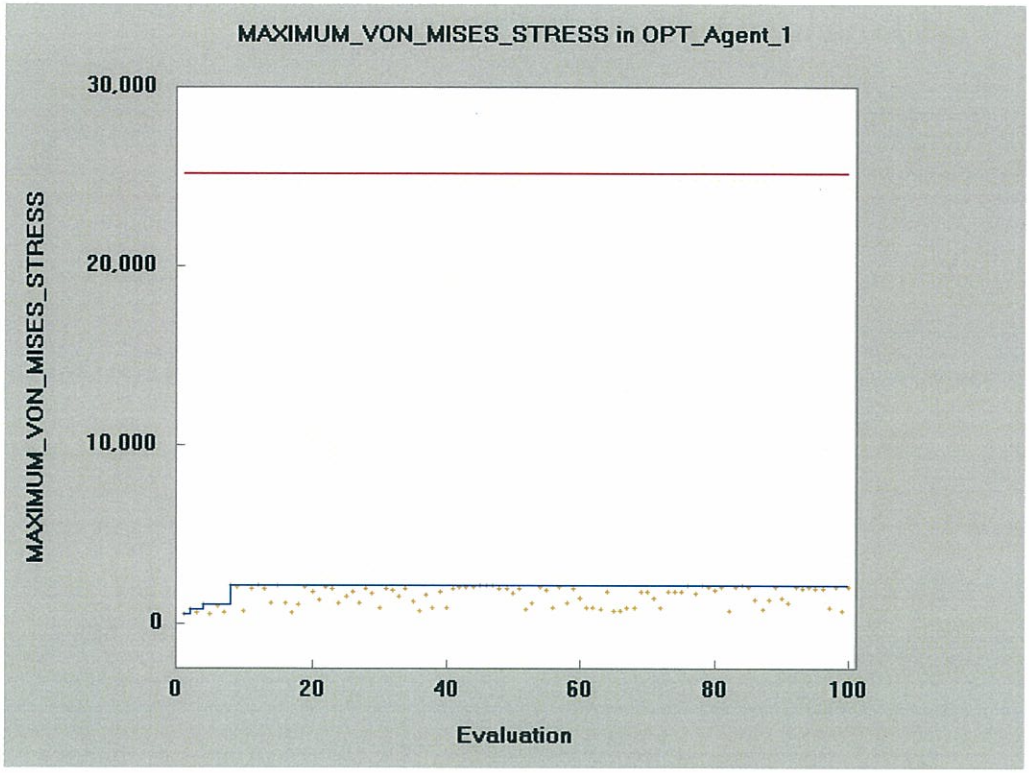

Figure 42-Max Von Mises Stress(psi) vs Design Iteration for Forks

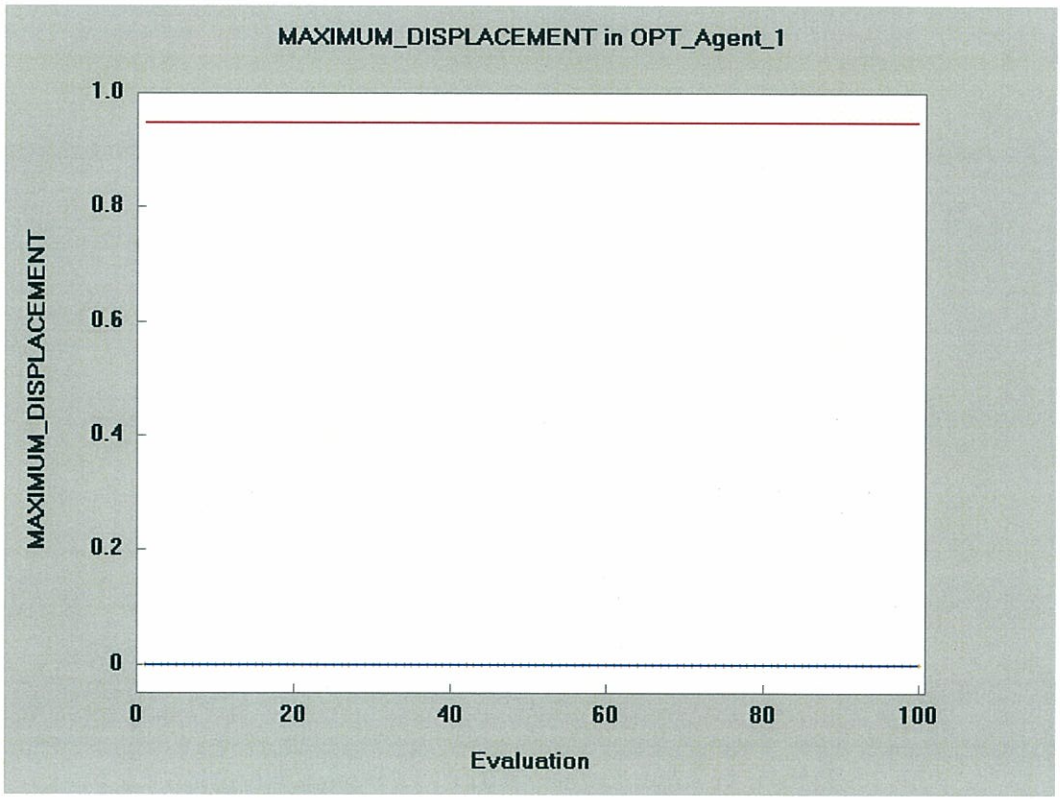

Figure 43-Max Displacement(in) vs Design Iteration for Forks

Main Frame Structural Optimization Results:

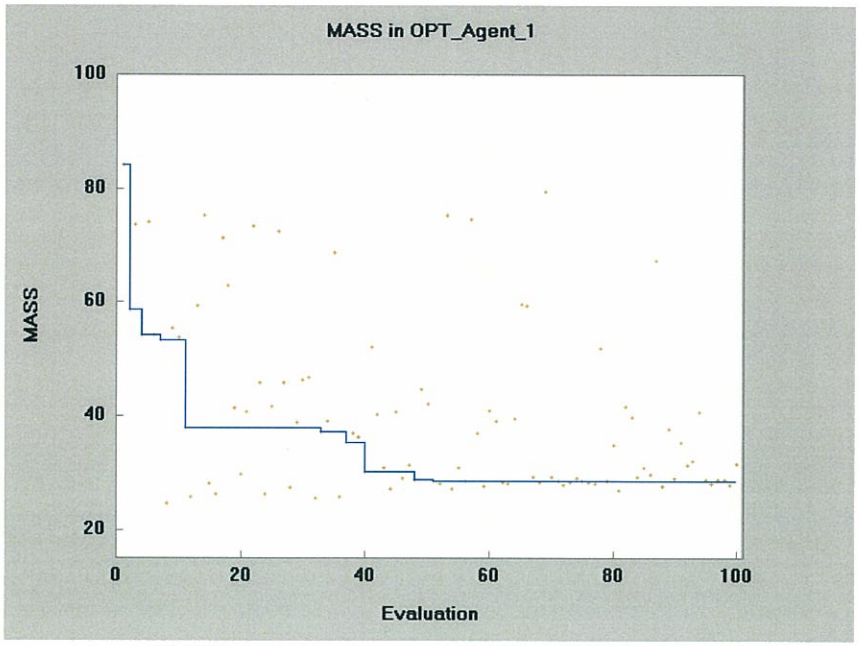

Figure 44-Mass(lb) vs Design Iteration for Main Frame

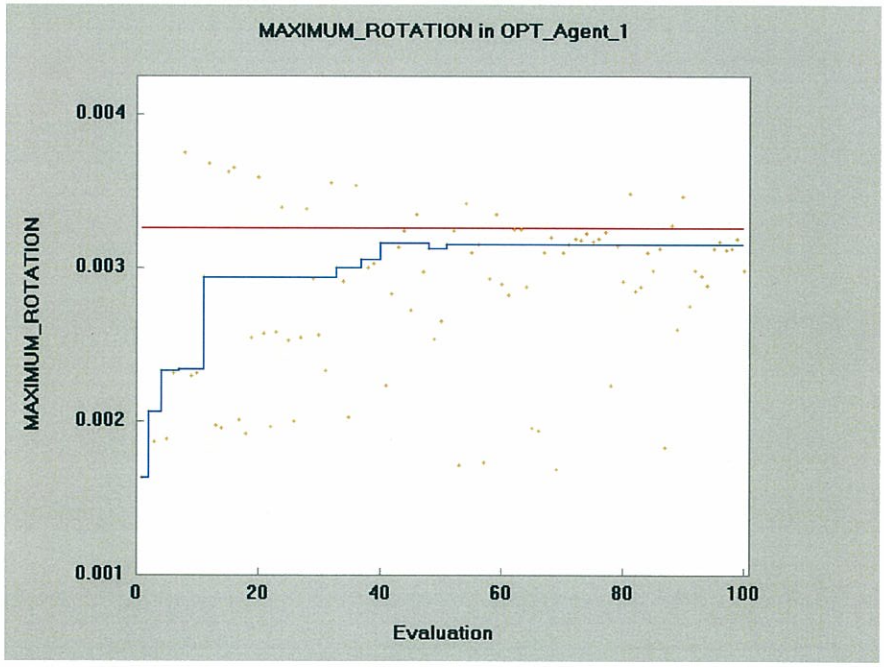

Figure 45-Max Rotation(deg) vs Design Iteration for Main Frame

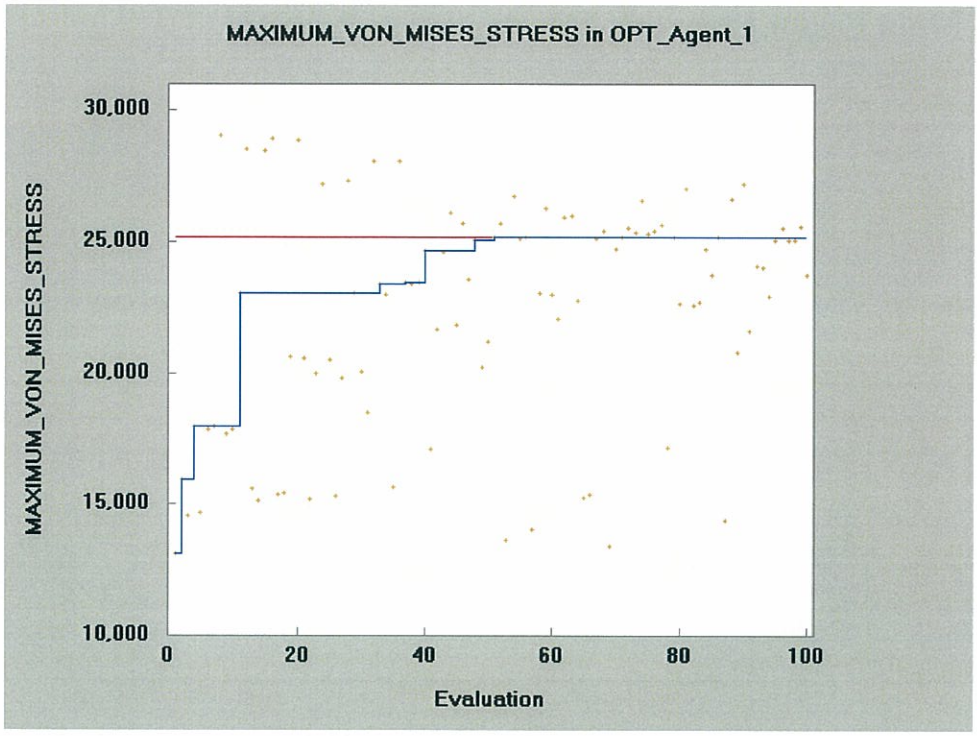

Figure 46-Max Von Mises Stress(psi) vs Design Iteration for Main Frame

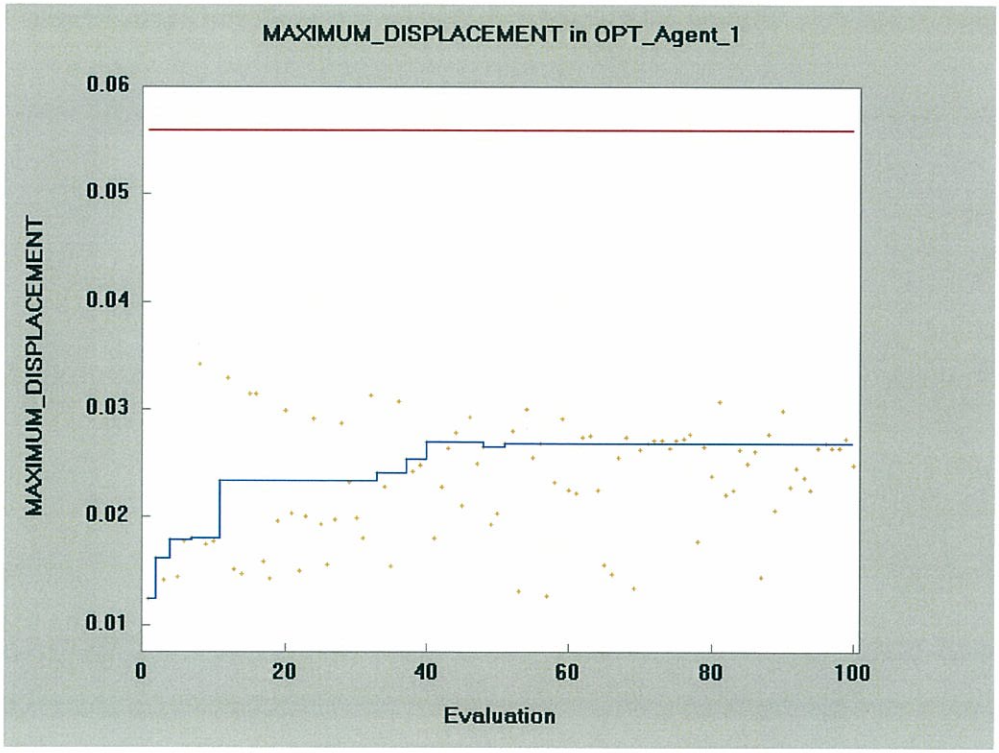

Figure 47-Max Displacement(in) vs Design Iteration for Main Frame

APPENDICIES C- Front Suspension Data

Velocity Ratio for Four Link Front Suspension Program:

```
clc,clear all, close all;

a=170;
b=28;
c=137;
d=190;
e=192;
f=583;
g=163.759;
h=352.668;

be=(pi/180)*(-3.1:0.1:23.7);  %(-3.1:1:23.7)

x4=0;
y4=a;

syms x

for n=1:length(be)
%pt1
x1(n)=b+d*cos(be(n));
y1(n)=d*sin(be(n));
SL(n)=sqrt((x4-x1(n))^2+(y4-y1(n))^2); %shock length

S=real(double(solve((x1(n)-c*cos(x))^2+(y1(n)-a+c*sin(x))^2 -e^2,x)));
%angle of the top link
all(1:2,n)=S;

x2(n)= c*cos(all(2,n));
y2(n)= a+c*sin(all(2,n));



%%%%wheel center path
x3(n)=x2(n)-x1(n)+g;
y3(n)=y1(n)-y2(n)-h;

end
CO=abs(SL(1)-SL(length(SL))) %compression
alld=all(1:2,:)*(pi/180);
T=abs(y3(1)-y3(length(be)))  %travel

figure
plot(x3,y3)
```

APPENDIX D – Rear Suspension Data

Front Hossack Suspension											
mm	%	%	degrees	degrees	mm.	mm.	mm.	mm.	mm.	mm.	mm.
Wheel Diplacement	Anti-Dive Rear Ext	Anti-Dive Rear Ext	Rake Rear Ext	Rake Rear Com	Trail Rear Ext	Trail Rear Com	Locus	Wheel Base	X Virtual Pivot	Y Virtual Pivot	Radius of Virtual Pivot
-0.05	18.89	-1.87	24.92	29.9	85.62	116.58	0	1380	-13114.9	1231.8	13546.7
0.96	19.08	-1.68	24.88	29.87	85.39	116.34	0.07	1380.1	-11379.8	1101.8	11806.8
1.98	19.26	-1.49	24.84	29.83	85.17	116.1	0.14	1380.1	-10057.2	1002.3	10480.6
3	19.43	-1.32	24.8	29.79	84.95	115.86	0.2	1380.2	-9015.3	923.6	9435.8
4.03	19.58	-1.16	24.77	29.76	84.74	115.62	0.27	1380.3	-8172.9	859.7	8591.1
5.05	19.73	-1.01	24.73	29.72	84.53	115.39	0.33	1380.3	-7477.6	806.6	7893.9
6.08	19.87	-0.87	24.7	29.68	84.32	115.17	0.39	1380.4	-6893.8	761.8	7308.5
7.11	20	-0.74	24.66	29.65	84.11	114.94	0.45	1380.5	-6396.4	723.4	6809.7
8.15	20.12	-0.62	24.63	29.62	83.91	114.72	0.51	1380.5	-5967.4	690.1	6379.6
9.18	20.24	-0.51	24.6	29.58	83.71	114.5	0.56	1380.6	-5593.6	661	6004.7
10.22	20.35	-0.41	24.56	29.55	83.52	114.29	0.62	1380.7	-5264.7	635.1	5674.9
11.26	20.45	-0.31	24.53	29.52	83.32	114.08	0.67	1380.7	-4973.1	612.1	5382.5
12.3	20.54	-0.22	24.5	29.48	83.13	113.88	0.72	1380.8	-4712.6	591.4	5121.4
13.35	20.63	-0.14	24.47	29.45	82.95	113.67	0.77	1380.8	-4478.5	572.7	4886.7
14.39	20.71	-0.07	24.44	29.42	82.77	113.47	0.82	1380.9	-4266.9	555.6	4674.5
15.44	20.78	0	24.41	29.39	82.58	113.28	0.86	1380.9	-4074.6	540.1	4481.7
16.49	20.85	0.07	24.38	29.36	82.41	113.08	0.9	1381	-3899	525.7	4305.6
17.54	20.92	0.13	24.35	29.33	82.23	112.89	0.94	1381.1	-3738	512.5	4144.2
18.6	20.98	0.18	24.32	29.3	82.06	112.71	0.98	1381.1	-3589.7	500.3	3995.6
19.65	21.04	0.23	24.29	29.27	81.89	112.52	1.02	1381.2	-3452.8	489	3858.3
20.71	21.09	0.27	24.26	29.24	81.73	112.34	1.06	1381.2	-3325.8	478.4	3731
21.77	21.14	0.31	24.24	29.22	81.57	112.17	1.09	1381.3	-3207.8	468.5	3612.7
22.84	21.18	0.35	24.21	29.19	81.41	111.99	1.12	1381.3	-3097.7	459.2	3502.3
23.9	21.22	0.38	24.18	29.16	81.25	111.82	1.15	1381.4	-2994.7	450.5	3399.1
24.97	21.26	0.41	24.16	29.14	81.09	111.66	1.17	1381.4	-2898.2	442.3	3302.4
26.04	21.3	0.44	24.13	29.11	80.94	111.49	1.2	1381.4	-2807.5	434.5	3211.5
27.11	21.34	0.46	24.11	29.09	80.8	111.33	1.22	1381.5	-2722.1	427.2	3125.9
28.19	21.37	0.49	24.08	29.06	80.65	111.17	1.24	1381.5	-2641.5	420.3	3045.1
29.26	21.4	0.51	24.06	29.04	80.51	111.02	1.26	1381.6	-2565.3	413.7	2968.8
30.34	21.43	0.53	24.03	29.01	80.37	110.87	1.28	1381.6	-2493.1	407.5	2896.4
31.42	21.46	0.54	24.01	28.99	80.23	110.72	1.29	1381.6	-2424.5	401.5	2827.8
32.5	21.48	0.56	23.99	28.97	80.1	110.57	1.3	1381.7	-2359.4	395.9	2762.5
33.59	21.51	0.58	23.97	28.94	79.97	110.43	1.31	1381.7	-2297.4	390.5	2700.4
34.67	21.53	0.59	23.94	28.92	79.84	110.29	1.32	1381.8	-2238.3	385.3	2641.2
35.76	21.56	0.61	23.92	28.9	79.71	110.15	1.33	1381.8	-2181.9	380.4	2584.7
36.85	21.58	0.62	23.9	28.88	79.59	110.02	1.33	1381.8	-2127.9	375.7	2530.7
37.95	21.61	0.64	23.88	28.86	79.47	109.89	1.33	1381.9	-2076.3	371.2	2479
39.04	21.63	0.65	23.86	28.84	79.35	109.76	1.33	1381.9	-2026.8	366.9	2429.4
40.14	21.66	0.67	23.84	28.82	79.24	109.64	1.33	1381.9	-1979.3	362.8	2381.8
41.24	21.69	0.69	23.82	28.8	79.13	109.52	1.32	1381.9	-1933.6	358.8	2336.1
42.34	21.71	0.7	23.8	28.78	79.02	109.4	1.31	1382	-1889.8	355	2292.2
43.44	21.74	0.72	23.79	28.76	78.91	109.29	1.3	1382	-1847.5	351.4	2249.9
44.55	21.77	0.75	23.77	28.75	78.81	109.18	1.29	1382	-1806.8	347.9	2209.1
45.66	21.8	0.77	23.75	28.73	78.71	109.07	1.28	1382	-1767.5	344.5	2169.8
46.77	21.84	0.79	23.74	28.71	78.61	108.96	1.26	1382.1	-1729.6	341.3	2131.8
47.88	21.87	0.82	23.72	28.7	78.52	108.86	1.24	1382.1	-1692.9	338.2	2095.2
49	21.91	0.85	23.7	28.68	78.43	108.76	1.22	1382.1	-1657.5	335.2	2059.7
50.11	21.95	0.89	23.69	28.67	78.34	108.67	1.2	1382.1	-1623.2	332.3	2025.4
51.23	21.99	0.92	23.68	28.65	78.26	108.58	1.17	1382.1	-1589.9	329.6	1992.1
52.36	22.04	0.96	23.66	28.64	78.17	108.49	1.14	1382.1	-1557.7	326.9	1959.9
53.48	22.09	1.01	23.65	28.62	78.09	108.4	1.11	1382.1	-1526.5	324.4	1928.6
54.61	22.14	1.06	23.63	28.61	78.02	108.32	1.08	1382.2	-1496.1	322	1898.3
55.74	22.2	1.11	23.62	28.6	77.94	108.24	1.05	1382.2	-1466.7	319.6	1868.8
56.87	22.26	1.16	23.61	28.59	77.87	108.16	1.01	1382.2	-1438	317.4	1840.1
58	22.32	1.22	23.6	28.57	77.81	108.09	0.97	1382.2	-1410.1	315.2	1812.2
59.14	22.39	1.29	23.59	28.56	77.74	108.02	0.93	1382.2	-1383	313.1	1785.1
60.28	22.46	1.36	23.58	28.55	77.68	107.96	0.89	1382.2	-1356.6	311.2	1758.7
61.42	22.54	1.44	23.57	28.54	77.62	107.89	0.84	1382.2	-1330.8	309.3	1732.9
62.57	22.62	1.52	23.56	28.53	77.57	107.84	0.79	1382.2	-1305.7	307.4	1707.8
63.71	22.71	1.61	23.55	28.53	77.52	107.78	0.74	1382.2	-1281.2	305.7	1683.3
64.86	22.8	1.7	23.54	28.52	77.47	107.73	0.69	1382.2	-1257.3	304	1659.4
66.02	22.9	1.8	23.53	28.51	77.42	107.68	0.64	1382.2	-1234	302.4	1636.1
67.17	23.01	1.91	23.53	28.5	77.38	107.63	0.58	1382.2	-1211.2	300.9	1613.2
68.33	23.12	2.03	23.52	28.5	77.34	107.59	0.52	1382.2	-1188.9	299.5	1591
69.49	23.23	2.15	23.51	28.49	77.31	107.56	0.46	1382.2	-1167.1	298.1	1569.2
70.65	23.36	2.28	23.51	28.48	77.27	107.52	0.4	1382.2	-1145.7	296.8	1547.8
71.82	23.49	2.42	23.5	28.48	77.25	107.49	0.33	1382.2	-1124.9	295.5	1526.9
72.99	23.63	2.57	23.5	28.48	77.22	107.46	0.26	1382.2	-1104.4	294.3	1506.5
74.16	23.77	2.72	23.5	28.47	77.2	107.44	0.19	1382.2	-1084.4	293.2	1486.5
75.34	23.93	2.89	23.49	28.47	77.18	107.42	0.12	1382.2	-1064.8	292.2	1466.8
76.52	24.09	3.06	23.49	28.47	77.17	107.41	0.05	1382.2	-1045.5	291.2	1447.6
77.7	24.26	3.24	23.49	28.46	77.15	107.4	-0.03	1382.2	-1026.6	290.3	1428.7
78.88	24.44	3.43	23.49	28.46	77.15	107.39	-0.11	1382.1	-1008.1	289.4	1410.2
80.07	24.63	3.64	23.49	28.46	77.14	107.38	-0.19	1382.1	-990	288.6	1392
81.26	24.82	3.85	23.49	28.46	77.14	107.38	-0.27	1382.1	-972.1	287.8	1374.2
82.45	25.03	4.08	23.49	28.46	77.15	107.39	-0.35	1382.1	-954.6	287.1	1356.7
83.65	25.25	4.31	23.49	28.46	77.15	107.4	-0.44	1382.1	-937.4	286.5	1339.4
84.85	25.47	4.56	23.49	28.47	77.16	107.41	-0.53	1382.1	-920.5	285.9	1322.5
86.06	25.71	4.82	23.49	28.47	77.18	107.43	-0.62	1382.1	-903.8	285.4	1305.9
87.26	25.96	5.1	23.5	28.47	77.2	107.45	-0.71	1382	-887.5	284.9	1289.5
88.48	26.22	5.38	23.5	28.48	77.22	107.48	-0.81	1382	-871.4	284.5	1273.4
89.69	26.49	5.68	23.5	28.48	77.25	107.51	-0.9	1382	-855.6	284.1	1257.6
90.91	26.78	6	23.51	28.49	77.28	107.54	-1	1382	-840	283.8	1242
92.13	27.07	6.32	23.52	28.49	77.32	107.58	-1.1	1382	-824.7	283.5	1226.7
93.36	27.38	6.67	23.52	28.5	77.36	107.62	-1.2	1382	-809.6	283.3	1211.6
94.59	27.71	7.02	23.53	28.51	77.4	107.67	-1.31	1381.9	-794.7	283.1	1196.7
95.82	28.04	7.4	23.54	28.52	77.45	107.73	-1.41	1381.9	-780.1	283	1182
97.06	28.39	7.79	23.55	28.53	77.5	107.79	-1.52	1381.9	-765.7	282.9	1167.6
98.3	28.76	8.19	23.56	28.54	77.56	107.85	-1.63	1381.9	-751.4	282.9	1153.3
99.55	29.14	8.62	23.57	28.55	77.63	107.92	-1.74	1381.8	-737.4	282.9	1139.3
100.8	29.53	9.06	23.58	28.56	77.69	107.99	-1.86	1381.8	-723.6	283	1125.5
102.06	29.95	9.52	23.59	28.57	77.76	108.07	-1.97	1381.8	-710	283.1	1111.8
103.32	30.37	10	23.6	28.58	77.84	108.16	-2.09	1381.8	-696.5	283.3	1098.3
104.58	30.82	10.49	23.62	28.6	77.92	108.25	-2.21	1381.8	-683.2	283.5	1085
105.85	31.28	11.01	23.63	28.61	78.01	108.34	-2.33	1381.7	-670.2	283.8	1071.9
107.12	31.76	11.55	23.65	28.63	78.1	108.44	-2.45	1381.7	-657.2	284.1	1059
108.4	32.26	12.11	23.67	28.65	78.2	108.55	-2.57	1381.7	-644.5	284.5	1046.2
109.69	32.78	12.69	23.68	28.66	78.31	108.66	-2.69	1381.7	-631.9	284.9	1033.6
110.97	33.32	13.29	23.7	28.68	78.42	108.78	-2.82	1381.6	-619.4	285.3	1021.1
112.27	33.88	13.92	23.72	28.7	78.53	108.91	-2.95	1381.6	-607.2	285.8	1008.8
113.57	34.46	14.57	23.74	28.72	78.65	109.04	-3.08	1381.6	-595	286.4	996.6
114.87	35.06	15.25	23.76	28.75	78.78	109.17	-3.21	1381.6	-583	286.9	984.6
116.18	35.68	15.95	23.79	28.77	78.91	109.32	-3.34	1381.6	-571.2	287.6	972.7
117.5	36.33	16.67	23.81	28.79	79.05	109.47	-3.47	1381.5	-559.5	288.2	961
118.82	37	17.43	23.83	28.82	79.19	109.63	-3.6	1381.5	-547.9	289	949.4
120.15	37.7	18.21	23.86	28.84	79.35	109.79	-3.74	1381.5	-536.5	289.7	938

Rear Suspension																
mm	N/mm		N/mm	N	N	N	N	N	N	N	N	N	N	J	%	%
Vetical Wheel Displacement	Shock Displacement	Motion Ratio	Actual Wheel Rate	Spring Load	Whee load	Pivot Load Total	Pivot Load Vertical	Pivot Load Horizontal	Rocker Load Total	Rocker Load Vertical	Rocker Load Horizontal	Link Force	Spring Stored Energy	Anti-Squat Percentage	Anti-squat Angle
0	0	0.4871	21.8154	0	0	0	0	0	0	0	0	0	0	139.87	30.76
1	0.4872	0.4873	21.8398	44.82	21.8398	53.08	-21.22	-48.65	64.97	-43.06	-48.65	-48.35	0.01	139.52	30.67
2	0.9745	0.4875	21.865	89.658	43.7048	106.27	-42.6	-97.35	130.11	-86.32	-97.35	-96.77	0.04	139.18	30.59
3	1.4621	0.4877	21.8907	134.513	65.5955	159.57	-64.16	-146.1	195.41	-129.77	-146.1	-145.27	0.09	138.84	30.5
4	1.9498	0.4878	21.9173	179.386	87.5128	212.99	-85.9	-194.9	260.89	-173.43	-194.9	-193.85	0.17	138.5	30.42
5	2.4378	0.488	21.9441	224.277	109.4569	266.52	-107.81	-243.74	326.53	-217.29	-243.74	-242.5	0.27	138.16	30.33
6	2.9259	0.4882	21.9718	269.186	131.4287	320.17	-129.89	-292.64	392.35	-261.35	-292.64	-291.24	0.39	137.82	30.25
7	3.4143	0.4885	22.0009	314.114	153.4296	373.94	-152.14	-341.58	458.34	-305.61	-341.58	-340.07	0.53	137.48	30.16
8	3.9028	0.4887	22.0303	359.061	175.4599	427.82	-174.58	-390.59	524.51	-350.07	-390.59	-388.98	0.69	137.13	30.08
9	4.3916	0.4889	22.0596	404.028	197.5195	481.84	-197.19	-439.64	590.86	-394.75	-439.64	-437.97	0.88	136.79	29.99
10	4.8806	0.4891	22.0911	449.014	219.6106	535.97	-219.97	-488.75	657.38	-439.63	-488.75	-487.06	1.09	136.45	29.91
11	5.3698	0.4893	22.1219	494.021	241.7325	590.23	-242.93	-537.92	724.09	-484.72	-537.92	-536.24	1.32	136.11	29.82
12	5.8592	0.4895	22.1528	539.049	263.8853	644.62	-266.07	-587.15	790.99	-530.02	-587.15	-585.51	1.57	135.77	29.74
13	6.3489	0.4898	22.1866	584.097	286.0719	699.14	-289.39	-636.44	858.07	-575.53	-636.44	-634.88	1.85	135.43	29.65
14	6.8388	0.49	22.2202	629.166	308.2921	753.79	-312.88	-685.79	925.34	-621.25	-685.79	-684.35	2.15	135.09	29.57
15	7.3289	0.4902	22.2547	674.257	330.5468	808.57	-336.56	-735.2	992.8	-667.19	-735.2	-733.91	2.47	134.75	29.48
16	7.8192	0.4905	22.2898	719.37	352.8366	863.49	-360.41	-784.68	1060.46	-713.34	-784.68	-783.58	2.81	134.41	29.4
17	8.3098	0.4907	22.3243	764.505	375.1609	918.54	-384.45	-834.22	1128.31	-759.71	-834.22	-833.35	3.17	134.07	29.31
18	8.8007	0.491	22.3607	809.663	397.5216	973.74	-408.67	-883.83	1196.35	-806.3	-883.83	-883.23	3.56	133.73	29.23
19	9.2918	0.4912	22.3997	854.844	419.9213	1029.07	-433.07	-933.5	1264.6	-853.1	-933.5	-933.21	3.97	133.39	29.14
20	9.7831	0.4915	22.4362	900.048	442.3575	1084.54	-457.66	-983.25	1333.05	-900.13	-983.25	-983.3	4.4	133.05	29.06
21	10.2747	0.4917	22.475	945.277	464.8326	1140.16	-482.42	-1033.07	1401.7	-947.38	-1033.07	-1033.51	4.85	132.71	28.97
22	10.7666	0.492	22.5127	990.529	487.3453	1195.92	-507.38	-1082.96	1470.56	-994.86	-1082.96	-1083.83	5.33	132.37	28.89
23	11.2588	0.4923	22.5549	1035.806	509.9002	1251.83	-532.51	-1132.92	1539.62	-1042.56	-1132.92	-1134.27	5.83	132.02	28.8
24	11.7512	0.4925	22.5987	1081.108	532.4989	1307.89	-557.84	-1182.96	1608.9	-1090.49	-1182.96	-1184.82	6.35	131.68	28.72
25	12.2439	0.4928	22.6364	1126.435	555.1353	1364.1	-583.35	-1233.08	1678.39	-1138.64	-1233.08	-1235.5	6.89	131.34	28.63
26	12.7368	0.4931	22.6768	1171.787	577.812	1420.47	-609.05	-1283.27	1748.09	-1187.03	-1283.27	-1286.3	7.46	131	28.55
27	13.2301	0.4934	22.7249	1217.166	600.5369	1476.99	-634.93	-1333.55	1818.02	-1235.65	-1333.55	-1337.22	8.05	130.66	28.46
28	13.7236	0.4937	22.7698	1262.571	623.3067	1533.67	-661.01	-1383.91	1888.16	-1284.5	-1383.91	-1388.28	8.66	130.32	28.38
29	14.2174	0.494	22.8098	1308.003	646.1165	1590.51	-687.28	-1434.35	1958.53	-1333.59	-1434.35	-1439.46	9.29	129.98	28.29
30	14.7115	0.4943	22.8585	1353.462	668.975	1647.51	-713.74	-1484.88	2029.12	-1382.92	-1484.88	-1490.78	9.95	129.64	28.21
31	15.206	0.4946	22.9028	1398.948	691.8779	1704.67	-740.39	-1535.49	2099.94	-1432.48	-1535.49	-1542.23	10.63	129.3	28.12
32	15.7007	0.4949	22.9532	1444.463	714.8311	1762	-767.23	-1586.19	2170.98	-1482.29	-1586.19	-1593.82	11.33	128.96	28.04
33	16.1957	0.4952	23.0023	1490.006	737.8334	1819.5	-794.27	-1636.98	2242.27	-1532.33	-1636.98	-1645.54	12.06	128.62	27.95
34	16.6911	0.4955	23.0487	1535.577	760.8821	1877.16	-821.5	-1687.86	2313.78	-1582.63	-1687.86	-1697.41	12.81	128.28	27.87
35	17.1867	0.4958	23.0992	1581.178	783.9813	1935.01	-848.93	-1738.84	2385.54	-1633.16	-1738.84	-1749.43	13.58	127.94	27.78
36	17.6827	0.4961	23.1471	1626.808	807.1284	1993.02	-876.56	-1789.91	2457.53	-1683.95	-1789.91	-1801.59	14.38	127.6	27.7
37	18.179	0.4965	23.2059	1672.468	830.3343	2051.21	-904.37	-1841.08	2529.77	-1734.98	-1841.08	-1853.91	15.2	127.26	27.61
38	18.6756	0.4968	23.2543	1718.159	853.5886	2109.59	-932.4	-1892.35	2602.26	-1786.27	-1892.35	-1906.38	16.04	126.92	27.53
39	19.1726	0.4971	23.3044	1763.88	876.8929	2168.14	-960.62	-1943.72	2675	-1837.81	-1943.72	-1959	16.91	126.58	27.44
40	19.6699	0.4975	23.3648	1809.633	900.2578	2226.88	-989.04	-1995.19	2747.98	-1889.61	-1995.19	-2011.78	17.8	126.24	27.36
41	20.1676	0.4978	23.419	1855.417	923.6768	2285.8	-1017.66	-2046.77	2821.22	-1941.66	-2046.77	-2064.72	18.71	125.9	27.27
42	20.6656	0.4982	23.472	1901.233	947.1487	2344.92	-1046.5	-2098.45	2894.72	-1993.98	-2098.45	-2117.83	19.65	125.56	27.19
43	21.1639	0.4985	23.5316	1947.081	970.6804	2404.22	-1075.52	-2150.24	2968.49	-2046.55	-2150.24	-2171.1	20.61	125.22	27.1
44	21.6626	0.4989	23.5906	1992.963	994.2709	2463.72	-1104.76	-2202.14	3042.51	-2099.39	-2202.14	-2224.54	21.59	124.88	27.02
45	22.1617	0.4993	23.6461	2038.877	1017.9171	2523.42	-1134.21	-2254.15	3116.8	-2152.5	-2254.15	-2278.16	22.6	124.53	26.93
46	22.6611	0.4996	23.7067	2084.825	1041.6238	2583.31	-1163.86	-2306.28	3191.36	-2205.87	-2306.28	-2331.95	23.63	124.19	26.85
47	23.161	0.5	23.7705	2130.808	1065.3943	2643.4	-1193.72	-2358.52	3266.2	-2259.51	-2358.52	-2385.92	24.68	123.85	26.76
48	23.6611	0.5004	23.8311	2176.824	1089.2253	2703.71	-1223.8	-2410.88	3341.31	-2313.43	-2410.88	-2440.07	25.76	123.51	26.68
49	24.1617	0.5008	23.8926	2222.876	1113.1179	2764.21	-1254.07	-2463.37	3416.7	-2367.62	-2463.37	-2494.41	26.86	123.17	26.59
50	24.6626	0.5011	23.9597	2268.964	1137.0776	2824.93	-1284.57	-2515.97	3492.37	-2422.09	-2515.97	-2548.93	27.98	122.83	26.51
51	25.164	0.5015	24.0231	2315.087	1161.1007	2885.86	-1315.28	-2568.7	3568.33	-2476.84	-2568.7	-2603.64	29.13	122.49	26.42
52	25.6657	0.5019	24.0878	2361.246	1185.1885	2947.01	-1346.21	-2621.56	3644.58	-2531.87	-2621.56	-2658.55	30.3	122.14	26.34
53	26.1679	0.5023	24.1556	2407.443	1209.3441	3008.37	-1377.35	-2674.55	3721.12	-2587.18	-2674.55	-2713.66	31.5	121.8	26.25
54	26.6704	0.5027	24.2272	2453.676	1233.5713	3069.95	-1408.71	-2727.66	3797.96	-2642.79	-2727.66	-2768.97	32.72	121.46	26.17
55	27.1733	0.5032	24.2924	2499.948	1257.8636	3131.76	-1440.3	-2780.92	3875.09	-2698.68	-2780.92	-2824.48	33.97	121.12	26.08
56	27.6767	0.5036	24.3608	2546.257	1282.2245	3193.8	-1472.1	-2834.3	3952.53	-2754.86	-2834.3	-2880.2	35.24	120.77	26
57	28.1805	0.504	24.4386	2592.605	1306.6631	3256.06	-1504.12	-2887.83	4030.28	-2811.34	-2887.83	-2936.14	36.53	120.43	25.91
58	28.6847	0.5044	24.5071	2638.992	1331.1702	3318.57	-1536.38	-2941.5	4108.34	-2868.11	-2941.5	-2992.28	37.85	120.09	25.83
59	29.1893	0.5049	24.5786	2685.419	1355.7488	3381.3	-1568.85	-2995.31	4186.72	-2925.19	-2995.31	-3048.65	39.19	119.75	25.74
60	29.6944	0.5053	24.6603	2731.885	1380.4091	3444.27	-1601.55	-3049.27	4265.41	-2982.56	-3049.27	-3105.24	40.56	119.4	25.66
61	30.1999	0.5057	24.7318	2778.393	1405.1409	3507.49	-1634.49	-3103.38	4344.43	-3040.25	-3103.38	-3162.05	41.95	119.06	25.57
62	30.7059	0.5062	24.807	2824.941	1429.9479	3570.95	-1667.65	-3157.63	4423.77	-3098.24	-3157.63	-3219.1	43.37	118.72	25.49
63	31.2123	0.5066	24.8896	2871.531	1454.8375	3634.67	-1701.05	-3212.05	4503.44	-3156.54	-3212.05	-3276.38	44.81	118.37	25.4
64	31.7192	0.5071	24.9705	2918.164	1479.808	3698.63	-1734.67	-3266.62	4583.45	-3215.16	-3266.62	-3333.9	46.28	118.03	25.32
65	32.2265	0.5076	25.0465	2964.838	1504.8545	3762.86	-1768.55	-3321.34	4663.8	-3274.09	-3321.34	-3391.66	47.77	117.69	25.23
66	32.7343	0.508	25.1298	3011.556	1529.9843	3827.34	-1802.65	-3376.24	4744.49	-3333.35	-3376.24	-3449.66	49.29	117.34	25.15
67	33.2426	0.5085	25.2145	3058.317	1555.1987	3892.08	-1837	-3431.29	4825.53	-3392.92	-3431.29	-3507.92	50.83	117	25.06
68	33.7513	0.509	25.297	3105.123	1580.4957	3957.09	-1871.58	-3486.52	4906.92	-3452.83	-3486.52	-3566.43	52.4	116.65	24.98
69	34.2606	0.5095	25.3877	3151.972	1605.8834	4022.38	-1906.4	-3541.91	4988.66	-3513.06	-3541.91	-3625.19	53.99	116.31	24.89
70	34.7703	0.51	25.4746	3198.868	1631.3571	4087.93	-1941.48	-3597.48	5070.77	-3573.63	-3597.48	-3684.23	55.61	115.96	24.81
71	35.2805	0.5105	25.5599	3245.809	1656.917	4153.77	-1976.8	-3653.23	5153.24	-3634.53	-3653.23	-3743.53	57.25	115.62	24.72
72	35.7913	0.511	25.6514	3292.796	1682.5684	4219.89	-2012.37	-3709.15	5236.08	-3695.78	-3709.15	-3803.1	58.92	115.27	24.64
73	36.3025	0.5115	25.7427	3339.83	1708.311	4286.29	-2048.19	-3765.26	5319.3	-3757.36	-3765.26	-3862.95	60.62	114.93	24.55
74	36.8143	0.512	25.8356	3386.911	1734.1466	4352.99	-2084.27	-3821.56	5402.9	-3819.3	-3821.56	-3923.08	62.34	114.58	24.47
75	37.3265	0.5125	25.9293	3434.041	1760.0759	4419.98	-2120.6	-3878.05	5486.89	-3881.58	-3878.05	-3983.49	64.09	114.23	24.38
76	37.8393	0.5131	26.0266	3481.218	1786.1025	4487.26	-2157.19	-3934.73	5571.26	-3944.22	-3934.73	-4044.2	65.86	113.89	24.3
77	38.3527	0.5136	26.1257	3528.445	1812.2283	4554.85	-2194.04	-3991.6	5656.03	-4007.22	-3991.6	-4105.21	67.66	113.54	24.21
78	38.8665	0.5141	26.2208	3575.722	1838.4491	4622.75	-2231.15	-4048.68	5741.2	-4070.57	-4048.68	-4166.51	69.49	113.19	24.13
79	39.381	0.5147	26.3226	3623.048	1864.7717	4690.96	-2268.52	-4105.96	5826.78	-4134.3	-4105.96	-4228.13	71.34	112.85	24.04
80	39.8959	0.5153	26.4261	3670.426	1891.1979	4759.49	-2306.17	-4163.45	5912.76	-4198.39	-4163.45	-4290.05	73.22	112.5	23.96
81	40.4115	0.5158	26.5278	3717.855	1917.7257	4828.33	-2344.08	-4221.15	5999.17	-4262.86	-4221.15	-4352.29	75.12	112.15	23.87
82	40.9276	0.5164	26.6346	3765.336	1944.3604	4897.5	-2382.26	-4279.06	6086	-4327.7	-4279.06	-4414.86	77.05	111.8	23.79
83	41.4442	0.517	26.7435	3812.87	1971.1039	4967	-2420.72	-4337.19	6173.25	-4392.93	-4337.19	-4477.75	79.01	111.46	23.7
84	41.9615	0.5175	26.8499	3860.457	1997.9537	5036.84	-2459.46	-4395.55	6260.95	-4458.54	-4395.55	-4540.98	80.99	111.11	23.62
85	42.4793	0.5181	26.9576	3908.097	2024.9114	5107.02	-2498.48	-4454.13	6349.08	-4524.55	-4454.13	-4604.55	83	110.76	23.53
86	42.9977	0.5187	27.074	3955.793	2051.9856	5177.54	-2537.77	-4512.95	6437.66	-4590.95	-4512.95	-4668.47	85.04	110.41	23.45
87	43.5168	0.5193	27.1875	4003.544	2079.1729	5248.42	-2577.36	-4571.99	6526.69	-4657.74	-4571.99	-4732.73	87.11	110.06	23.36
88	44.0364	0.5199	27.3008	4051.35	2106.4736	5319.65	-2617.23	-4631.28	6616.19	-4724.95	-4631.28	-4797.36	89.2	109.71	23.27
89	44.5567	0.5206	27.4204	4099.213	2133.894	5391.24	-2657.39	-4690.81	6706.14	-4792.56	-4690.81	-4862.35	91.32	109.36	23.19
90	45.0775	0.5212	27.5396	4147.134	2161.4336	5463.2	-2697.85	-4750.59	6796.58	-4860.59	-4750.59	-4927.71	93.47	109.01	23.1
91	45.599	0.5218	27.6619	4195.112	2189.0955	5535.53	-2738.6	-4810.63	6887.49	-4929.03	-4810.63	-4993.45	95.65	108.66	23.02
92	46.1212	0.5225	27.7849	4243.148	2216.8804	5608.24	-2779.66	-4870.92	6978.89	-4997.9	-4870.92	-5059.58	97.85	108.31	22.93
93	46.644	0.5231	27.9092	4291.245	2244.7896	5681.33	-2821.01	-4931.47	7070.78	-5067.2	-4931.47	-5126.09	100.08	107.96	22.85
94	47.1674	0.5238	28.0386	4339.401	2272.8281	5754.81	-2862.68	-4992.29	7163.17	-5136.94	-4992.29	-5193.01	102.34	107.6	22.76
95	47.6915	0.5244	28.1682	4387.618	2300.9963	5828.69	-2904.65	-5053.38	7256.08	-5207.11	-5053.38	-5260.33	104.63	107.25	22.68
96	48.2163	0.5251	28.2993	4435.896	2329.2957	5902.97	-2946.94	-5114.75	7349.5	-5277.73	-5114.75	-5328.07	106.95	106.9	22.59
97	48.7417	0.5258	28.4331	4484.236	2357.7288	5977.66	-2989.54	-5176.4	7443.44	-5348.8	-5176.4	-5396.22	109.29	106.55	22.5
98	49.2678	0.5265	28.5691	4532.64	2386.2979	6052.77	-3032.47	-5238.34	7537.92	-5420.33	-5238.34	-5464.81	111.66	106.19	22.42
99	49.7946	0.5272	28.7087	4581.106	2415.0066	6128.3	-3075.71	-5300.57	7632.93	-5492.32	-5300.57	-5533.83	114.06	105.84	22.33
100	50.3222	0.5279	28.8491	4629.638	2443.8557	6204.26	-3119.29	-5363.1	7728.5	-5564.79	-5363.1	-5603.3	116.49	105.48	22.25
101	50.8504	0.5286	28.9915	4678.235	2472.8472	6280.65	-3163.19	-5425.94	7824.62	-5637.72	-5425.94	-5673.22	118.95	105.13	22.16
102	51.3793	0.5293	29.1384	4726.898	2501.9856	6357.49	-3207.44	-5489.08	7921.31	-5711.14	-5489.08	-5743.6	121.44	104.78	22.07
103	51.909	0.53	29.2864	4775.628	2531.372	6434.78	-3252.02	-5552.54	8018.57	-5785.05	-5552.54	-5814.45	123.96	104.42	21.99
104	52.4394	0.5308	29.4363	4824.425	2560.7083	6512.52	-3296.94	-5616.33	8116.42	-5859.45	-5616.33	-5885.78	126.51	104.07	21.9
105	52.9706	0.5315	29.5894	4873.291	2590.2976	6590.74	-3342.21	-5680.44	8214.86	-5934.35	-5680.44	-5957.6	129.09	103.71	21.82
106	53.5025	0.5323	29.7461	4922.227	2620.0437	6669.42	-3387.84	-5744.89	8313.9	-6009.76	-5744.89	-6029.92	131.7	103.35	21.73
107	54.0351	0.5331	29.9045	4971.232	2649.9482	6748.59	-3433.82	-5809.68	8413.56	-6085.69	-5809.68	-6102.74	134.33	103	21.64
108	54.5686	0.5338	30.0657	5020.309	2680.0139	6828.25	-3480.16	-5874.82	8513.84	-6162.14	-5874.82	-6176.09	137	102.64	21.56
109	55.1028	0.5346	30.23	5069.458	2710.2439	6908.41	-3526.86	-5940.31	8614.75	-6239.12	-5940.31	-6249.96	139.69	102.28	21.47
110	55.6378	0.5354	30.3972	5118.68	2740.6411	6989.07	-3573.94	-6006.17	8716.3	-6316.63	-6006.17	-6324.36	142.42	101.92	21.39
111	56.1736	0.5362	30.5669	5167.975	2771.208	7070.25	-3621.39	-6072.4	8818.51	-6394.7	-6072.4	-6399.32	145.18	101.56	21.3
112	56.7103	0.537	30.7405	5217.345	2801.9485	7151.96	-3669.22	-6139	8921.39	-6473.32	-6139	-6474.83	147.97	101.21	21.21
113	57.2477	0.5379	30.9163	5266.792	2832.8647	7234.2	-3717.44	-6205.99	9024.94	-6552.5	-6205.99	-6550.91	150.79	100.85	21.13
114	57.786	0.5387	31.0959	5316.314	2863.9607	7316.99	-3766.04	-6273.37	9129.18	-6632.25	-6273.37	-6627.58	153.64	100.49	21.04
115	58.3252	0.5396	31.2788	5365.914	2895.2395	7400.33	-3815.05	-6341.16	9234.12	-6712.58	-6341.16	-6704.83	156.52	100.13	20.95
116	58.8651	0.5404	31.4653	5415.593	2926.7048	7484.23	-3864.45	-6409.35	9339.77	-6793.5	-6409.35	-6782.69	159.43	99.77	20.87